A STUDY OF THE MOLECULAR ORIENTATION OF ISOTACTIC POLYPROPYLENE AS A FUNCTION OF DRAW RATIO AND THE EFFECT OF ANNEALING TIME ON THE SAME.

BY

TOM OCHIENG OGADA , B.ED (SCIENCE)

A THESIS SUBMITTED IN PARTIAL FULFILMENT OF THE REQUIREMENTS FOR THE DEGREE OF MASTER OF SCIENCE

IN

THE DEPARTMENT OF PHYSICS

KENYATTA UNIVERSITY,

P.O. BOX 43844,

NAIROBI.

MAY, 1988.

This thesis is my original work and has not been presented for a degree in any other University.

Signature----------

TOM OCHIENG OGADA

This thesis has been submitted for examination with my approval as University Supervisor

Signature----------

DR. S.K. KATIA.

DEPARTMENT OF PHYSICS

KENYATTA UNIVERSITY.

ACKNOWLEDGEMENT.

I would like to give special thanks to my Supervisor, Dr. S.K. Katia, who offered tireless guidance throughout the whole period of this work. His encouragement and valuable advice in Polymer physics enabled me to get over crucial decisions and difficult moments over the experimental work. His support has undoubtedly made this piece of work a reality.

Secondly, I am grateful to Dr. Sarhene of the Physics Department, University of Nairobi, who offered me guidance on certain experimental aspects of polymer studies. His advice supplemented my skills and knowledge on the conduct of certain experimental techniques.

I am very thankful to the departments of Civil and Mechanical Engineering, University of Nairobi, for allowing me to use their equipment for the preparation of my samples. On the same note, I am deeply indepted to the Department of Geology, University of Nairobi, for availing me the polarising microscope that I used to carry out birefringence measurements.

I would also like to thank the Geology Department, of the Ministry of Environment and

Natural Resources for the use of the X-ray Diffractometer. In this regard I thank Mr. Kamagundho of the Geology Department for his technical assistance.

Lastly, but not least, I would like to thank Mrs. Francisca Osiemo and Miss Irene Nyambura for their tireless and dedicated efforts in typing this work.

DEDICATION.

This work is dedicated to my parents
and brothers, for, from them I received
moral and psychological support
I badly needed.

"Absolute certainty is the privilege
of uneducated minds - and fanatics.
It is for Scientific folks an
unattainable ideal"
C.J. Keyser.

CONTENTS

LIST OF FIGURES AND TABLES

LIST OF SPECIMEN CODES USED IN TABLES

1. Re-stretched specimens: SR-1, 2, 3, 4, 5 (Table 1).

2. Specimens with varied thickness and constant extension: ST-1, 2, 3, 4, 5, 6 (Table 2).

3. Specimens with controlled thickness and varied extensions: SE-1, 2, 3, etc. (Table 3).

4. Specimens annealed for 10, then 30 minutes after stretch.

   SA-A1, A2, A3, etc. (Table 4).

5. Specimens annealed for 10, then 60 minutes after stretch.

   SA-B1, B2, B3, etc. (Table 5).

6. Specimens annealed before stretch for:

   1½ hours; SB-A1, A2, A3, etc. (table 6)

   2½ hours; SB-B1, B2, B3, etc. " 7

   3 hours; SB-C1, C2, C3, etc. " 8

   6 hours; SB-D1, D2, D3, etc. " 9

   22 hours; SB-E1, E2, E3, etc. " 10

   47 2/3 hours; SB-F1, F2, F3, etc. " 11

   72 hours; SB-G1, G2, G3, etc. " 12.

7. Specimens for degree of crystallinity measurement:

DC-1, DC-2, DC-3, etc. (Table 13).

8. Specimens for Debye-Scherrer Camera:

DS-1, DS-2, DS-3, etc. (Table 16).

9. Specimens for IR-Scan:

IR-1, IR-2, IR-3, etc. (Table 19).

ABSTRACT

The birefringence (BF) due to molecular orientation induced in isotactic polypropylene (IPP) films by hot-stretching at 115°C has been studied, as a function of annealing time and draw (extension) ratio. The specimens were stretched between 20% and 600% (draw ratios of 1.2 to 7).

The general variation of BF versus extension and "orientation function" (OF) versus extension curves appeared to be described by an inverse tangential function, suggesting that there is a tendency of BF and OF values towards equilibrium values.

The films that had been pre-stretch annealed for varying times showed a lowering of BF with pre-stretch annealing times at low extensions (0-200%) but tended to a common magnitude irrespective of the annealing time, at higher extensions. The observed lowering of BF in the low extensions ceased after a certain period of annealing. These observations have been explained by invoking the crystalline and amorphous nature of the IPP, and the microstructural changes, that result from the applied tensile stresses under the given thermal conditions.

INTRODUCTION

One of the important characteristics of polymers is the ease with which molecules and crystallites are oriented when the polymers are deformed through such processes as stretching or extrusion. When a polymer is stretched many of its properties may be modified or changed altogether. The polymer may become anisotropic with respect to its optical properties. Molecular orientation in polymers is very important in the study of drawn fibres, especially in the textiles industry where tensile strength and elastic modulus can be effected by uniaxial tension.[1] Such properties are desirable in a number of textiles applications e.g. marine lines, howsers and in strap for heavy packing application. Uniaxial tension in many cases increases stiffness and as such has been useful in making brush bristles. High orientation along machine direction creates easy tear in the same direction relative to the transverse direction and could be useful in certain packing operations where unidirectional tear is desirable. Biaxial orientation is also of interest in applications where superior tensile properties, improved flexibility, toughness and increased shrinkability may be desirable.

Polycrystalline (semi-crystalline) polymers have generated a special interest because of their

two-phase structure that makes it possible to provide a wide range of different physical properties.

Polypropylene is a semi-crystalline polymer and as such articles of different physical properties can be fabricated from it. Its versatility and formability has made it an industrially important polymer. Its chemical formula is given below:

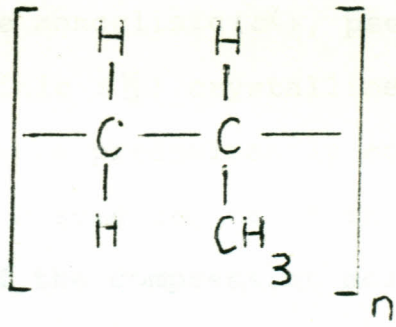

Fig. 1 Chemical formula of polypropylene.

The square brackets enclose the monomer , and the "n" outside the brackets denotes the number of monomer molecules in the chain. As a result of the methyl group the polymer acquires a helical structure. The positions of the methyl group along the chain determines whether it is atactic, syndiotactic or isotactic. When it occurs randomly along the carbon backbone the form is atactic. The form is syndiotactic or isotactic according to whether the methyl group occurs alternately or on the same side of the chain respectively. While the atactic form is amorphous,

isotactic and syndiotactic forms are semi-crystalline. These latter two forms are made by Ziggler-Natta Catalysts as addition polymerisation products. Isotactic polypropylene is the more widely used industrially. It was the one used for this work and has a melting point in the range 165-175°C. [2-4]

Isotactic polypropylene is a polymorphic material, and those forms that have been investigated widely are the monoclinic(α), pseudo-hexagonal (β) and the triclinic (γ) crystalline forms.[5] The samples used were predominantly monoclinic in structure, with some amount of the triclinic form, as a result of the compression molding process[6].

CHAPTER I

LITERATURE REVIEW

Studies on the molecular orientation of polymers have been of interest to many researchers. Most of these investigations have been related to orientation induced by processing methods such as extrusion and also to orientation caused by uniform uniaxial or biaxial deformation. Some of the commonly applied methods in these types of investigation have been: (i) birefringence, (ii) wide and small angle X-ray diffraction (iii) infrared dichroism (iv) sonic modulus and (v) low and wide angle light scattering. The birefringence method is applied in the investigation when the material is transparent[7-10]

The birefringence approach has been employed under varying conditions. Moore and Gieniewski[11] have made dynamic birefringence studies on certain polymers and obtained information about time dependence of orientation processes. They assumed affine deformation of the samples.

Extensive investigation on molecular orientation of isotactic polypropylene by applying wide angle and small angle X-ray diffraction, birefringence, infrared and sonic modulus has been carried out by Samuels.[12] He obtained values of crystalline and amorphous

orientation functions and intrinsic birefringences of the two phases.

Stein [13] has also made studies on orientation in stretched polyethylene by means of X-ray diffraction, birefringence and infrared. General uniaxial orientation was considered, and the assumption made that the contributions to birefringence and infrared dichroism were completely described in terms of three orientation functions. These, by definition were:

$$f_\alpha = \tfrac{1}{2}\,(3\langle\cos^2\alpha\rangle - 1)$$

$$f_\beta = \tfrac{1}{2}\,(3\langle\cos^2\beta\rangle - 1)$$

$$f_\gamma = \tfrac{1}{2}\,(3\langle\cos^2\gamma\rangle - 1)$$

where the angles α, β and γ were measured between the z-axis (the stretching direction) and the a, b, and c cystallographic axes respectively.

Orientation studies have also been carried on cold-drawn samples. Petermann and Schultz[14] have studied the microstructure and annealing behavior of cold-drawn isotactic polypropylene. A number of experimenters[15-19] have also studied semi-crystalline polymers in the oriented state. Such studies have led to the establishment of three basic morphologies:

(i) Extended-chain crystals with lamella overgrowths.[19]

(ii) Stacking sequence of oriented crystal lamellae[20].

(iii) Fringe-micelle type[21].

Fischer and Goddar[22] and Statton[16] from their work have come up with two principal models for cold-drawn and annealed semi-crystalline polymers:

(i) A defect crystal with many chainfolds randomly incorporated in the crystalline lattice, and the accumulation of these chainfolds during annealing lead to lamellar structure[22].

(ii) An oriented fringe-micelle model of structure, where one molecule penetrates several crystallites[16].

Horsely and Nancarrow[23] have investigated the stretching and relaxing of polyethylene. They used an X-ray beam of very small cross-sectional area to obtain diffraction patterns over the neck region that is produced when randomly oriented polyethylene is stretched. The results indicate that the orientation over the neck region produced by stretching at room temperature and lower is abnormal in that it does not consist of a gradual alignment of the polymer chains with the direction of stretch, but that at intermediate stretches the preferred orientation is such that the (011) axis was parallel to the stretch direction. At higher stretches, there is gradual tilting of the

crystallites until they are finally aligned with their chain axis parallel to the axis of the monofilament.

Deformation of polypropylene during extrusion has been investigated by Bahadur[24] at different temperatures, and he has found that this leads to c-axis orientation of the monoclinic unit cell. The unit cell aligns itself parallel to the direction of extrusion and the lamellar structure is orderly arranged.

Peterlin[17] has, from studies on plastically deformed polyethylene and isotactic polypropylene using electron microscopy, X-ray diffraction and photography, and infrared, developed a microfibrillar model of fibrous structure. The model points out to the existence of three stages in the cold-drawing process, although they are, to some extent intermixed in the neck region. They are

(i) Plastic deformation of the original spherulitic structure,

(ii) the discontinous transformation of the spherulite into fibre structure by micronecking,

(iii) plastic deformation of the fibre structure.

Also, Peterlin and Baltá-Calleja[25] have studied plastic deformation of polypropylene by the method of small angle X-ray scattering in the neck region.

Among their findings is the observation that the transformation from the spherulitic to fibrillar structure is a discontinuous process. The small angle X-ray scattering also yields information about the continous deformation and orientation of the lamellae within the spherulites before the final destruction takes place.

Investigations on the drawing and annealing of fibrous material by small angle X-ray scattering have also been performed by Peterlin [26]. He has observed a more than linear increase in elastic modulus with draw ratio after annealing, and a recovery upon standing at room temperature for a sample annealed with fixed ends. The observations were explained by the microfibrillar model of fibrous structure.

McRae, et al.[27] have reported on infrared spectroscopic and X-ray diffraction study of cold-drawn high density polyethylene and have found their results to be consistent with the Peterlin model.

Brown,[28] Stein and Norris,[29] and Aggarwal et al.[30] have applied a variety of techniques to follow the morphological changes during the cold-draw of polyethylene.

Shinozaki and Groves[31] have also made studies on the

molecular mechanisms in annealing of oriented polypropylene by means of low and wide angle X-ray photography. The mechanisms involve shear processes (intermolecular, interlamellar and fibrillar), normal processes (interlamellar separation and fibrillar separation) and twinning processes within the lamellae. While the wide angle X-ray photography showed no orientation over the whole range of annealing time and temperature, at 100°C the low angle X-ray photography showed a progressive change in the orientation of the lamella normal to the molecular axis. At higher temperatures of 130°C and 140°C the lamella normal became parallel to the molecular axis and a stable structure appeared to have formed. The specimens had been deformed by strains of 64% and 100% respectively. The explanations on low angle X-ray photography follow earlier reasoning by Shinozaki and Groves[31]. The same mechanisms have been studied by other authors[32-34].

Other studies on the stretching and relaxing of polyethylene have been made by Brown[28]. The stretching was done at 96°C and the observation made indicates orientation of crystallites in which the long axis is parallel to the direction of stretch. The orientation is low at low elongations and becomes progressively stronger with increasing extension. When polyethylene is stretched at room temperature the crystalline structure becomes more complex with

further extension. The orientation of the crystallites in the shoulder of the necked region of polyethylene is also such that the "011" axis aligns in the stretching direction.

Measurements by Rhodes and Stein[35] using low angle light scattering on the annealing of drawn polyethylene samples have showed that the observed orientation, especially at 200% extension suggests three regions of orientation as previously deduced from X-ray diffraction studies by Stein and Norris[29]. Changes in morphology of structures having sizes upto several microns occured upon annealing as revealed by the low angle photographic light scattering technique. These results agree with previously observed changes in the orientation of individual crystals by the authors. The observations appear to indicate that the explanation to the changes must be compatible with the accompanying change in the superstructure.

Sasaguri et al.[36] have investigated the relation between morphology and deformation mechanisms of polyolefins by slow drawing at room temperature, and noted that the birefringence of polyolefins changes from negative values at low elongations to positive values at higher elongations. The extent of the negative contribution depends on the tacticity of the sample, its thermal and mechanical history, and the temperature of measurement.

Crystal and Hansen[37] have also performed cyclic cold-drawing and annealing of polypropylene samples. They observed that while the first drawing proceeded by neck deformation and propagation, the subsequent drawings were homogeneous. Micrographs of sections cut from the polypropylene showed a spherulitic structure that was retained throughout the drawing and annealing.

The studies reviewed above involved affinely deformed, cold drawn and annealed samples. The stretchings and annealings had been performed at various temperatures. The morphological changes were examined by X-ray, infrared, and light scattering methods while the bulk properties were examined by birefringence and modulus measurements. If the birefringence is taken in particular, the studies carried only touched on annealings during or after stretching. There seemed to have been no mention of studies on birefringence involving initial physical state, such as crystallinity, as a function of draw ratio. The properties of such samples after hot stretching to different draw ratios could be important in extending our knowledge on drawn semi-crystalline polymers. Such a study would indicate how molecular orientation is influenced by varying the initial physical states for given draw ratios. This investigation aimed at determining the

effects on the molecular orientation of polypropylene caused by:

(i) Varying the draw ratio at constant temperature

(ii) annealing after stretching

(iii) stretching, annealing and re-stretching

(iv) varying the annealing time.

The specimens examined were drawn to low (0-100%), medium (about 100-200%) and high (300% and above) extensions. The method of wide angle X-ray diffraction was used to determine crystallinity as well as the change in Bragg spacings. Infrared dichroism was used along with birefringence to relate the two to the draw ratio.

CHAPTER 2

THEORY

2.0 INTRODUCTION

The molecular orientation of a material can be suitably studied by a number of quantitative methods. The methods that were of interest in this study were birefringence, infrared dichroism and wide angle X-ray diffraction.

2.1 BIREFRINGENCE

In the unoriented state the isotactic polypropylene molecules, although anisotropic individually, are in random conformations, and crystallites are randomly arranged. Thus the crystalline and amorphous regions exhibit macroscopic isotropy. When uniaxial orientation is applied, it sets up anisotropy in the macro-level. A difference is thus set between refractive indices parallel and perpendicular to the stretch direction. This difference, defined as birefringence is related to the phase change caused to the polarised light beam that passes through the film. The birefringence is given by:

$$\Delta n = n_1 - n_2$$

where n_1 and n_2 are refractive indices parallel and perpendicular to the direction of stretch repectively.

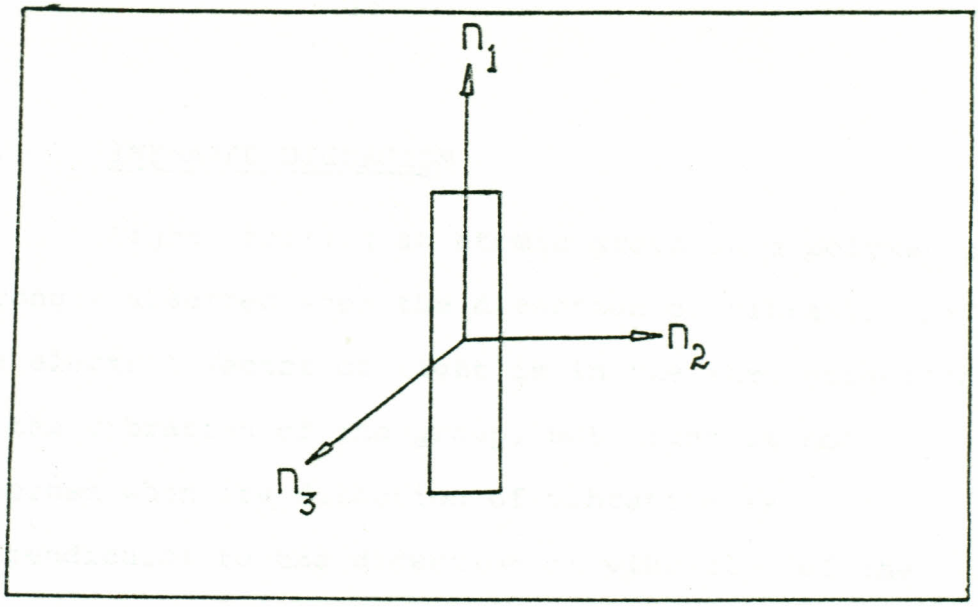

FIG. 2 The refractive indices, n_1, n_2 and n_3 are mutually perpendicular.

The phase difference,

$$R = \frac{\delta}{2\pi}\lambda$$

where δ is the phase difference in radians, and λ is the wavelength in nanometers.

R is the phase difference in nanometers.

The birefringence is related to the phase change by:[12]

$$\Delta n = \frac{\delta}{2\pi}\,\frac{\lambda}{t} \qquad \ldots \quad (1)$$

$$= \frac{R}{t} \qquad \ldots \quad (2)$$

where t is the thickness of the specimen in nanometers.

The films are composed of two phases, the crystalline and amorphous, whose physical structures are different, and therefore exhibit different birefringences. The polarising light microscope will, however, yield only the average birefringence of the film material.

2.2 INFRARED DICHROISM

Light striking an atomic group in a polymer is strongly absorbed when the direction of vibration of the electric vector of light is in the same direction as the vibration of the group, but light is not absorbed when its direction of vibration is perpendicular to the direction of vibration of the group. Thus when an oriented polymer is examined with polarised infrared light, the intensity of the absorption band depends on the direction of the electric vector of the incident light relative to the axis of orientation. The effects of orientation on an absorption band is characterized by the dichroic ratio, D defined as[38].

$$D = \frac{A_{\parallel}}{A_{\perp}} \qquad \ldots.(3)$$

where $A_{\parallel}$ and $A_{\perp}$ are the absorbances parallel and perdendicular to the direction of stretch respectively.

Absorbance is generally defined as:

$$A = \log\frac{I_o}{I} \qquad \ldots. (4)$$

where I_o, I are the incident and transmitted intensities respectively.

By considering an oriented material as consisting of all molecules oriented at some average angle θ relative to the orientation direction, Samuels obtained the expression for dichroic ratio

as[12]:

$$D = \frac{1 + (D_o + 1)\ \langle \cos^2\theta \rangle}{1 + \tfrac{1}{2}(D_o - 1)\ \langle \sin^2\theta \rangle} \qquad \ldots\ (5)$$

Where D_o is the dichroic ratio of an ideally oriented polymer.

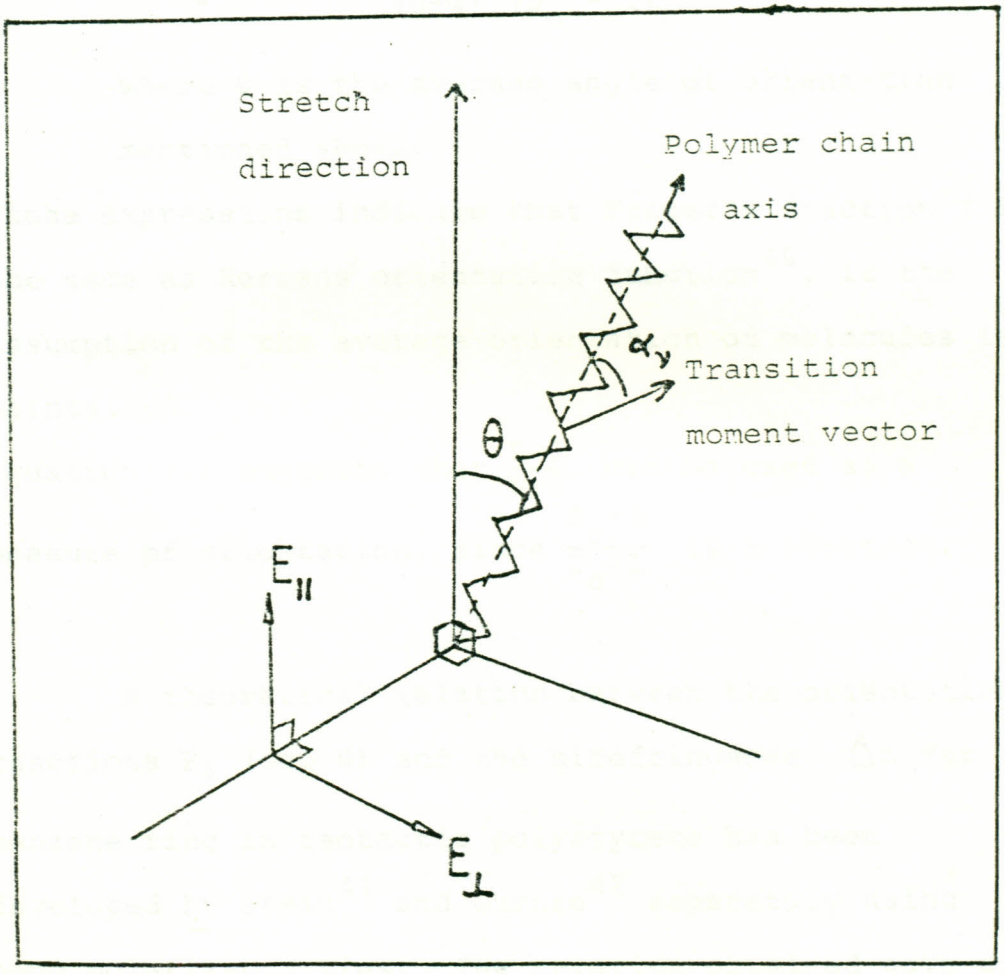

FIG. 3 Polymer molecule inclined at average angle θ to the direction of stretch.
α_ν is the transition moment angle, and $E_{\parallel}$, $E_{\perp}$ are the parallel and perpendicular components of the electric vector.

On relating the above expression to one earlier obtained by Fraser,[39] where the oriented sample was

considered to have a fraction f of perfectly oriented chains and (1-f) randomly oriented chains new expressions were arrived at[12]:

$$\frac{3\langle\cos^2\theta\rangle - 1}{2} = \frac{(D-1)\ (D_o + 2)}{(D+2)\ (D_o - 1)} = f \qquad \ldots(6)$$

where θ is the average angle of orientation mentioned above.

These expressions indicate that Fraser's fraction f is the same as Hermans' orientation function[40], if the assumption of the average orientation of molecules is maintained.

Equation (6) suggests that $\frac{D-1}{D+2}$ can be used as a measure of orientation, since $\frac{D_o+2}{D_o-1}$ is a constant.

A theoretical relation between the orientation functions P_2 (cos θ) and the birefringence Δn for benzene ring in isotactic polystyrene has been developed by Stein[41] and Gurnee[42] separately using bond polarizabilities. The relation obtained gave a linear relation.

$$\Delta n = \left[0.194 - 0.51\langle\cos^2\alpha'\rangle\right] P_2\langle(\cos\theta)\rangle \qquad \ldots(7)$$

where α' is the angle between the normal to the benzene ring and the chain axis.

Now since

$$\langle P_2(\cos\theta)\rangle = \frac{3\langle\cos^2\theta\rangle-1}{2} = \frac{D-1}{D+2}\,\frac{D_o+2}{D_o-1} \quad \ldots\ldots (8)$$

equation (8) becomes

$$\Delta n = \left[0.194-0.51\langle\cos^2\alpha'\rangle\right]\frac{D-1}{D+2}\,\frac{D_o+2}{D_o+1} \quad \ldots\ldots (9)$$

such a relation where birefringence varies linearly with $\frac{D-1}{D+2}$ may be expected for isotactic polypropylene given that their backbones are similar except for the benzene and methyl groups. The crystalline nature of polypropylene may also create some deviation from linearity.

2.3 X-RAY DIFFRACTION

The semi-crystalline structure of the polymer makes the X-rays be diffracted in such a manner that particularly strong reflections are recorded at some glancing angles. Bragg's law is obeyed during such interaction between the radiation and the polymer material and the strong reflections are obtained at Bragg angles θ such that

$$2d_{hkl}\sin\theta = n\lambda \quad \ldots\ldots (10)$$

d_{hkl} represents the Bragg spacing of planes with the miller indices (hkl).

θ is the Bragg angle,

λ is the wavelength of the X-rays in Angstroms.

and

n is the order of the reflection.

The relation between the Bragg angle θ and the arc length S is simply related by reference to fig. 4 below.

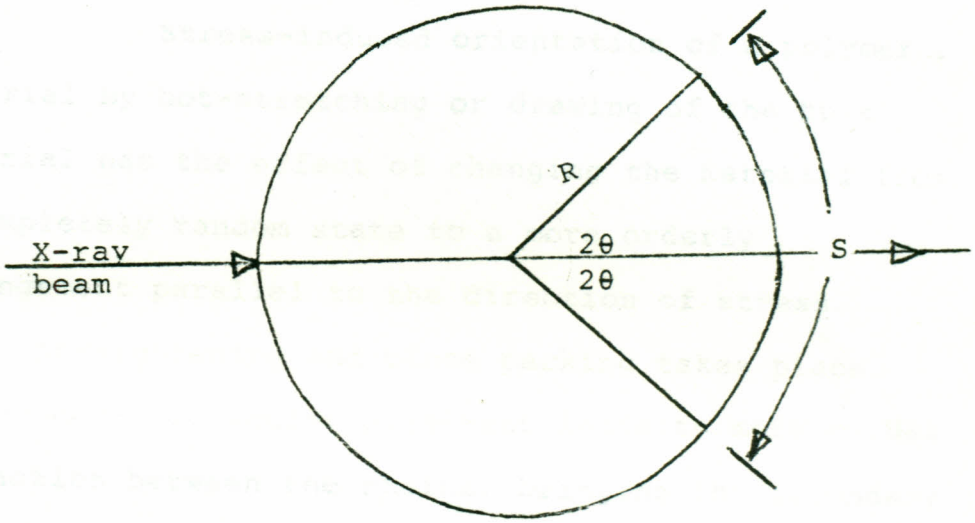

FIG. 4. X-ray beam, strikes sample at centre of DS camera.

S is the arc length;

θ is the Bragg angle

R is the camera radius

$$4\theta = \frac{S}{R} \text{ radians}$$

$$\text{or} \quad \theta = \frac{S}{4R} \text{ radians}$$

$$= \left[\frac{180}{\pi} \cdot \frac{1}{4R}\right] \; S \text{ degrees} \quad \ldots.(11)$$

Camera diameter = 57.3 cm $\left[\simeq \frac{180}{\pi}\right]$

Hence $\theta = \frac{S}{2}$ degrees.

Correction is made to measured value of S to take care of the distance between the collimeter hole

and the exit hole on the film. The exact distance is 90mm. An alternative way to obtain θ is from a diffractogram.

2.4 GENERAL REMARKS ON THE CRYSTALLIZATION AND DRAWING PROCESSES.

Stress-induced orientation of a polymeric material by hot-stretching or drawing of the bulk material has the effect of changing the material from a completely random state to a more orderly arrangement parallel to the direction of stress. Chain straightening and close packing takes place. The ensuing molecular alignment leads to more mutual attraction between the chains, bringing the secondary valence forces to the greatest possible effect. This mutual attraction is enhanced the more symmetrical and the more polar the molecules are.

If the temperature of draw is below the glass transition temperature, the chains are rigid, and rupture is likely to occur during drawing. A high stress may have to be applied and the material may whiten. At the glass transition temperature, the molecules attain a certain degree of freedom, and they may start unfolding under stress. Above the glass transition temperature, a mass of randomly coiled and entangled chains may be drawn out. The applied stress will lead to chain disentanglement,

straightening and slip.

The stretching process thus has three major components:[43]

(i) instantaneous elastic deformation, as a result of valence angle deformation or bond stretching. This is completely recoverable when stress is removed.

(ii) Molecular alignment deformation caused by uncoiling. This involves more molecular alignment, and the stress is frozen in when the material is cooled.

(iii) Non-recoverable viscous flow which is caused by the molecules sliding past one another.

The desirable of the major components is (ii) since it is the orienting component. The factors that will be favourable to various levels of orientation include the temperature of draw, rate of draw, and the initial state of the material. The conditions that were chosen ensured the material was ductile enough, and a combination of cooling and deformation rates which exceeded the relaxation rate.

The stretching of unoriented polymer leads to a structural reorganisation which in turn leads to changes in both mechanical and optical properties. The deformation may be affine or non-affine.

If the deformation is affine, the Wilchinsky[44] model that relates orientation function to the draw ratio may be applied. Supposing the initial state of the molecular chains and crystallites is random, then the orientation parameter for the crystal C-axis, assumed to align in the same direction as a line vector in an affine deformation, in a uniaxial elongation may be given by:

$$\langle \cos^2\theta \rangle = \frac{\lambda^3}{\lambda^3 - 1}\left[1 - \frac{\tan^{-1}(\lambda^3 - 1)^{\frac{1}{2}}}{(\lambda^3 - 1)^{\frac{1}{2}}}\right] \quad \ldots(12)$$

where $\langle \cos^2\theta \rangle$ is the orientation parameter

λ is the draw ratio (extension ratio)

Non-affine deformation may occur during hot-stretching, such as when necking down or "cold-drawing" occurs. This kind of deformation leads to fibrous structure and may be explained by the microfibrillar model of fibrous structure developed by Peterlin[17]. The deformation of non-fibrous semi-crystalline polymer destroys the stacks of thin and wide parallel lamellae of the starting material and transforms them into densely packed and well aligned extremely long and thin microfibrils of the final fibrous structure.

If a stretched semi-crystalline polymer is subjected to annealing, the process leads to perfecting of the crystal structure, makes sharper the boundary between crystal blocks and amorphous surface layers and relaxes the amorphous chains. From the work done on semi-crystalline polymers relating to the effects of annealing, two principal models (see lit. review pg. 6) have been proposed.

The annealing of the polymeric material before stretching also has the effect of increasing the crystalline content. As the process of crystal perfection proceeds, residual strains are relaxed, dislocations and vacancies are healed and the lamellae thicken[2]. The process approaches an equilibrium state, and the lamellar thickenings can then be explained by irreversible thermodynamic processes[45].

CHAPTER 3

EXPERIMENTAL PROCEDURE AND TECHNIQUES

3.0 INTRODUCTION

In order to study the molecular orientation of isotactic polypropylene, the methods of birefringence, infrared dichroism and X-ray diffraction were employed. All the methods were expected to be sensitive to changes in orientation. The specimens were prepared to suit examination by the above methods.

3.1 SAMPLE PREPARATION

Two mild-steel mold plates (fig. 5) of effective surface dimensions of 22.5x7.0 cm were used in the compression molding of the polypropylene films.

The isotactic polypropylene pellets labelled as FINAPROP PPH 3060s of melt-flow index 1.7 and tensile strength of about 35 Nmm^{-2}, were obtained from East Africa Bag and Cordage Co. Ltd., Juja, Kenya.

Before preparation, aluminium foil was placed on the polished surface of the plates to prevent sticking of the films after compression. Pellets were arranged on the surface of the bottom plate (fig. 5) and both plates placed in the oven, which had been set at a temperature of 250 °C. They were left for 25 minutes for the pellets to melt. The top plate was then lowered to cover the melted pellets (fig. 6), and

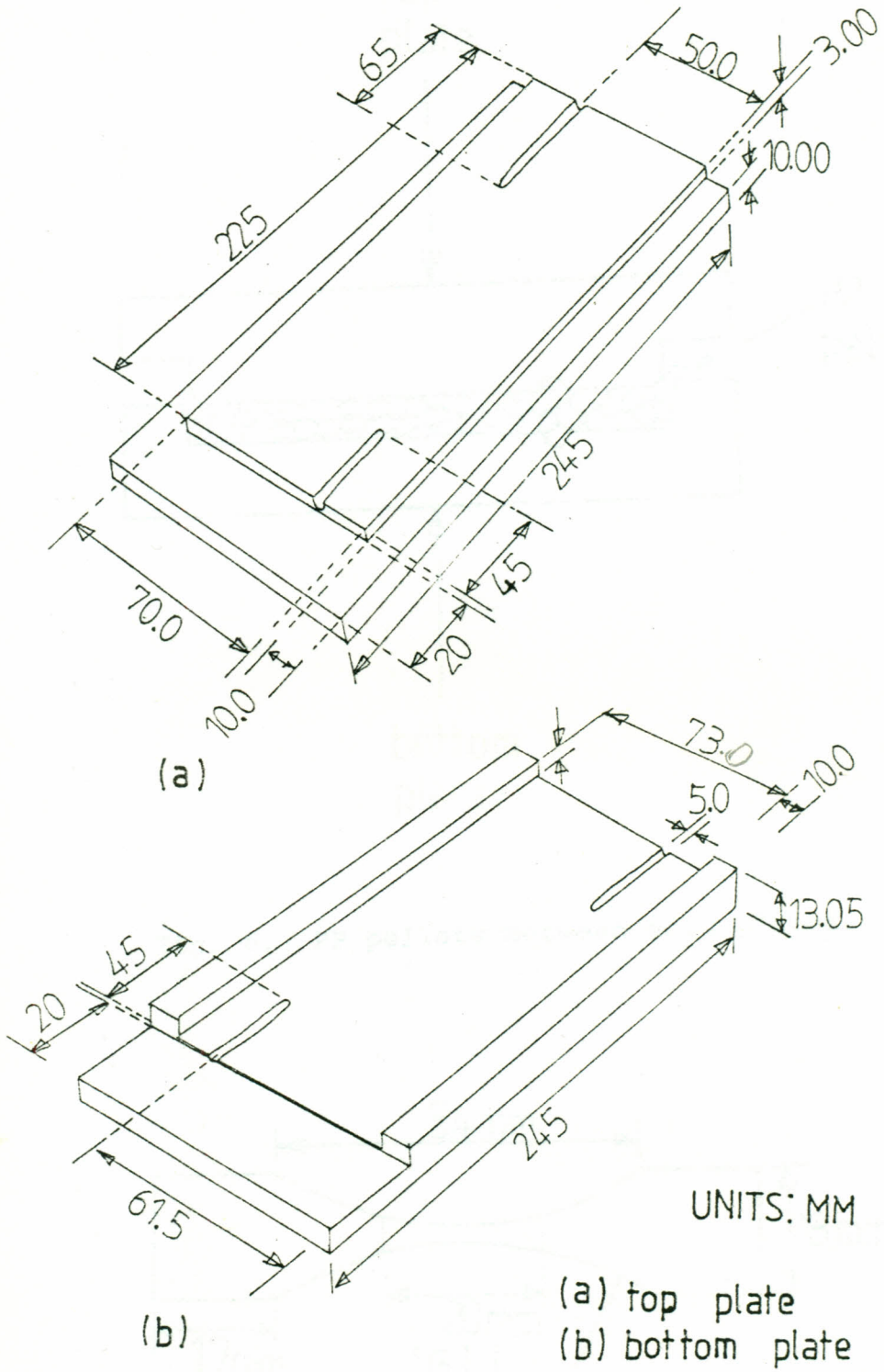

Fig. 5. The Mold plates.

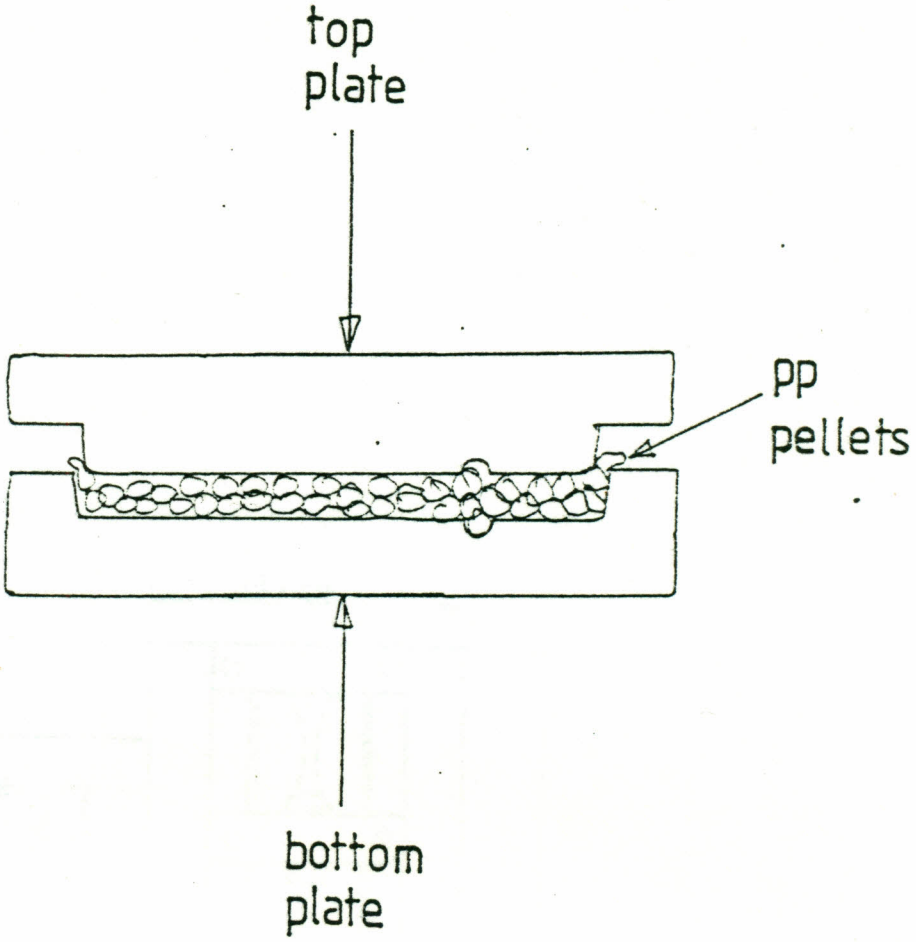

Fig. 6. PP pellets between mold plates.

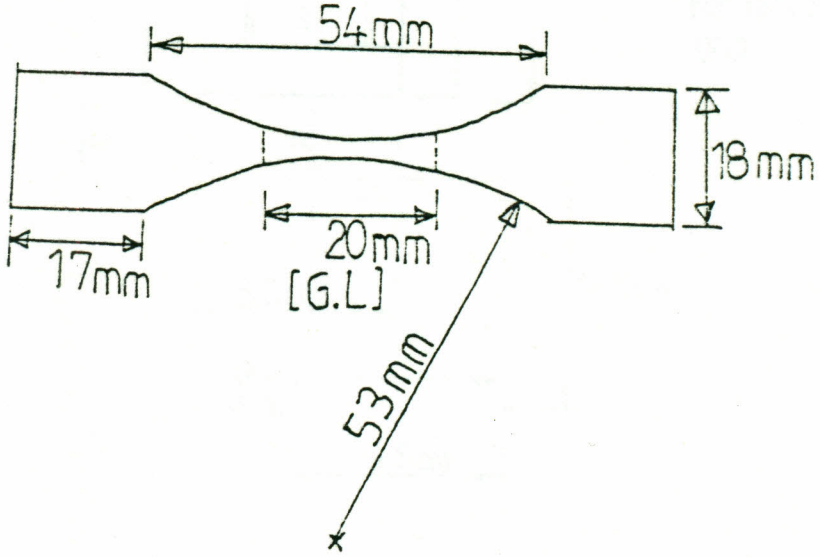

Fig. 7. Specimen profile for stretching, narrowest section width = 3 mm.

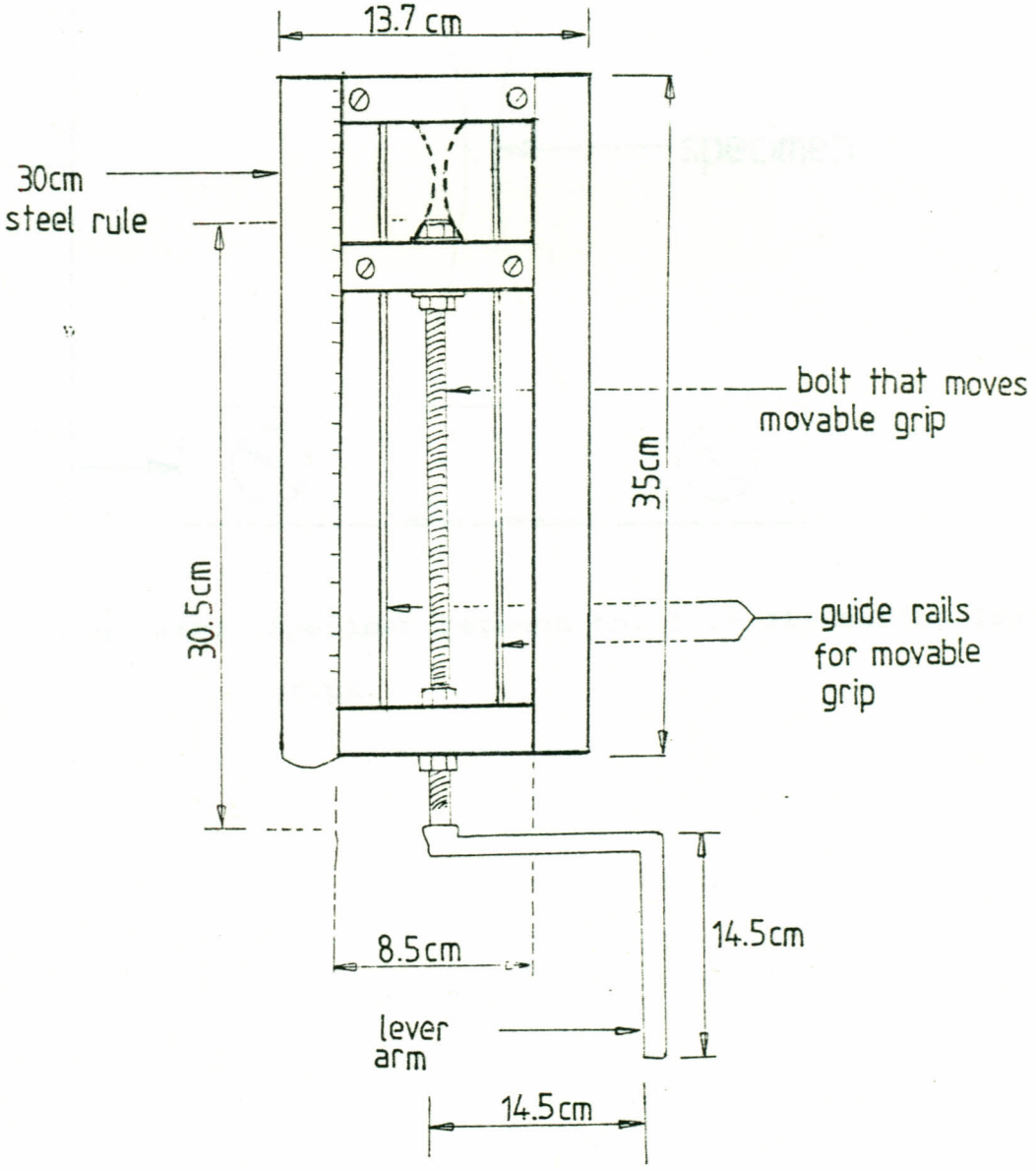

Fig. 8(a) The film-stretching frame.

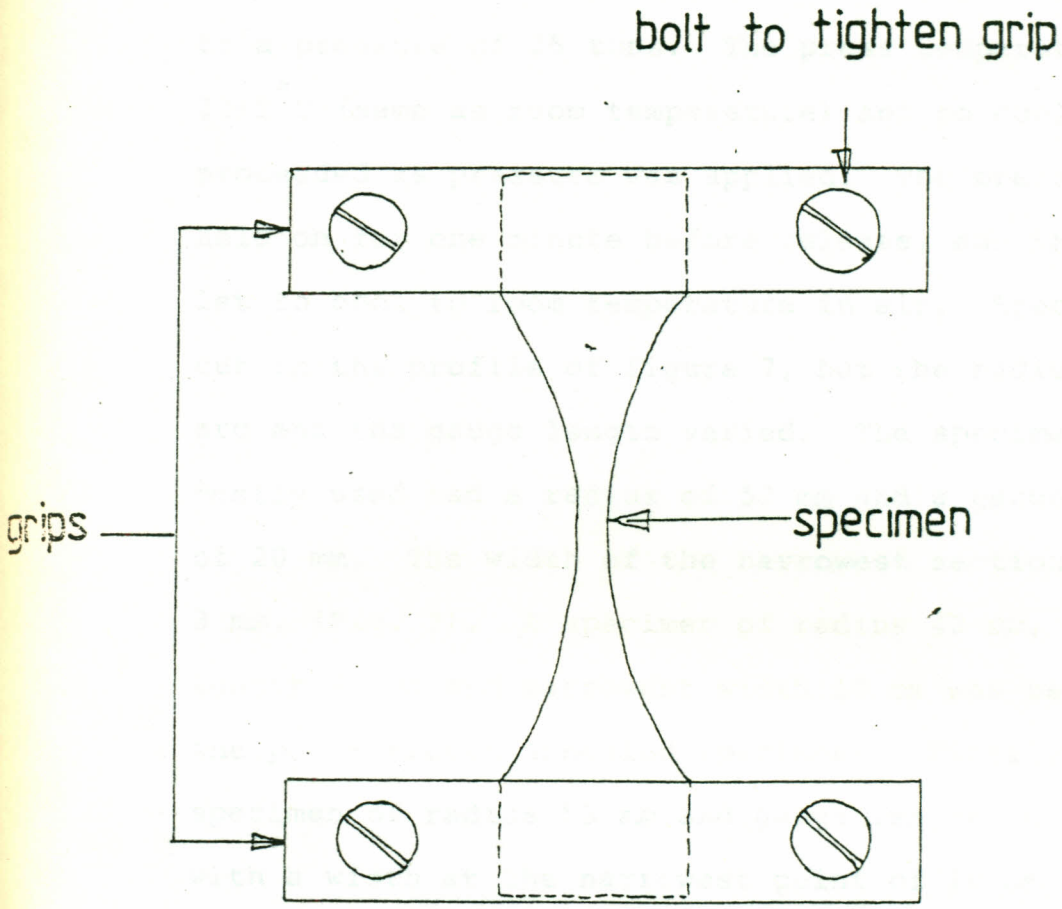

Fig. 8(b) Specimen between the film-stretching frame grips.

the mold taken to the compression machine and pressed to a pressure of 25 tons. The press temperature was 20±2°C (same as room temperature) and so cooling proceeded as pressure was applied. The pressure was held on for one minute before release, and the set-up let to cool to room temperature in air. Specimens were cut in the profile of figure 7, but the radius of the arc and the gauge length varied. The specimen profile mostly used had a radius of 53 mm and a gauge length of 20 mm. The width of the narrowest section was 3 mm. (Fig. 7). A specimen of radius 42 mm, gauge length 40 mm and narrowest width 10 mm was used for the post-stretch annealed specimens. Finally, a specimen of radius 53 mm and gauge length 20 mm but with a width at the narrowest point of 10 mm was used for infrared measurements. The mean thickness of the specimens was 0.10±0.08 mm.

The narrower width of 3 mm of the pre-stretch annealed specimens helped in reducing the time of annealing after stretch to 10 minutes, and was also reasonable for use in the microscope. The width of 10 mm for the infrared specimens was needed because it provided a width suitable for use at the beam slit. However, as a result of the width, the annealing time after stretch was extended to 15 minutes.

The profile chosen for the specimens was preferred to the dumbbell, because preliminary tests revealed that the specimen tended to fail at the shoulder of the specimen or the edge of gauge length. This type of profile has been used by Vincent,[46] also in preference to the dumbbell. The actual dimensions of his specimens were different. He explained the difficulty he found as related to the machining of the specimens. They also tended to suffer slippage and fracture near the clamps. The disadvantage that was evident in the shape was that it had no parallel gauge length which made measurements of strain rather inaccurate. The benefit, however, of having all the specimens starting to deform around the centre by necking made the study of the deformed region more consistent, and the effect of strain measurement minimized.

3.2 STRETCHING OF THE SPECIMENS

The stretching of the films was performed with the aid of a film stretching frame (fig.8), made in the science workshop of Kenyatta University. Film specimens were locked at the grips of the stretching-frame before being extended. Portions of the film under the grips were covered by emery cloth to improve the gripping and to prevent heat damage from the hot metal grips. When this precaution was not taken,

specimens failed at the grips. After the films were held (fig.8) the frame was placed in an air-circulated oven set at 115°C. The specimens were left to heat for six minutes after which the oven door was partially opened and stretching done by rotating the lever arm of the frame (fig.8).

3.3 APPARATUS USED

The apparatus used included

(i) 2 mild-steel mold plates.

(ii) 1 film-stretching frame.

(iii) 2 ovens, one of which was air-circulated, and a press.

(iv) An X-ray diffractometer.

(v) An Infrared Spectrophotometer.

(vi) A polarising Microscope and Compensator.

(vii) Auxilliary equipment- a micrometer screw gauge, a film measuring equipment (Debye-Scherrer Camera) and a planimeter.

3.3.0 The mold plates

The mold plates were machined, ground and polished at the mechanical engineering department of Nairobi University. The final polishing was done with grade 600 emery paper. Their dimensions were as shown in fig. 5.

3.3.1 The film-stretching frame

The frame (fig.8a) was made at the Science

Workshop, Kenyatta University. It was capable of giving an extension within 20 mm gauge-length of the specimen upto 8 times (700% necked extension). Four large G-clamps and two small G-clamps were used to support both the steel rule and the frame. Four steel rods held by the four G-clamps and supported by wooden rectangular blocks ensured that the frame was only directly heated by the circulating hot air and radiation. Aluminium bolts were used to lock specimens on the grips (Fig. 8b).

3.3.2 Ovens and the press

An oven and press at the Civil Engineering Department, University of Nairobi, were used for heating of the isotactic polypropylene pellets to melt and for compression molding respectively. The press was a Dennison Compression Testing Machine with a capacity of 180 Tons on the 11½ in (29.2 cm) ram.

Another oven at the Mechanical Engineering Department, that was equipped with a fan for air circulation was used for the stretching and annealing purposes. The films that were subjected to annealing before stretch had been placed between mold plates before being kept in the same oven. The oven had stable temperature within $\pm 2^{\circ}C$ and had a temperature range $0\text{-}300^{\circ}C$.

This oven was also large enough to accommodate the film stretching frame.

3.3.3. X-ray diffractometer

A Phillips Norelco Diffractometer and an accompanying Debye-Scherrer Camera were used for the wide-angle X-ray measurements. These were located at the Mines and Geology Department of the Ministry of Natural Resources. The diffractometer was operated at an anode voltage and current of 40KV and 30 mA respectively. The films had rectangular dimensions of 6 x 29 mm. Specimens for the camera had a width of 0.5 mm, and were long enough to project into the path of the X-ray beam.

3.3.4. Infrared spectrophotometer

A Perkin-Elmer spectrophotometer model 598 apparatus at the Chemistry Department, Kenyatta University, produced a partially polarised infrared beam. A rectangular slit 7 x 7 mm was made in a cardboard to ensure the same beam area passed through the film when the specimen was placed vertically or horizontally. The scan time was set to 4 minutes and the reference medium was air.

3.3.5 Polarising microscope and compensator

A Carl Zeiss Standard Polarising

Microscope and a Carl Zeiss Ehringhaus Compensator located in the Department of Geology University of Nairobi, were used for the measurement of phase difference caused to polarised light by the isotactic polypropylene films.

3.3.6 Auxilliary Equipment

(a) A micrometer screw gauge was used to measure the thickness of the specimens.

(b) Special ruler scale with a vernier was used to measure the diameters of the rings and arcs formed on the X-ray film from the DS camera. It had an accuracy of $\pm$ 0.1 mm.

(c) A planimeter was used to measure the areas of the crystalline and amorphous regions in the diffractograms for the purpose of calculating the degree of induced crystallinity.

3.4 EXPERIMENTAL PROCEDURES

3.4.0 INTRODUCTION

The specimens used had their rates of stretch calculated by dividing the extension by the time taken. The mean rates of stretch were such that:

(a) Specimens unannealed before stretch, followed by annealing for 10, 30 and 60 minutes (post-stretch annealing) had a rate of 40.0 ± 2.5 mm/min.

(b) Specimens annealed before stretch (pre-stretch annealing) for $1^1/_4$, $2^1/_4$, 3, 6, 22, 47 and 72 hours followed by a post-stretch annealing of 10 minutes had a rate of 30.5±3.0 mm/min.

(c) Specimens for infrared scan, unannealed before stretch but annealed for 15 minutes after stretch had a rate of 29.0±2.4 mm/min.

All the annealing was done at a temperature of 115±2°C.

3.4.1 Birefringence measurements by microscopy techniques.

All the specimens used in the study were examined for their birefringence. A specimen to be examined was placed on the stage of a polarising microscope mounted with an Ehringhaus compensator. The compesator had quartz combination plates (formed by a pair of quartz plates). The Phase difference caused by each specimen was calculated. The specimens were set between crossed polars at 45° from the position of extinction with their draw axes perpendicular to the axis of the compensator (fig.9) When the quartz combination plates were rotated in white light, a number of coloured fringes crossed the field of view until the compensating dark band was obtained. The angle through which the plates rotated was observed while the compensating band

was at the intersection of the cross-hairs. Readings were made for the plates' inclination in two directions i.e. one to the right and the other to the left and an average reading computed from the two.

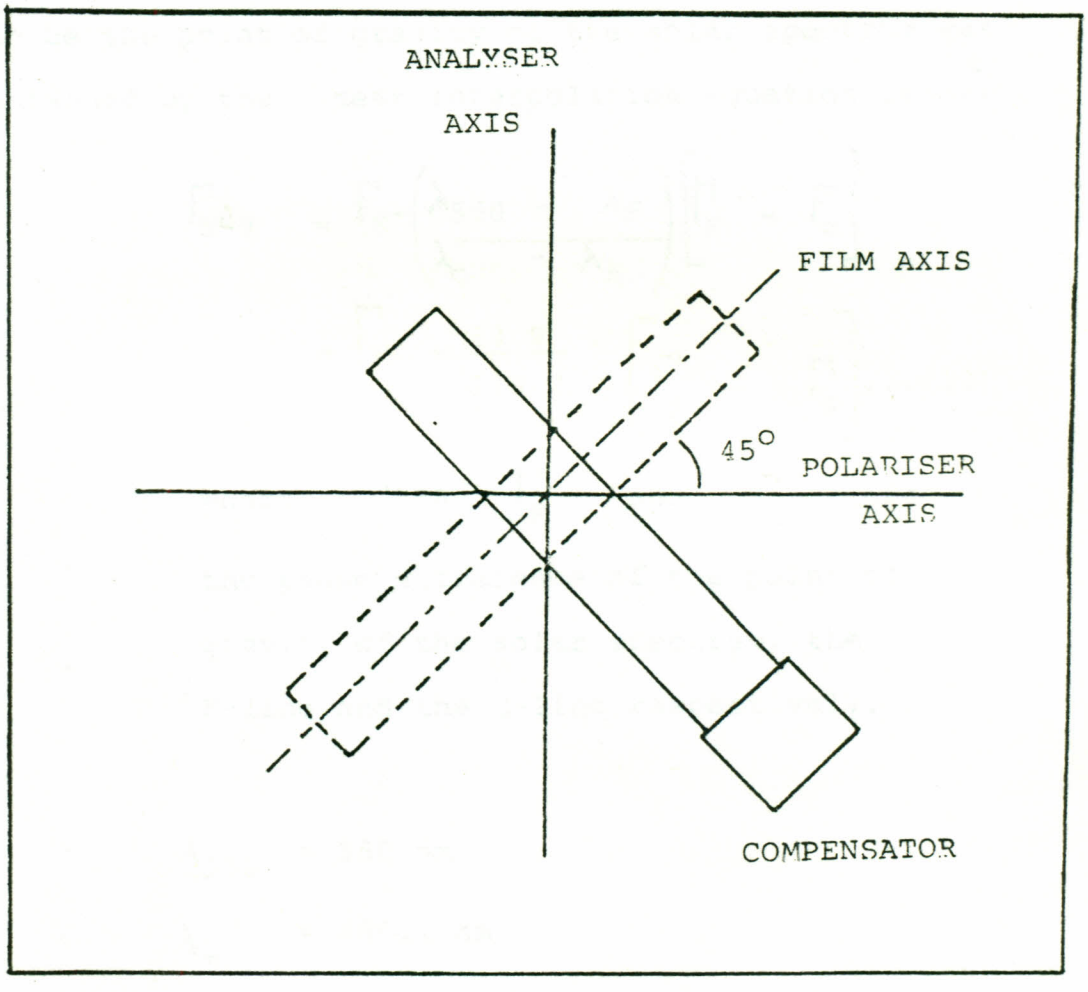

Fig. 9. Specimen between crossed polars

About five pairs of readings were made to have better mean values, and an overall mean worked out. The thickness of the specimens at the point of observation was measured using a micrometer screw gauge.

The phase difference obtained was worked out using the angle-phase difference tables for quartz combination plates. Phase differences for the F-line and the C-line were read from the tables and linear interpolation performed where necessary. The Phase difference for the wavelength λ= 550 nm, considered to be the point of gravity of the solar spectrum was obtained by the linear interpolation equation below:[47]

$$\Gamma_{550} = \Gamma_F - \left(\frac{\lambda_{550} - \lambda_F}{\lambda_C - \lambda_F}\right)\left[\Gamma_F - \Gamma_C\right]$$

$$= \Gamma_F - \frac{63.9}{170.2} \cdot \left[\Gamma_F - \Gamma_C\right] \quad \ldots(13)$$

Where Γ_{550}, Γ_F and Γ_C are the phase difference of the point of gravity of the solar spectrum, the F-line and the C-line respectively.

λ_{550} = 550 nm

λ_F = 486.1 nm

λ_C = 656.3 nm

The birefringence was then calculated from

$\Delta n = \frac{R}{t}$, where Δn, R and t are defined in equation (2)

Now $R = \Gamma_{550}$

3.4.2 Crystallinity Measurement by Wide-Angle X-ray.

X-ray diffraction represents one of the methods that may be used to find the degree of crystallinity of a polymer. The other methods include density, nuclear magnetic resonance, differential thermal analysis and infrared spectroscopy. The X-ray method turns out to be very convenient because of the ease with which it can be performed. There are a number of approaches that could be used even with the X-ray method, and may involve either "internal" or "external" measurements. The method that was adopted in this work was an "internal" one, and rested on the contention that the intensities of the crystalline peaks are in principle related through the unit cell to structure factors, and therefore their ratio should be invariant.[48]

This approach means therefore that the resolution of the crystalline and amorphous regions is done, keeping the crystalline area as a whole, rather than considering individual peaks as had been done by Natta and Corradini[49] or Hermans and Weidinger[50]. Thus a single correction factor

is applied to the crystalline area as a whole rather than individual correction factors for each peak[48].

$$X = \frac{A_c}{A_c + KA_a} \qquad \ldots.(14)$$

Where A_c is the crystalline area,

A_a is the amorphous area,

and K is a factor which takes into account the fact that the centre of the intensity of a group of crystalline reflections occurs at a higher θ value than does the maximum corresponding to the amorphous peak.

The calculated value of K of 0.98 in the range $6^\circ < 2\theta < 33^\circ$ was used in crystallinity calculation to give the expression[51]:

$$X = \frac{A_c}{A_c + 0.98A_a} \qquad \ldots. (15)$$

The factor to multiply the crystalline area is unity.

The diffractograms observed in this experiment had prominent peaks occuring close to 14°, 16°, 16.8°, 18.4°, 21°, and 21.8°. Small peaks occured around 25.4° and 28.4° (figs. 36-42). During resolution, a line was drawn to separate the region of air scatter and incoherent radiation from the amorphous area

(Figs. 36-42) between the angular limits of $2\theta = 10^{\circ}$ and 31°. No peaks were observed outside these limits.

3.4.3 Bragg Spacing Measurement by Wide-Angle X-ray.

The Bragg spacing of the specimens that had been annealed (table 14) was calculated from angles registered on the diffractograms (Figs. 36-42). However, the measurement of Bragg spacing of the stretched specimens was done by the Debye-Scherrer approach. The specimens were cut into fibre-like pieces of width 0.5 mm. A fibre holder was used to support the pieces at the centre of the camera, and centring done to ensure that the specimen was always in the path of the beam when rotating[52]. Non-screen X-ray film strips of dimensions 3.5 x 7 cm were cut from a film plate. The exposure proceeded for 30 minutes, at an anode voltage and current of 40 kV and 30 mA respectively.

After processing the films, the diameters of the rings or arcs obtained were measured by a special ruler scale, with a vernier enabling readings accurate to ±0.1 mm to be made. Accuracy of the measured distances was checked by considering the sum (table 19) $X_1 + X_2$ to within ±0.1mm. The

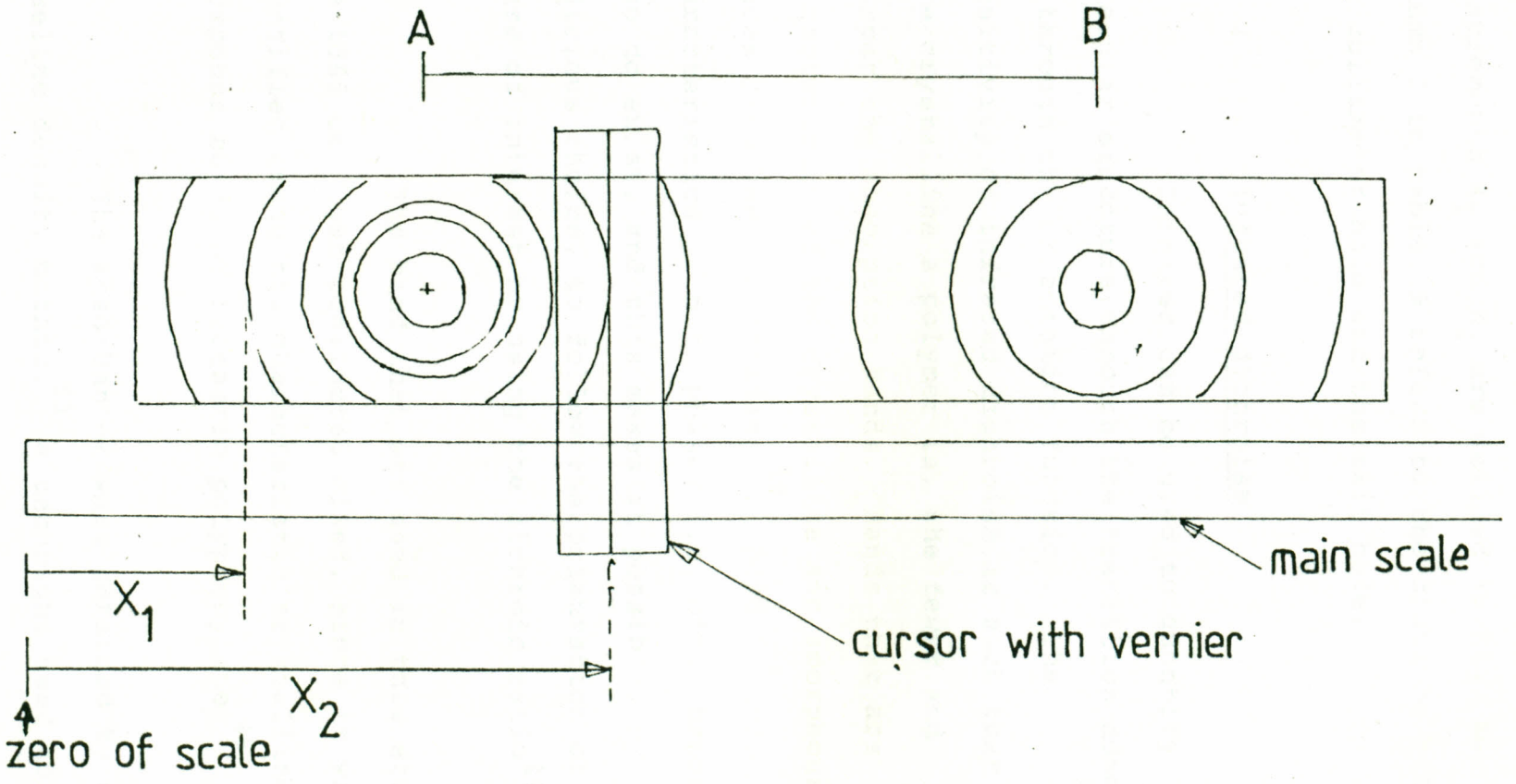

Fig. 10. Schematic diagram of X-ray film on film measuring equipment.

measurements X_1 and X_2 are defined in Fig. 10. The column 2 in table 19 refers to the distance between the collimeter hole and the exit hole.

3.4.4 Infrared dichroism

Infrared can be used to quantify molecular structure through the transition moment or through the orientation function. The sensitivity of infrared dichroism is such that the more crystalline a polymer is, the fewer and sharper the absorption bands. Bands that are characteristic of the crystalline and amorphous phases have been indentified[48]. Band characteristics of both phases i.e. mixed bands also do exist, and this makes it possible, by judicious choice, to follow the orientation of the phase of interest by using the dichroic ratio[12].

The band that was used in this study, i.e 1365 cm^{-1} was considered mixed, since it was not identified among the characteristic crystalline or amorphous bands of isotactic polypropylene[48].

The absorbances were obtained by the baseline density method,[53] a technique used to reduce losses resulting from reflection, scattering and background absorption of other components.

The resolution was done by drawing a line XY (see fig. 11) tangentially between the absorbance minima (transmission maxima) occuring on either side of the band. An ordinate FHG is drawn parallel to the ordinate axis to pass through "H" (frequency absorption maximum) cutting "XY" at G. Thus the absorbance for this frequency is given by:

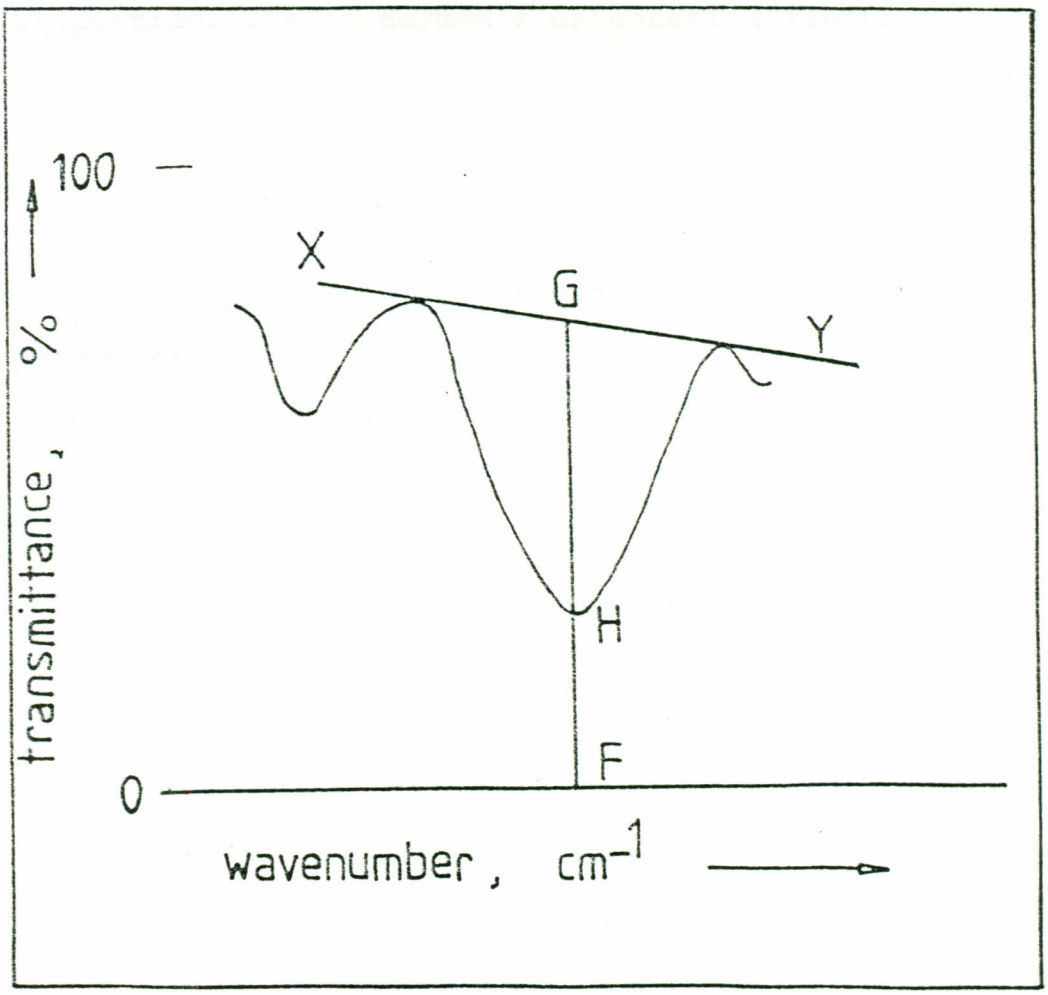

FIG: 11 Resolution by baseline-density method.

$$A = \log (FG/GH) \qquad \ldots.(16)$$

The dichroic ratio, D can then be computed from the definition in equation (3). Samples indicating the frequency 1365 cm^{-1} for horizontal and vertical positions of film are given in figs. 30 and 31. The quantity $\frac{D-1}{D+2}$, where the vertical lines refer to modulus was computed and considered as the "orientation function", because of its proportionality to Herman's orientation function,

$$f = \frac{3\langle\cos^2\theta\rangle - 1}{2}$$

where $\langle\cos^2\theta\rangle$ is the orientation parameter.

CHAPTER 4

RESULTS

4.0 INTRODUCTION

The various measurements made using the methods described in the preceeding Chapter are outlined below.

(i) Birefringence of all specimens annealed before and after stretch.

(ii) Crystallinity of the specimens annealed before stretch

(iii) Bragg spacing calculations, made from diffractograms and the DS-camera films.

(iv) Infrared dichroism measurements.

A list of figures and tables depicting measurements made in this study is furnished in the pages (i) to (vi)

The results obtained have been arranged as follows:

4.1 BIREFRINGENCE

The tables and graphs relating to birefringence are described as shown below:

(i) Table 1 provides information on the effect of re-stretch on birefringence.

(ii) Table 2 and figure 12 display the variation of birefringence with thickness at a constant extension of 25%.

(iii) Table 3 and figure 13 indicate the variation of birefringence with extension within the thickness range of specimens of 0.085-0.095 mm.

(iv) Tables 4 and 5, and the figures 14 and 15 show the effects of annealing time on birefringence of the stretched specimens.

(v) The effects of annealing specimens for various times before stretching (pre-stretch annealing) are respresented in tables 6 to 12 and figures 16 to 22.

(vi) Table 13 and figure 25 shows the variation of birefringence with pre-stretch annealing time for various extension ratios (or draw ratios).

(vii) Table 14 and figure 32 give the variation of birefringence with extension for the specimens used in infrared dichroism.

(viii) Figures 23 and 24 show superimposed graphs of various pre-stretch annealing periods.

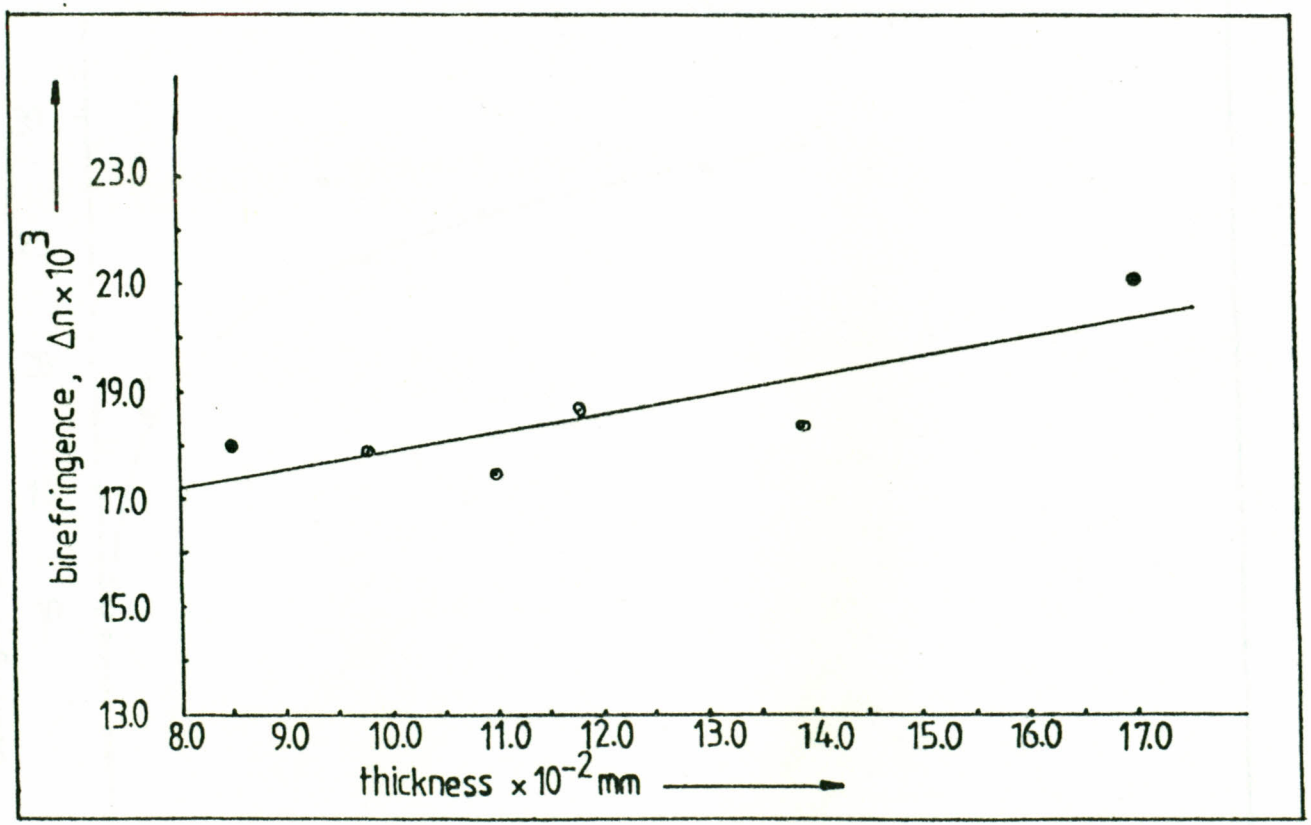

Fig. 12. Variation of birefringence with film thickness for film of 25% extension.

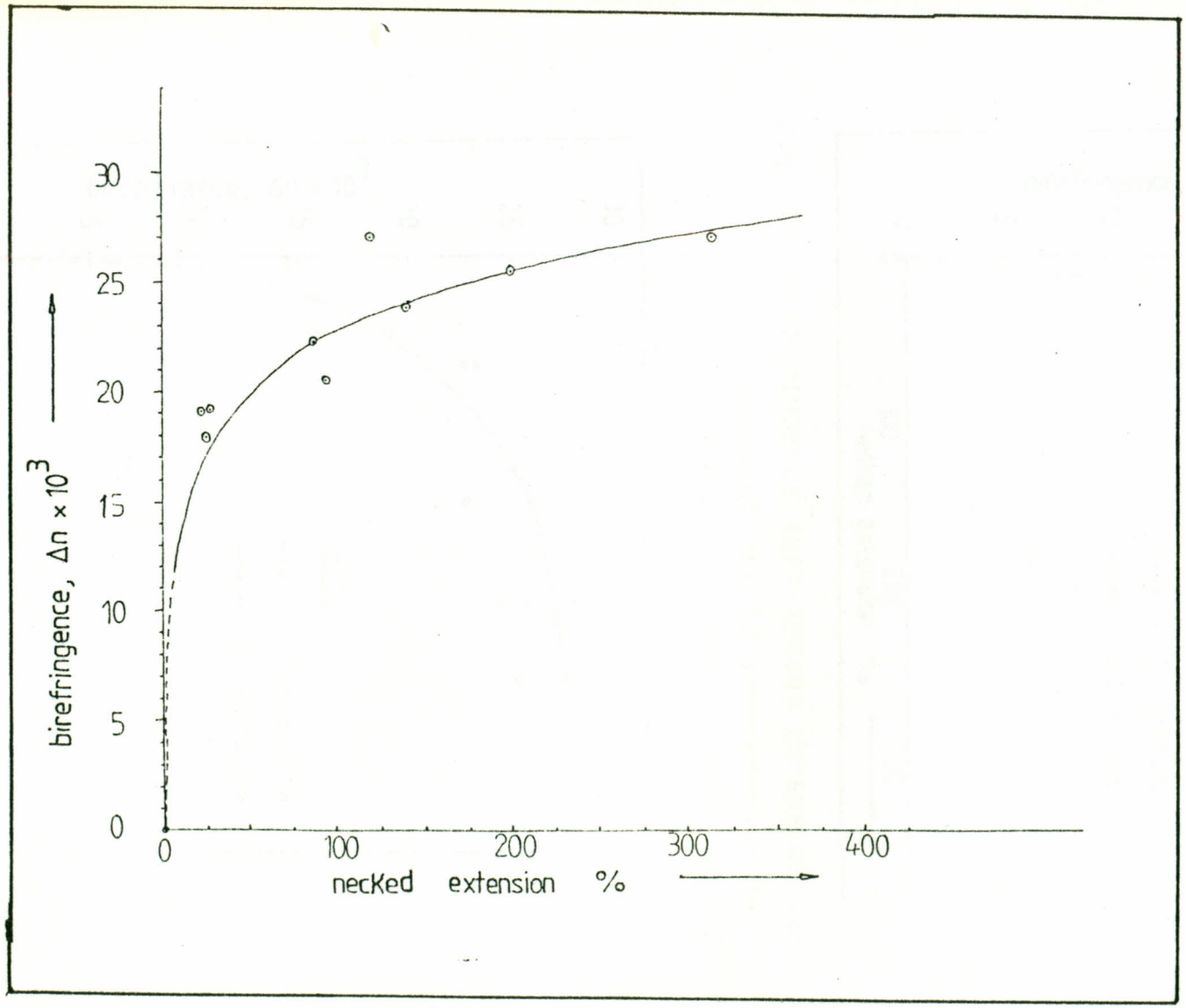

Fig. 13. Variation of birefringence with extension. Thickness range of specimens=0.085÷0.095mm

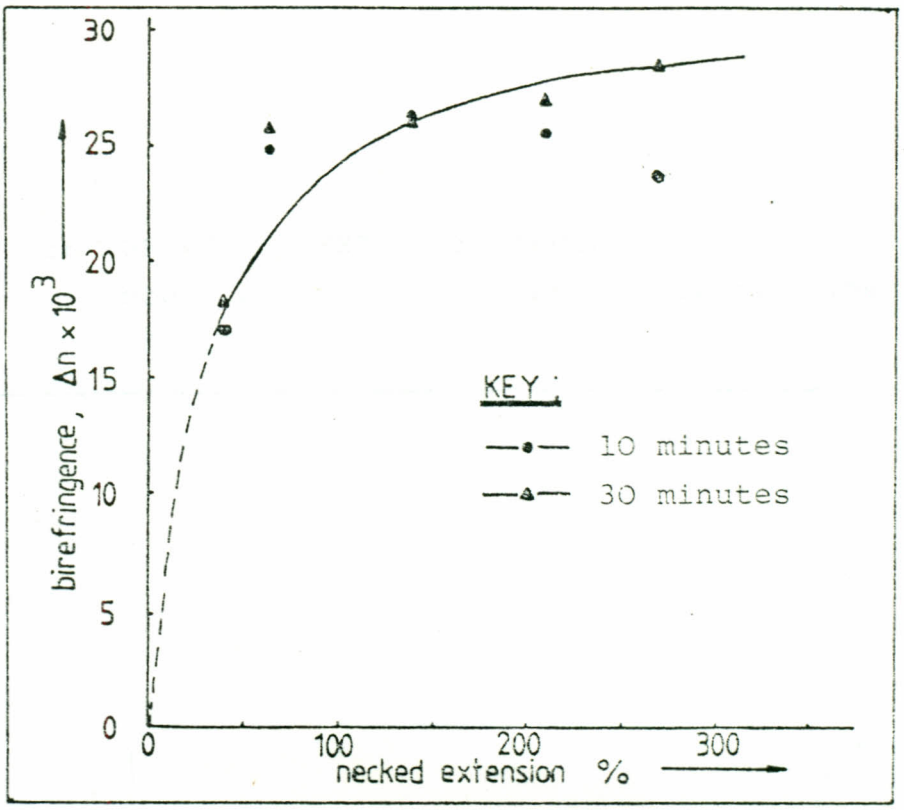

Fig. 14. BIREFRINGENCE (BF) VERSUS EXTENSION (EXT.) for films annealed for 10 (——•——), then 30 minutes (——▲——) after stretch at 115 °C.

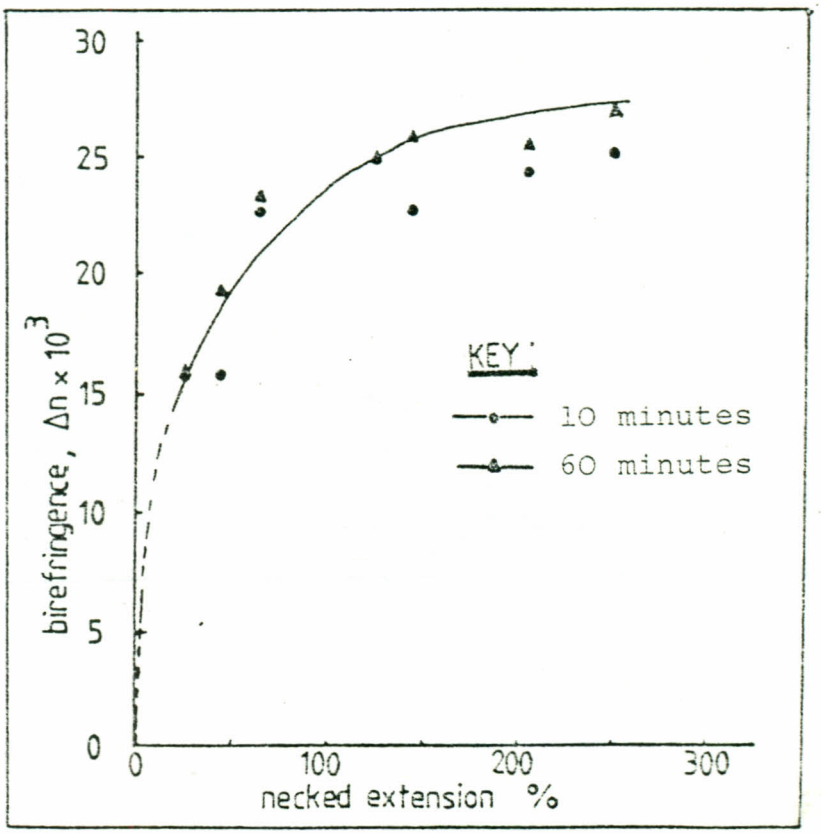

Fig. 15 BF VERSUS EXT. for films annealed for 10 (——•——), then 60 minutes (——▲——) after stretch at 115 °C.

Fig. 16 BF VERSUS EXT. for specimens annealed for $1\frac{1}{4}$ hours before stretch at annealing temperature of 115 °C.

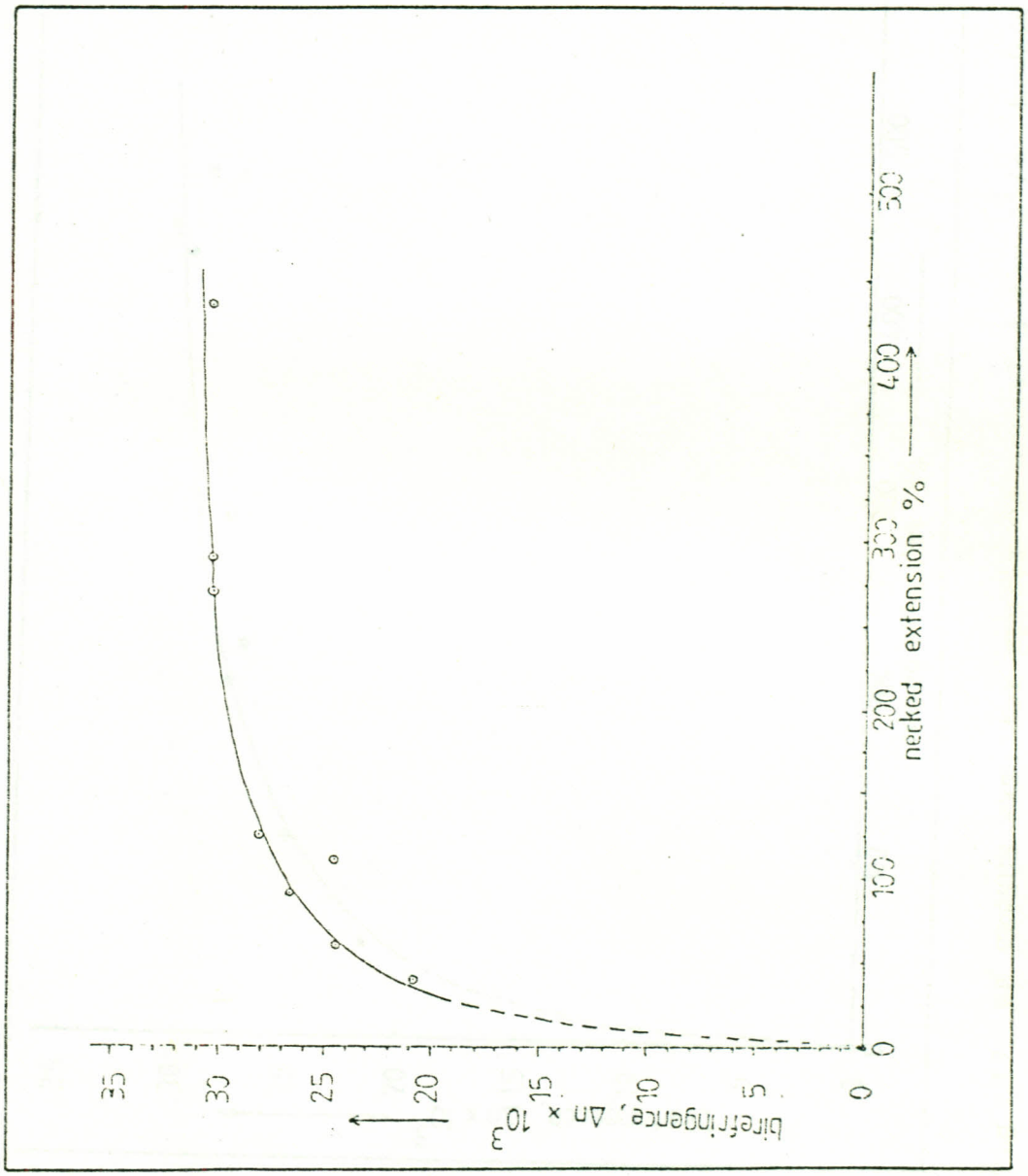

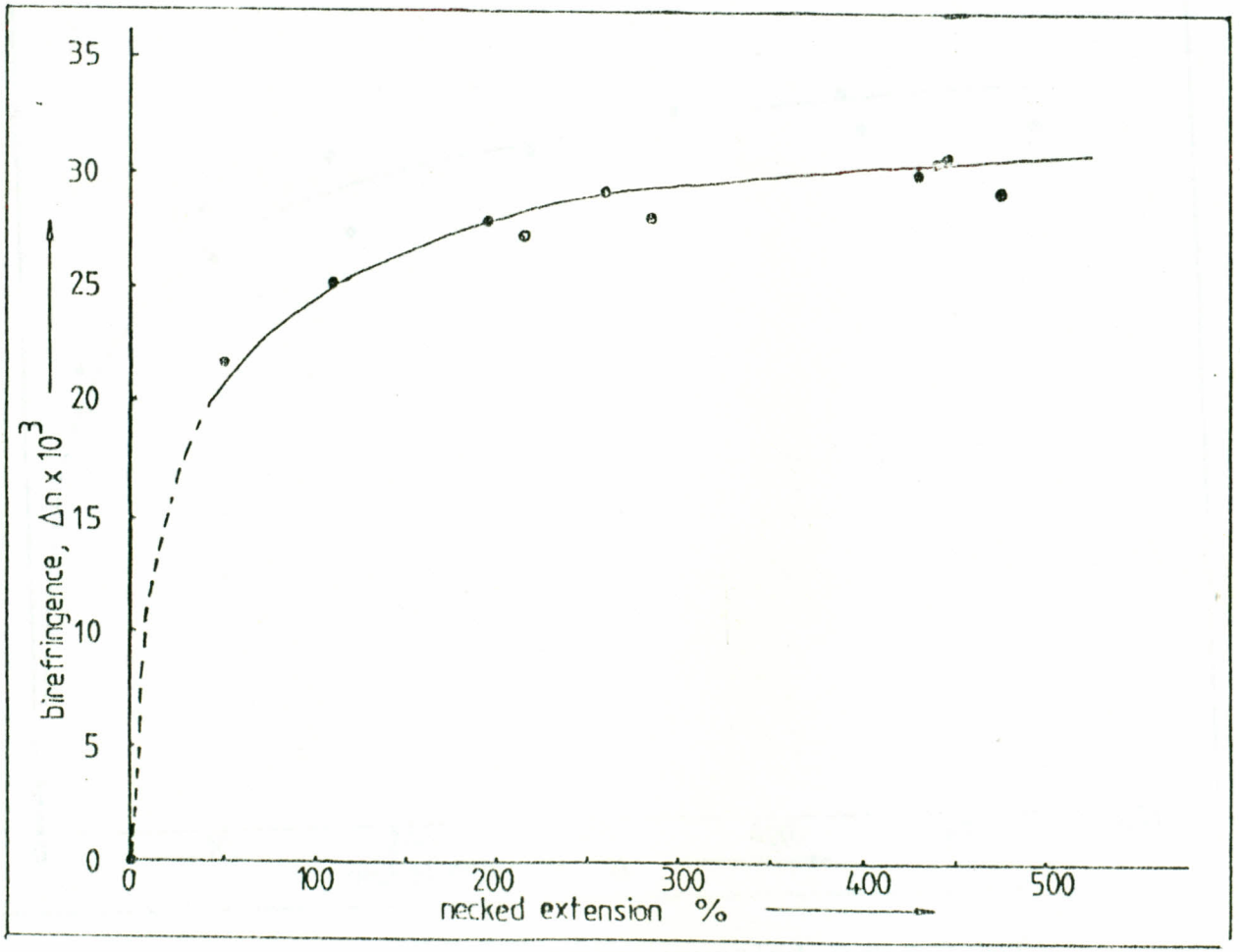

Fig. 17 BF VERSUS EXT. for specimens annealed for $2^{1}/4$ hours before stretch at annealing temperature of 115 °C.

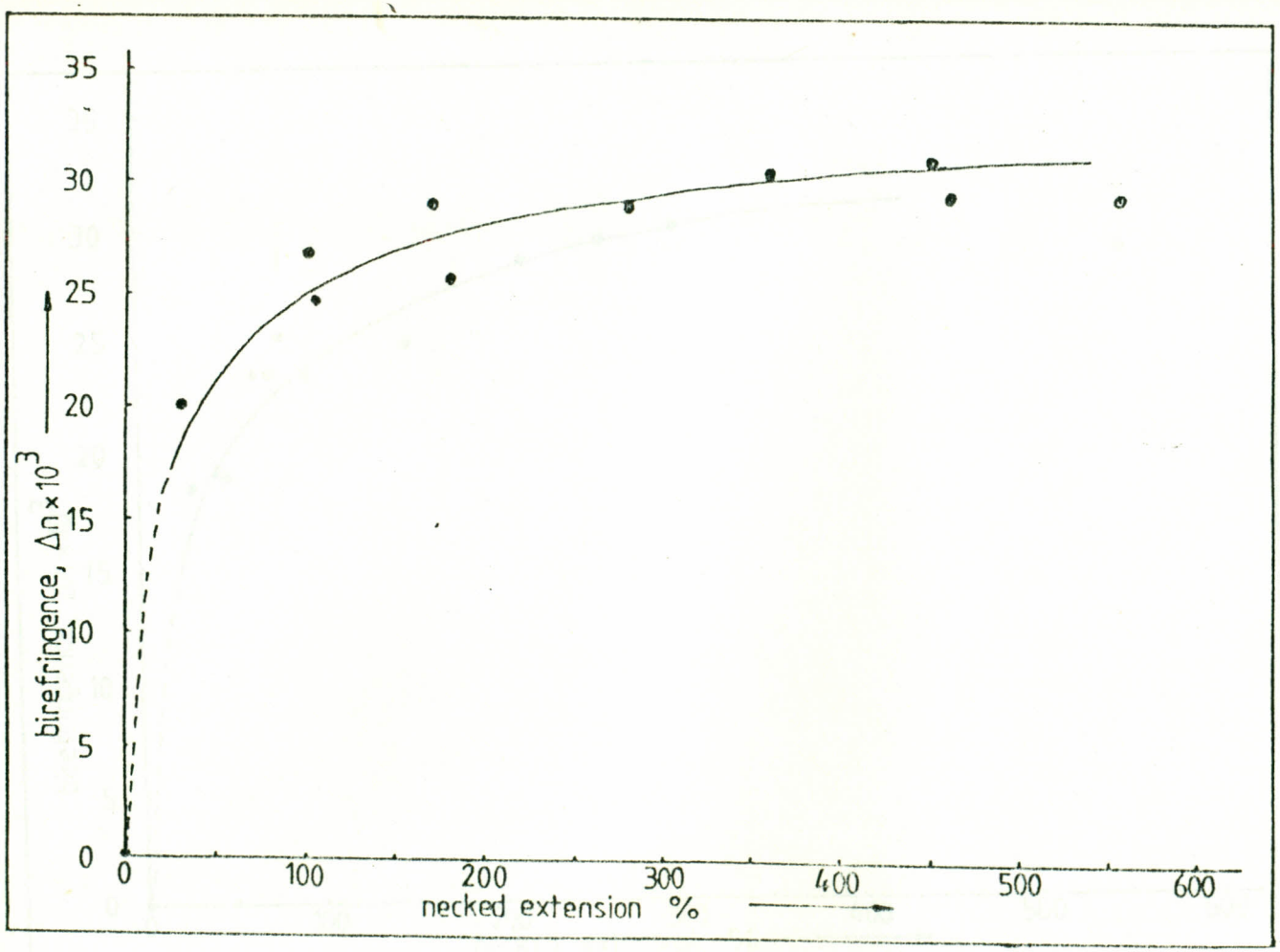

Fig. 18 BF VEPSUS EXT. for specimens annealed for 3 hours before stretch at annealing temperature of 115 °C.

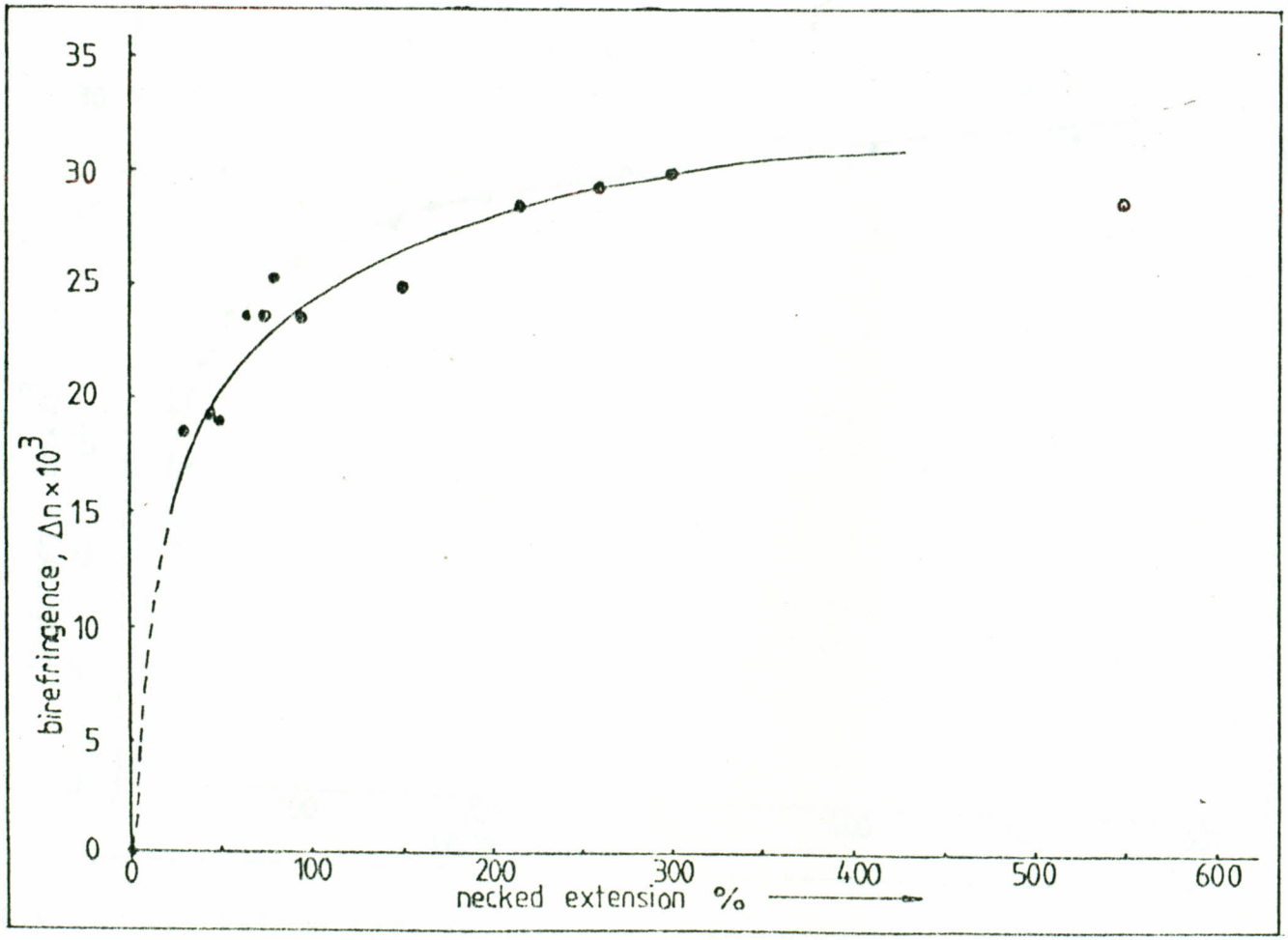

Fig. 19 BF VERSUS EXT. for specimens annealed for 6 hours before stretch at annealing temperature of 115°C.

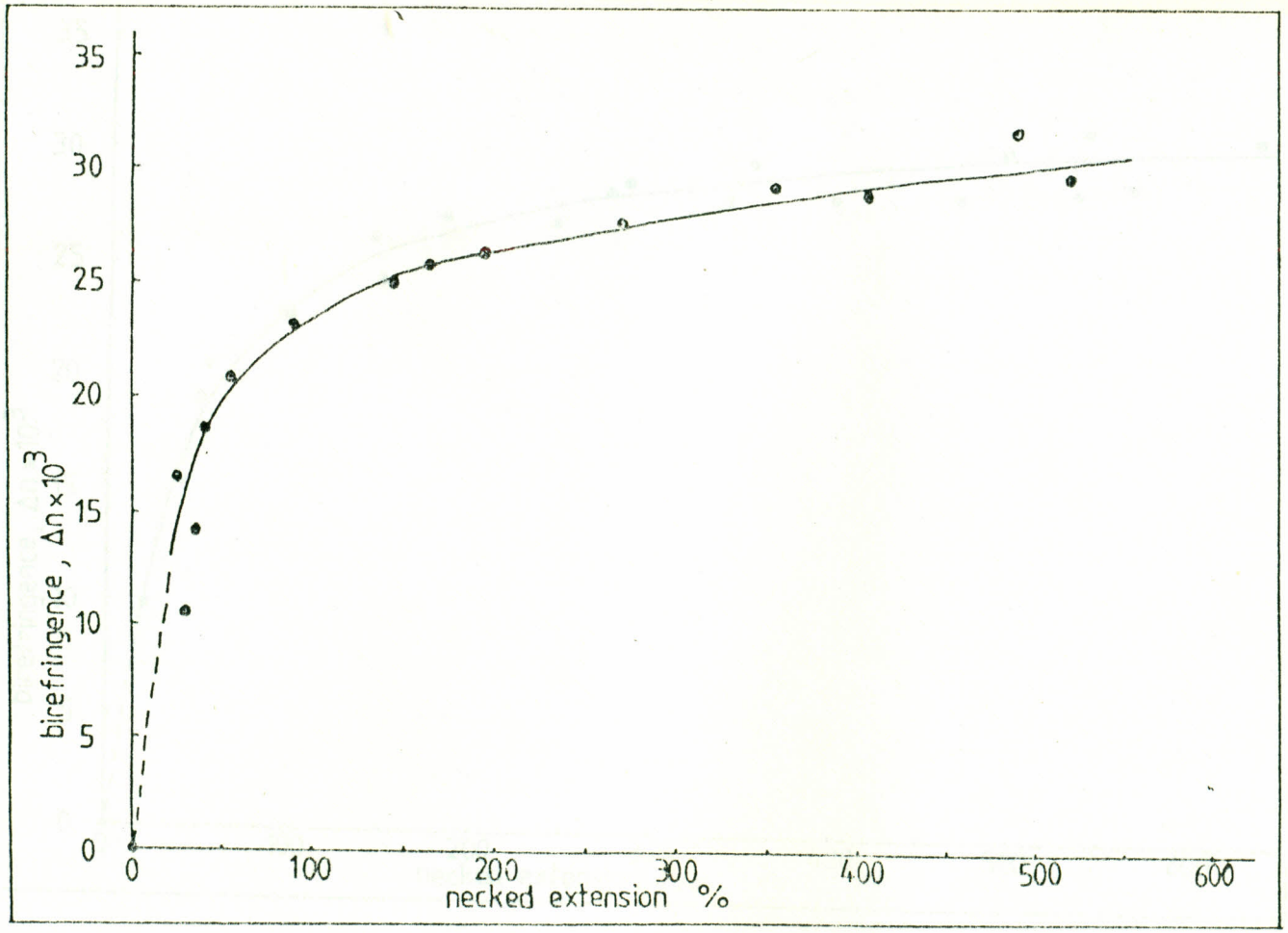

Fig. 20 BF VERSUS EXT. for specimens annealed for 22 hours before stretch at annealing temperature of 115°C.

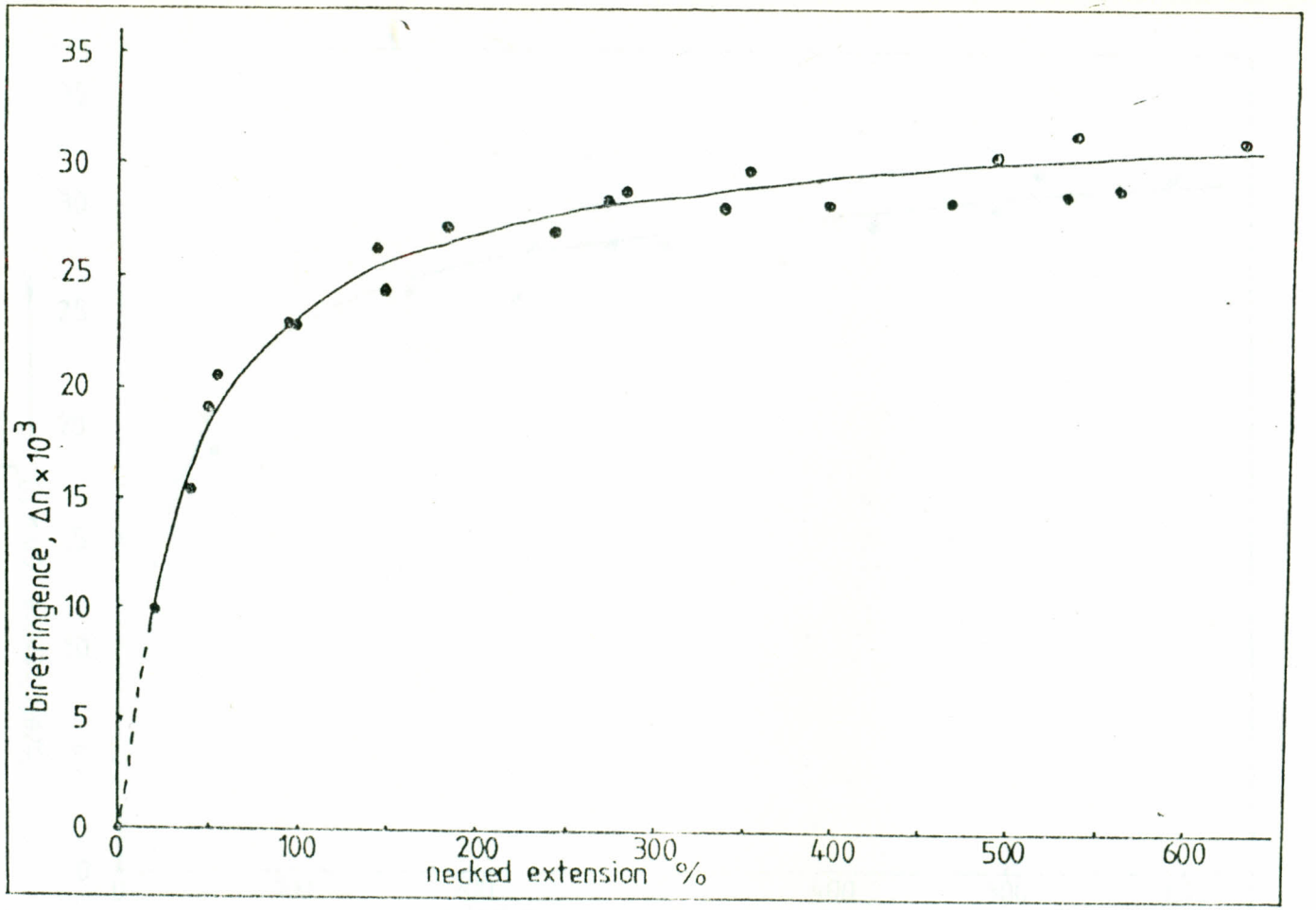

Fig. 21 BF VERSUS EXT. for specimens annealed for $47^2/3$ hours before stretch at annealing temperature of 115 °C.

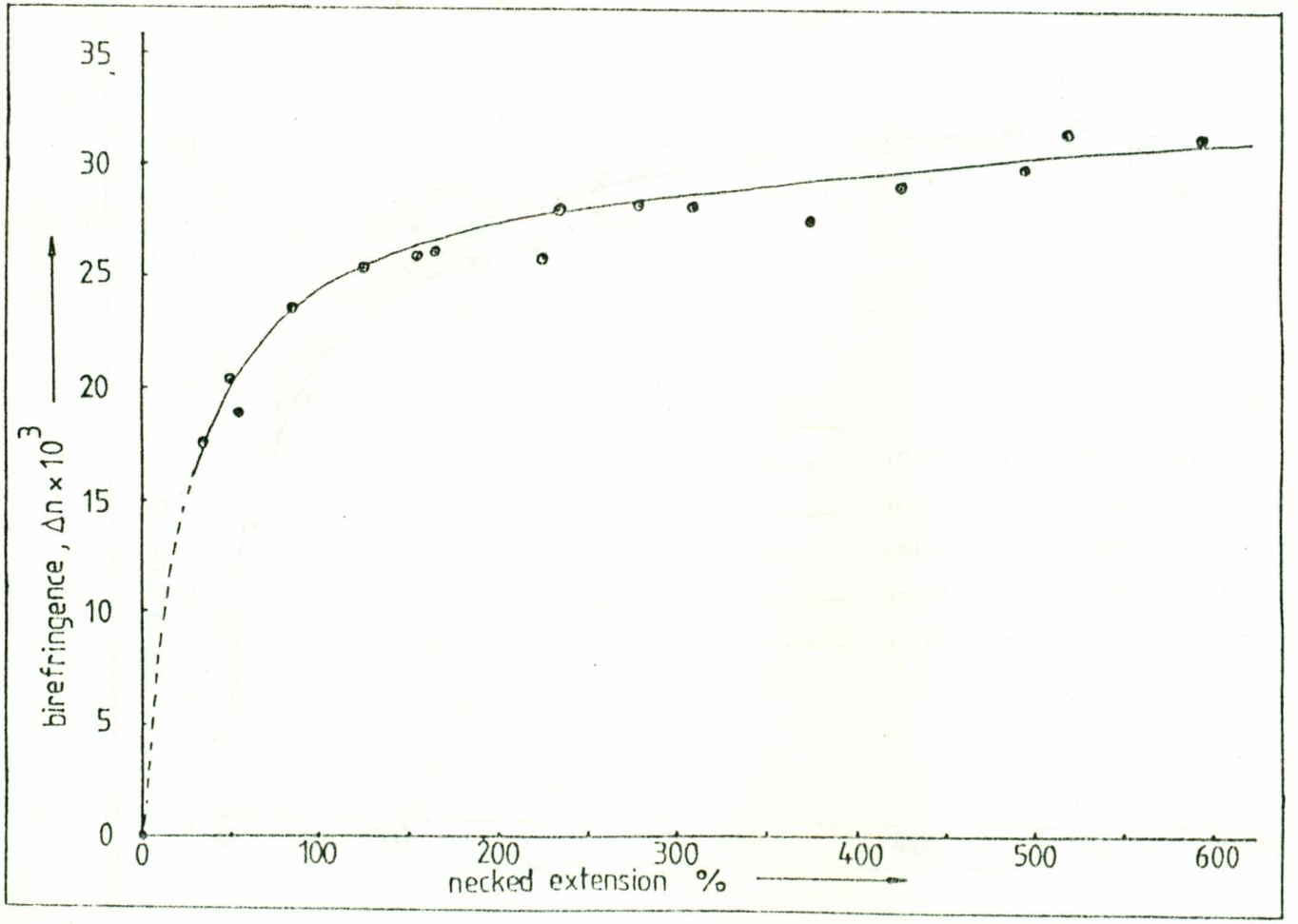

Fig. 22 BF VERSUS EXT. for specimens annealed for 72 hours before stretch at annealing temperature of 115 °C.

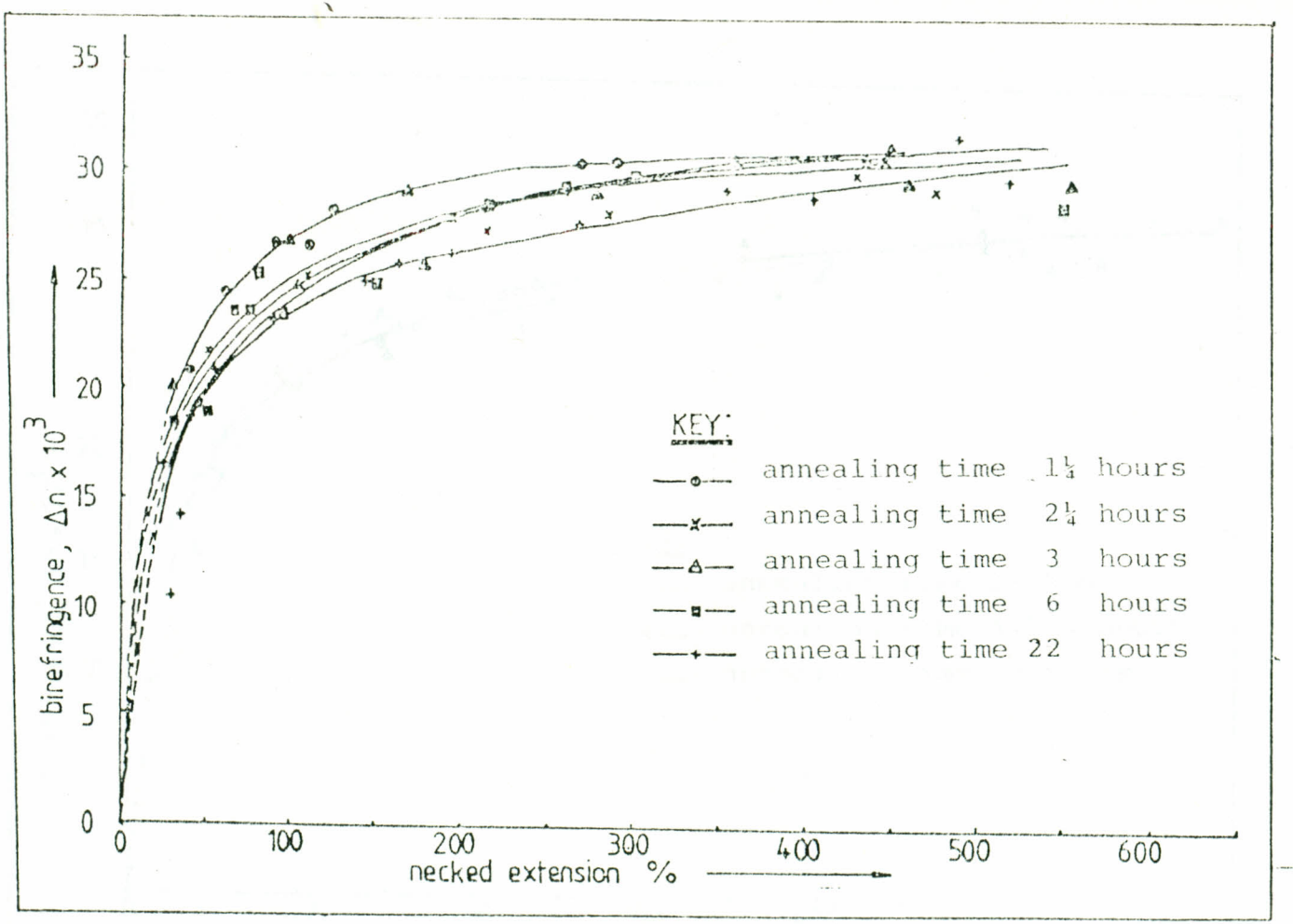

Fig. 23 BF Versus EXT. for specimens annealed for $1^{1}/4$, $2^{1}/4$, 3, 6, 22 hours before stretch at annealing temperature of 115°C.

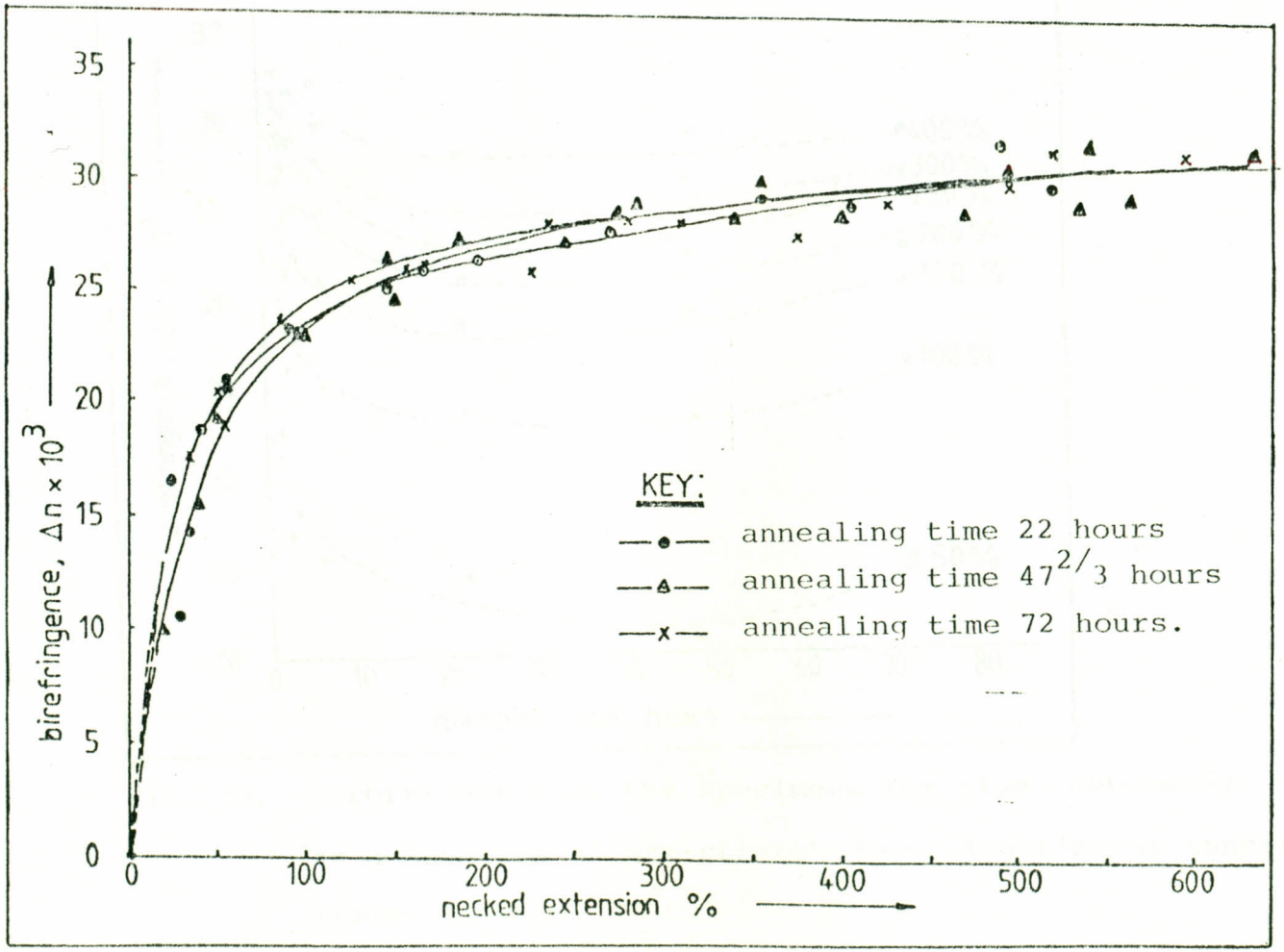

Fig. 24 BF versus EXT. for specimens annealed for 22, $47^{2}/3$ and 72 hours before stretch at annealing temperature of 115°C.

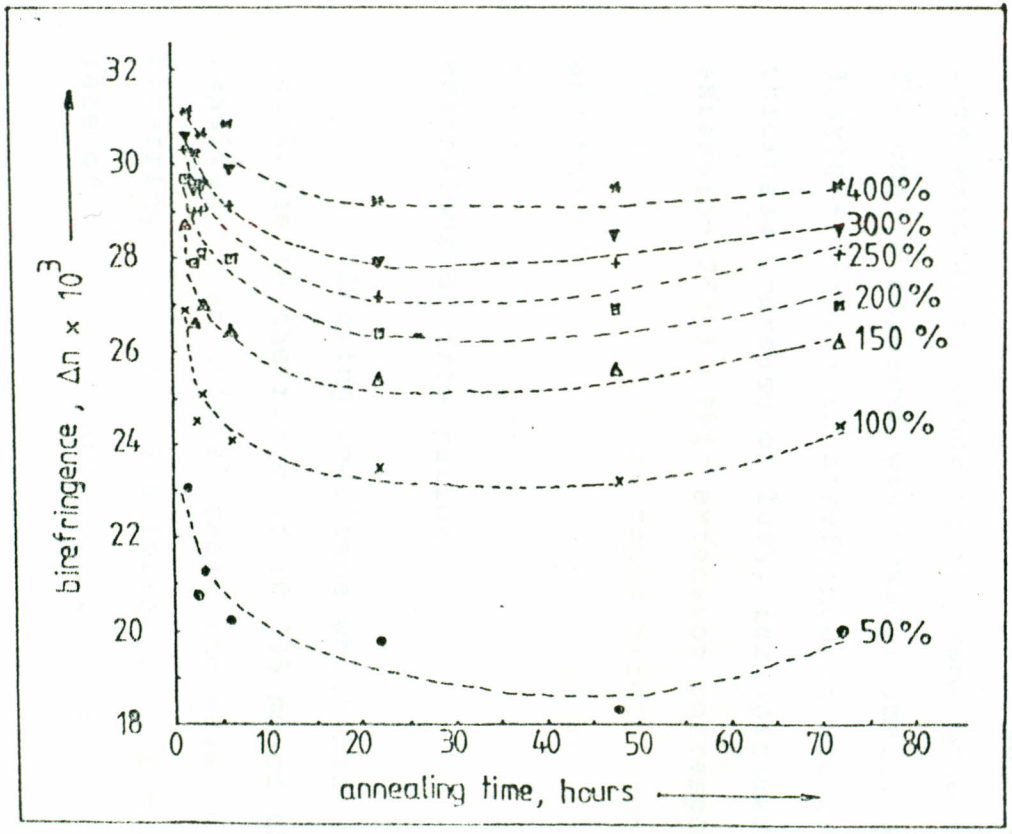

Fig. 25. Birefringence of the specimens for given extensions as a function of pre-stretch annealing time at annealing temperature of 115 °C.

Most of the re-stretched specimens showed that birefringence increases with re-stretch (table 1). It was observed that the birefringence increased nearly linearly with specimen thickness for a given extension (table 2, fig. 12). It would have been expected from theory that the birefringence remain constant for the same extension, assuming the same molecular orientation. The change observed was however small; an increase of 3.4×10^{-2} or 21% in birefringence was caused by a thickness increase of 100%, for specimens of necked extension 25%.) This extension corresponded to one of the regions of most rapid birefringence increase, and therefore indicated less changes in birefringence for thickness variations corresponding to other extensions or draw ratios.

Drawing specimens which had a controlled thickness in the range of ±0.005 mm of the mean value resulted in an initial rapid increase in birefringence upto 100% followed by a much reduced rate of increase (table 3, fig. 13).

Specimens that had been stretched earlier were annealed first for 10 minutes and then for 30 and 60 minutes. (Post stretch annealing). There was an observed increase in birefringence although small. Extensions from 0 to about 250%

were considered, and in this region birefringence was a rising function of extension.

The sets of specimens that had been annealed for various periods before stretch (pre-stretch annealing) yielded trends (tables 6-12, figs 16-22) similar to that observed for fig. 15. There was an initial rapid rise in the value of birefringence with extension upto 100%, after which there was a substantial decrease in the rate of increase and the curve appeared to approach a limiting experimental value in the neighbourhood of 31×10^{-3} (figs. 16-22).

The various graphs of pre-stretch annealed specimens were superimposed for comparative purposes (figs. 23-24). By considering specimens pre-stretch annealed for $1^{1}/4$, $2^{1}/4$, 3, 6, and 22 hours (fig. 23) it was observed that below 200% (approximately) the value of birefringence tended to lower with longer pre-stretch annealing periods, for a given extension percent. Beyond 22 hours this trend changed as birefringence slightly rose for the 47 and 72 hours respectively (Fig. 24). Graphs were deduced from the superimposed curves (fig.25) and these gave a clearer picture of how birefringence varied with annealing times for a number of fixed extensions. From the graphs (table 13, fig. 25)

it can be inferred that the decrease in birefringence with annealing time is highest at low extensions, and as the extension gets higher the birefringence values narrow down to an almost common value for a given extension.

The trend of variation of birefringence with extension for the specimens used in infrared dichroism (table 14, fig. 32) was similar to that observed in the above specimens (figs. 13, 16-22) but the limiting birefringence was noted to be about 26×10^{-3}, for 500% extension. This was attributed to the width of the gauge length of the unstretched specimens of 10 mm at the narrowest section, as compared to 3 mm at the narrowest section for the specimens used in figs. 12, 16-22. The justification for difference in widths was given in Chapter 3 page 25.

4.2 WIDE-ANGLE X-RAY DIFFRACTION

The X-ray diffractograms that were obtained from specimens annealed before stretch provided information on the state of crystallinity as well as on the Bragg spacing. Below are the obtained tables and figures.

(i) Table 15 and figure 26 display the variation of crystallinity with annealing time.

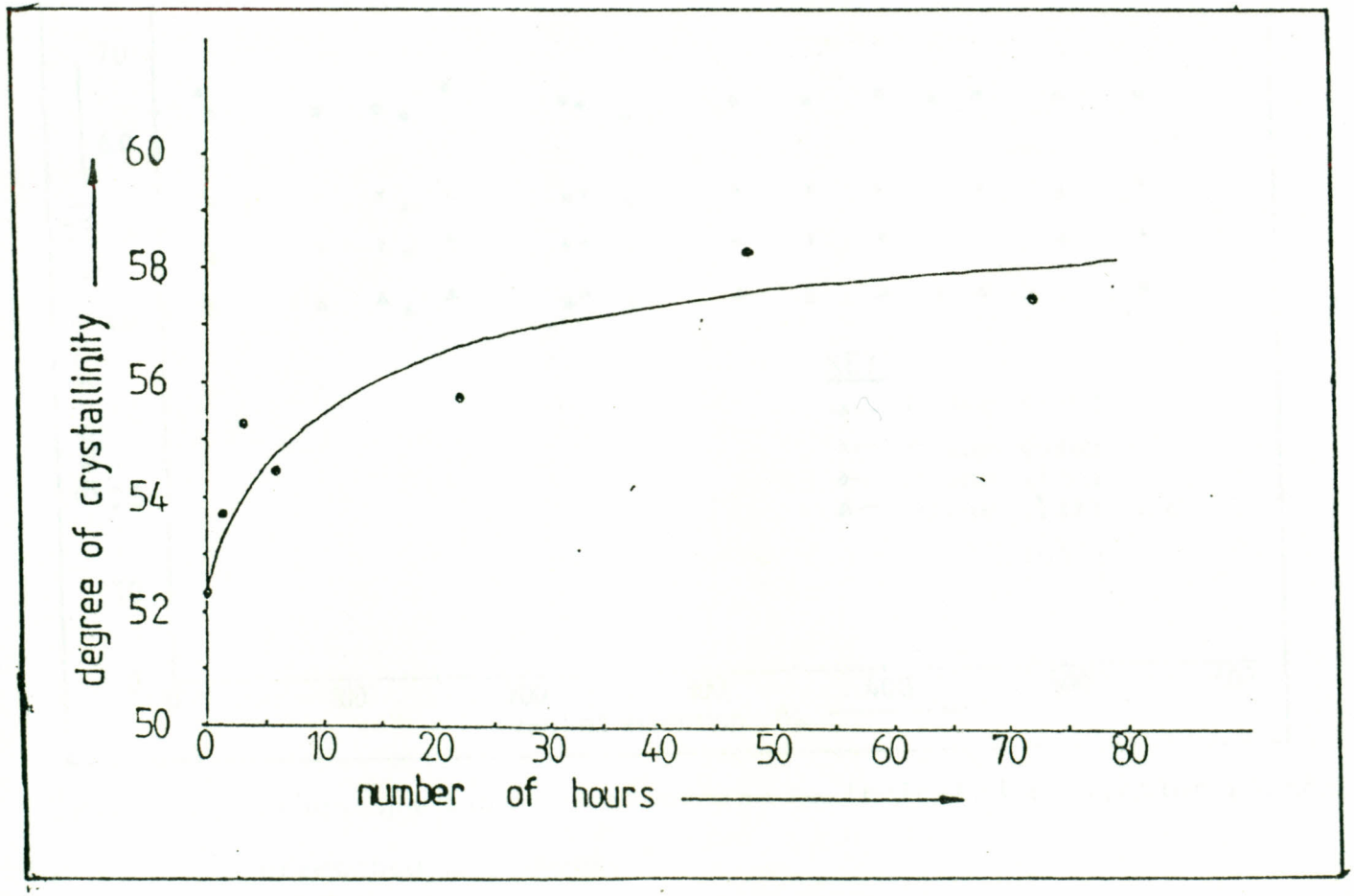

Fig. 26. Variation of crystallinity with annealing time.

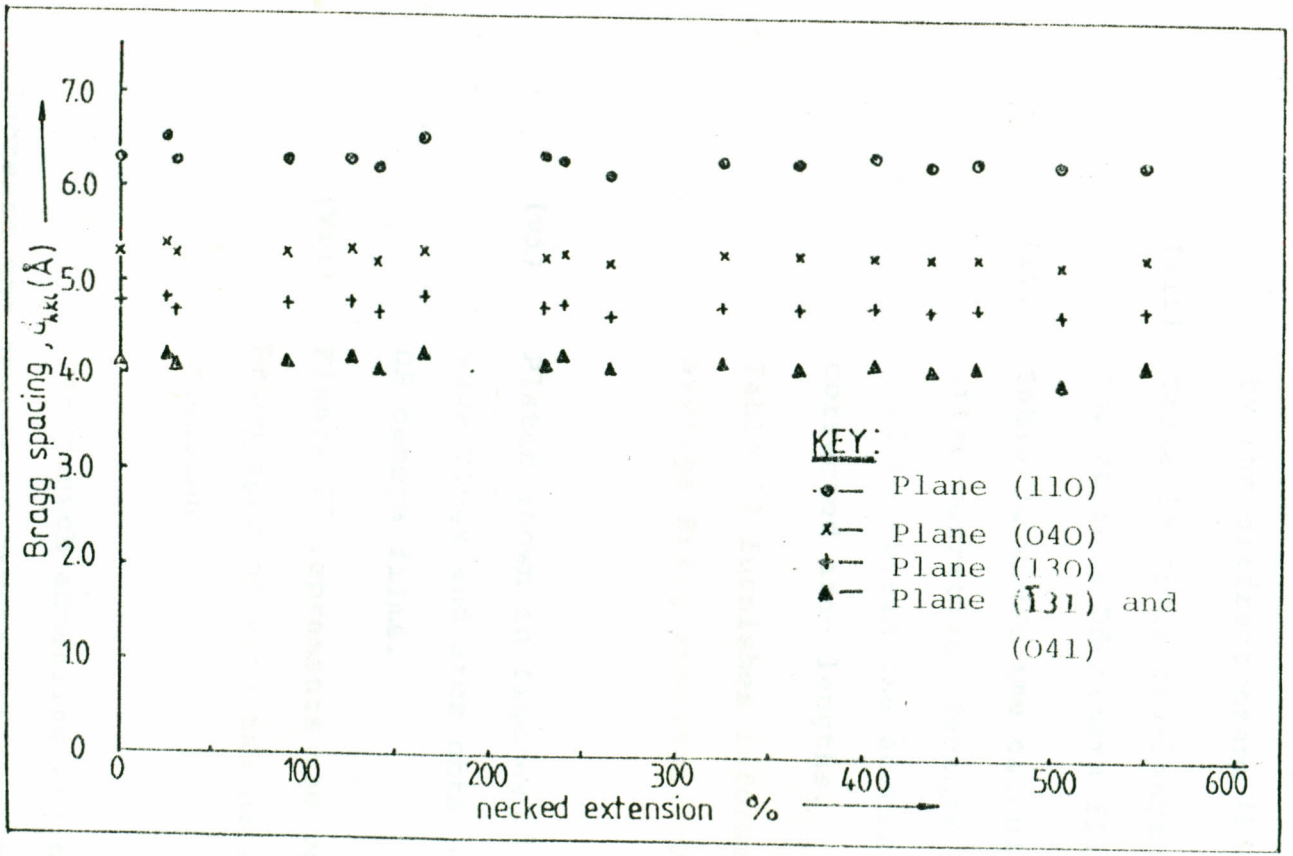

Fig. 27. Bragg Spacings corresponding to indicated reflection planes for stretched specimens.

(ii) Table 16 shows Bragg spacings as a function of annealing time, as given by the diffractograms (Figs. 36 - 42).

(iii) Table 19 gives arc-length measurements for various DS-camera films.

(iv) Table 20 gives the calculated d-spacings, after correction factors have been used to obtain the accurate or corrected arc- lengths.

(v) Table 17 furnishes information on the average Bragg spacings, calculated from table 20.

(vi) Plates shown in figures 28 a, b, c, d show rings and arcs obtained from DS camera films.

(vii) Figure 27 represents the variation of Bragg spacing with the necked extension.

Pre-stretch annealing was observed to increase the degree of crystallinity. The initial rise in crystallinity was rather steep and then levelled off as the time became longer. The shape of the graph was inverse tangential or logarithmic. (table 15, fig. 26).

There was a tendency of the 2θ values to rise with longer annealing periods, an indication of decrease in Bragg spacings (table 16).

The Debye-Scherrer (DS) camera method was used to record changes in the crystalline reflection planes of a number of stretched specimens. The small size of these specimens rendered them unsuitable for examination by the diffractometer. The DS camera photographs showed a ring structure for the unstretched specimens and a breaking of the ring structure into arcs as the extension was increased. The rings and arcs located on the films were identified as (110), (040) (130) and the overlap of $(\bar{1}31)$ and (041) (refs. 6 ; 54, 55, 56 .)

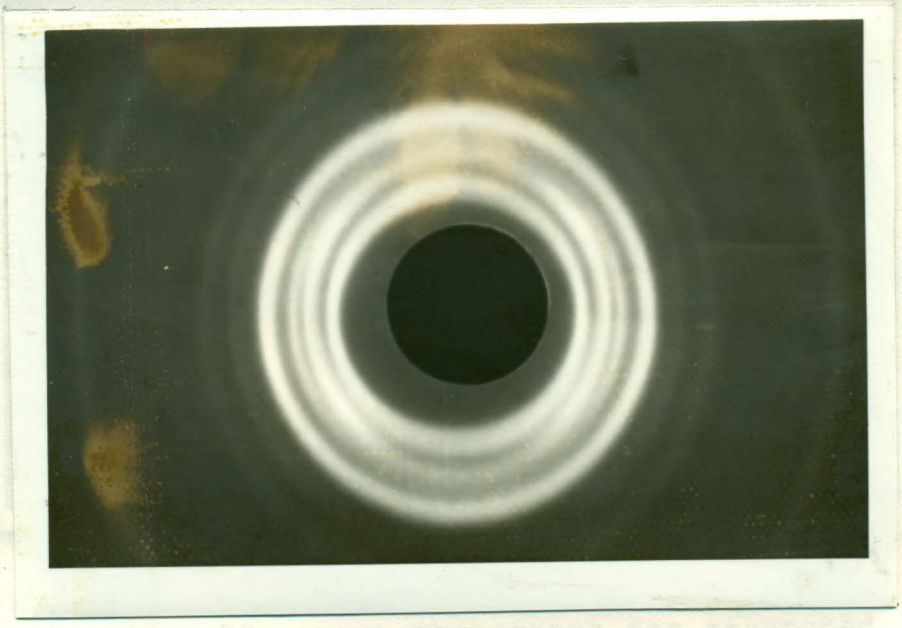

FIG. 28a. DS Camera photograph for unstretched specimen; draw ratio=1

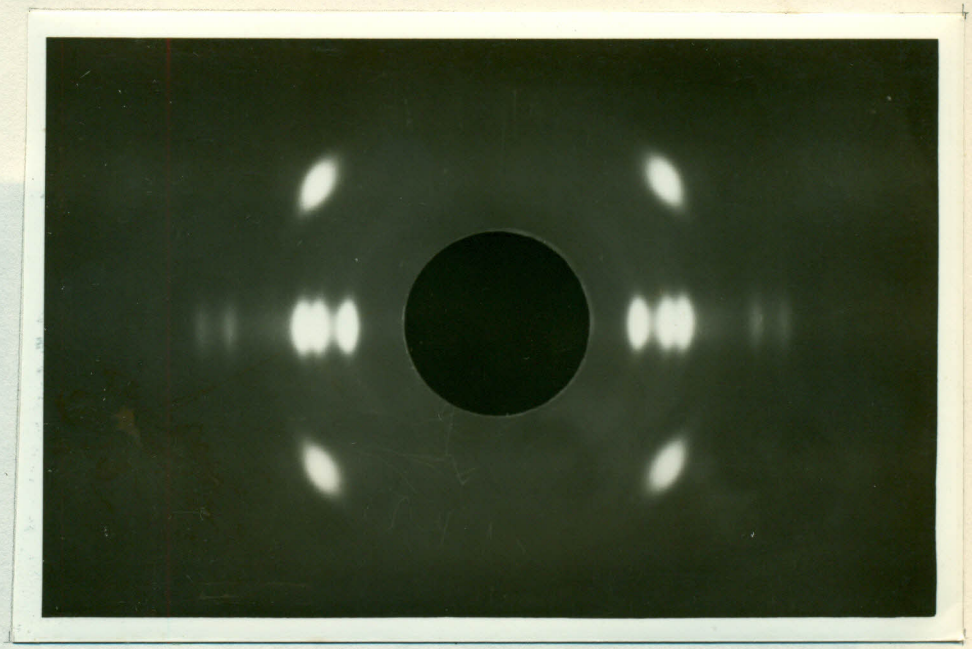

Fig. 28b. DS Camera photograph for stretched specimen; draw ratio = 2.25

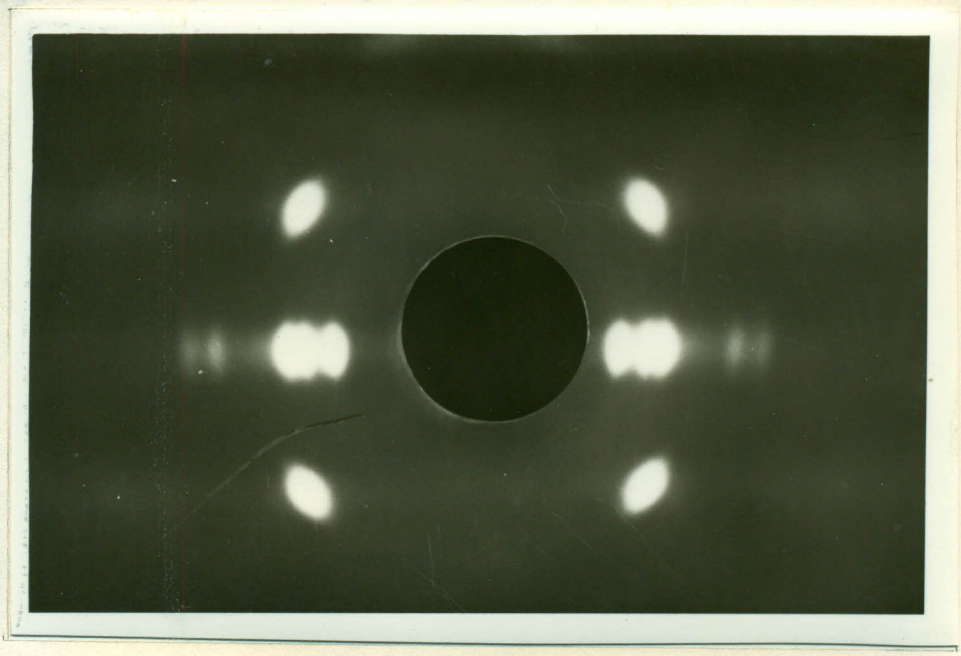

Fig. 28c DS camera photograph for stretched specimen; draw ratio = 3.4

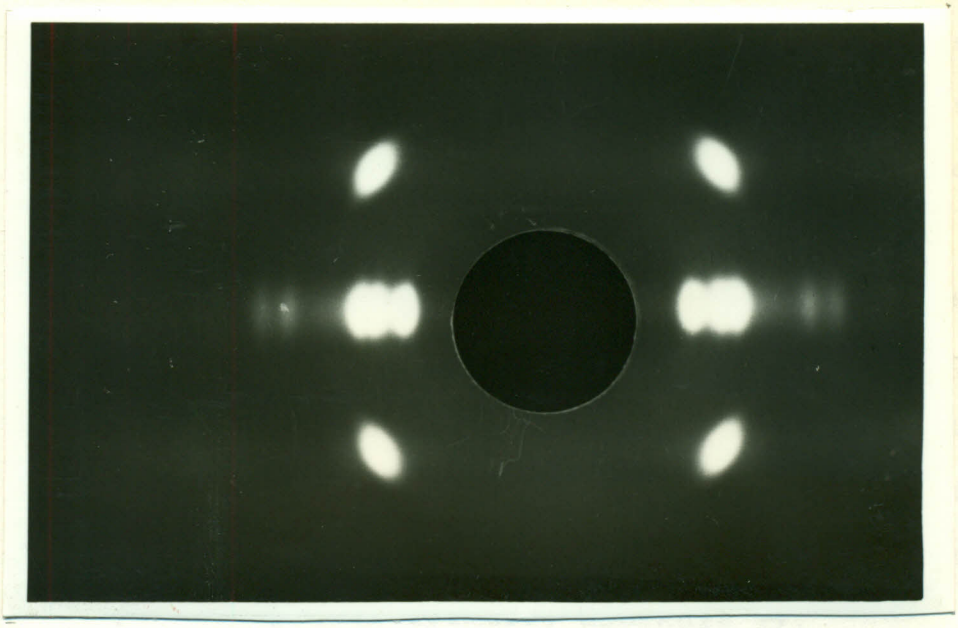

Fig. 28d. DS Camera photograph for stretched specimen, draw ratio = 4.25

On examining the Bragg spacings calculated from the oriented specimens (table 17, 19 and 20 and fig. 27) it was noted that there was an initial fluctuation of the values, but these values became steady as the orientation approached higher values. There was a general but slight decrease in the spacings for the various planes with increasing extension (or draw ratio). Assuming a linear fit, the slopes of the graphs (fig. 27 for the planes (110) (040), (130) and the doublet (131) and (041) would be -1.02, -1.05, -0.86, -1.61($\times 10^{-4}$) respectively (see formula, appendix 1).

4.3 INFRARED DICHROISM

The dichroic ratio, D, and the function $\left|\frac{D-1}{D+2}\right|$, hereby referred to as the "Orientation function" were obtained. $\left|\frac{D-1}{D+2}\right|$ was referred to as the "Orientation function", because of its proportionality to Herman's orientation function,[12,39]

$$f = \tfrac{1}{2}(3\langle\cos^2\theta\rangle - 1)$$

The figures and tables relating to infrared dichroism are:

(i) Figure 29 is an infrared scan of unstretched isotactic polypropylene used in this work, taken between the wavenumbers 4000-200 cm^{-1}.

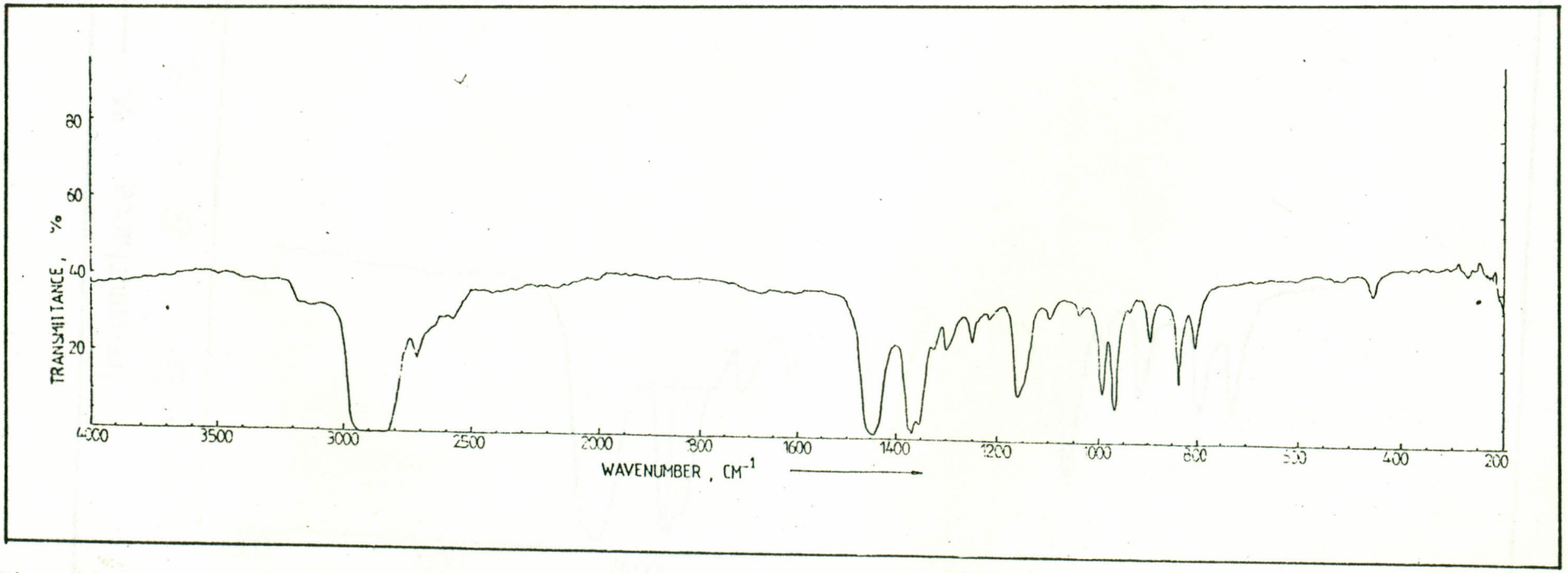

Fig. 29. Infrared scan for unoriented polypropylene (Isotactic) film.

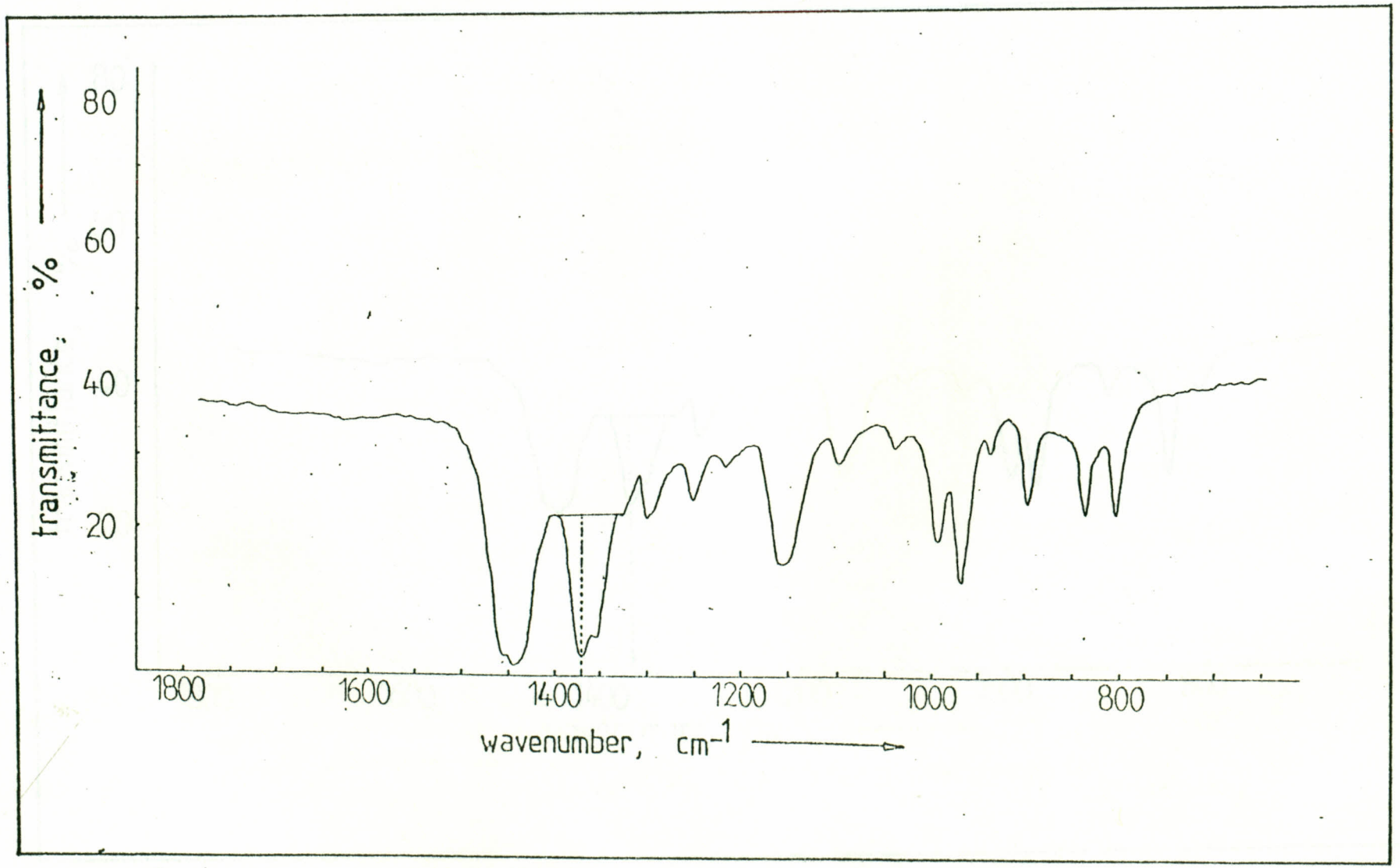

Fig. 30. Infrared scan specimen; stretch direction vertical.

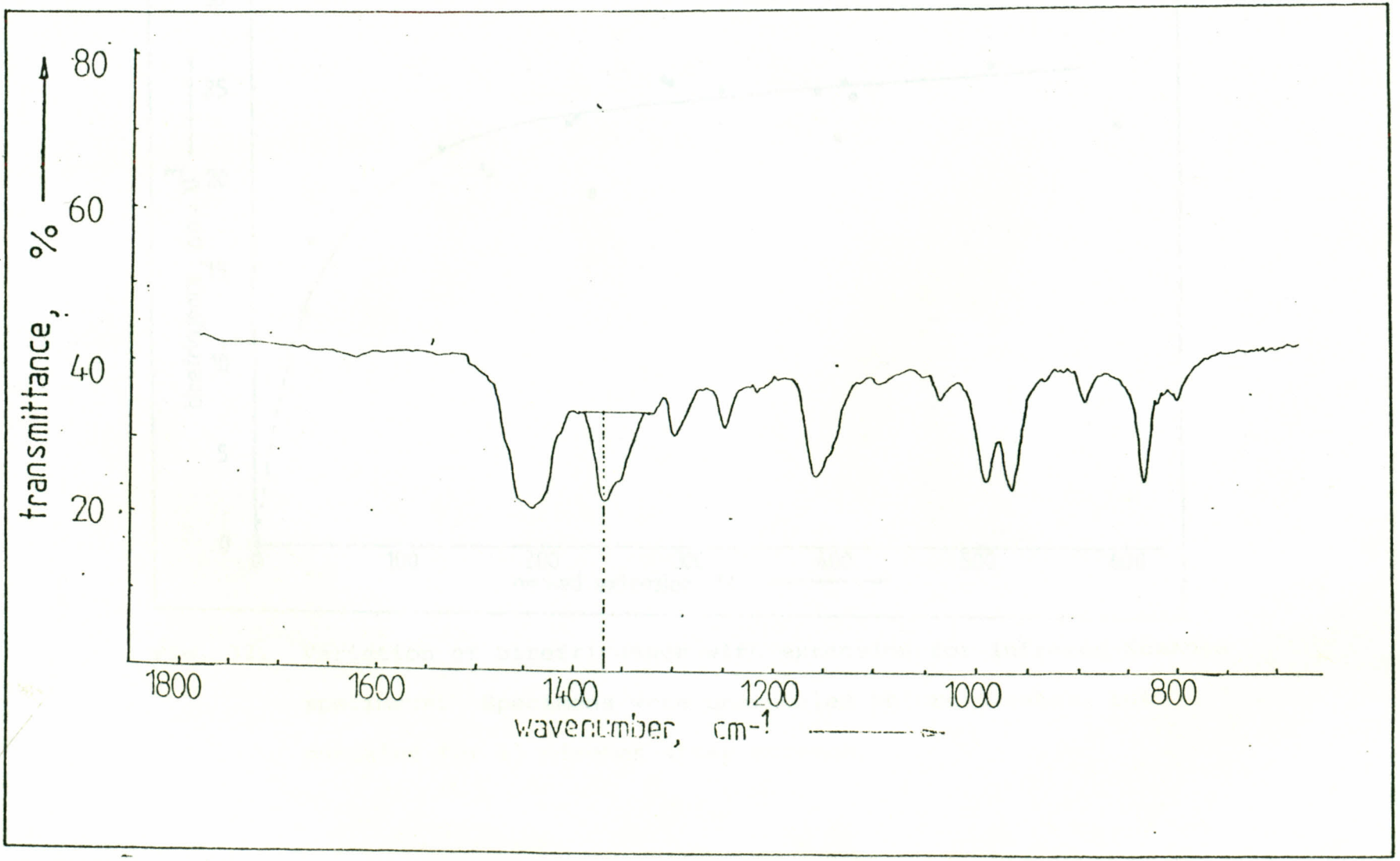

Fig. 31. Infrared scan specimen; stretch direction horizontal.

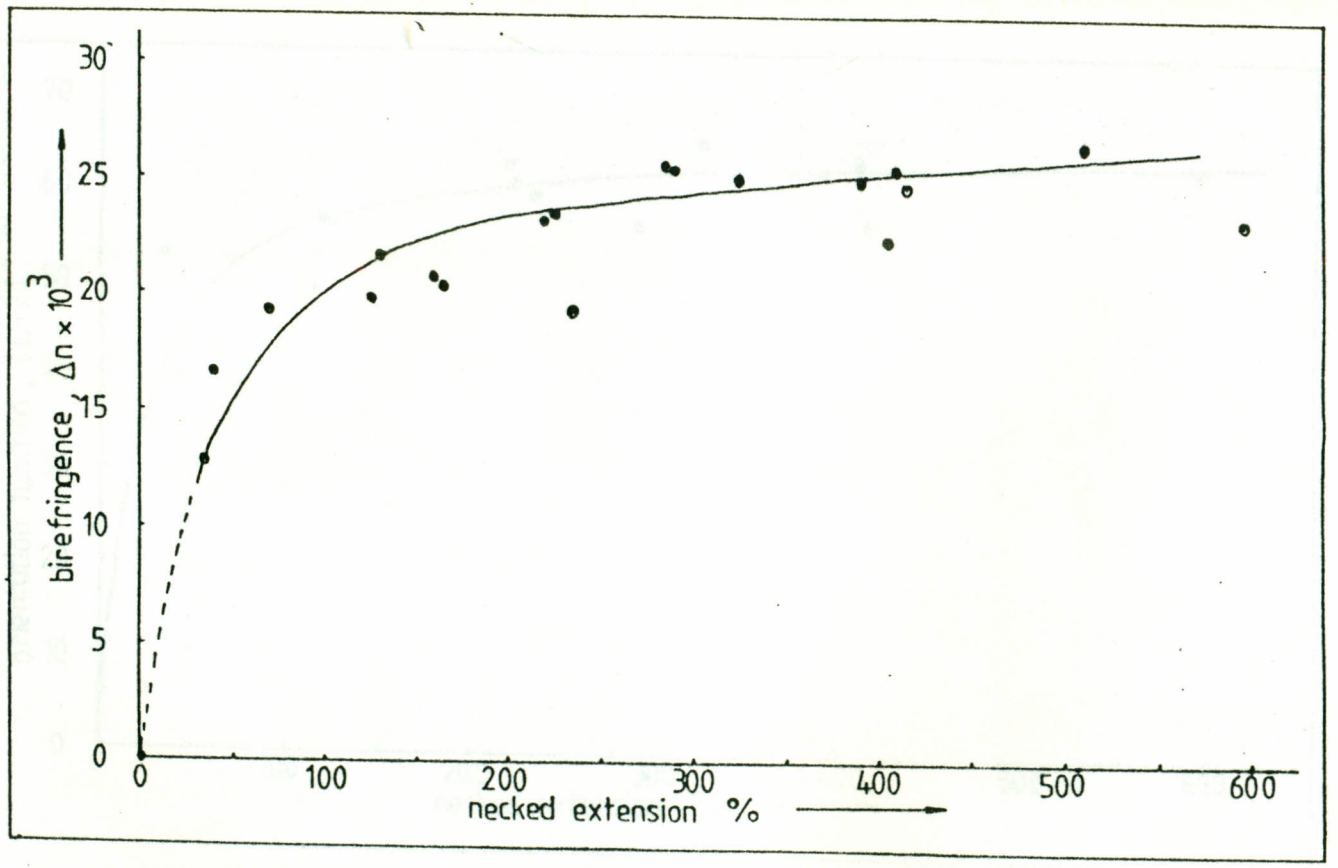

Fig. 32. Variation of birefringence with extension for Infrared-Scanned specimens. Specimens were unannealed before stretch, but annealed for 15 minutes after stretch.

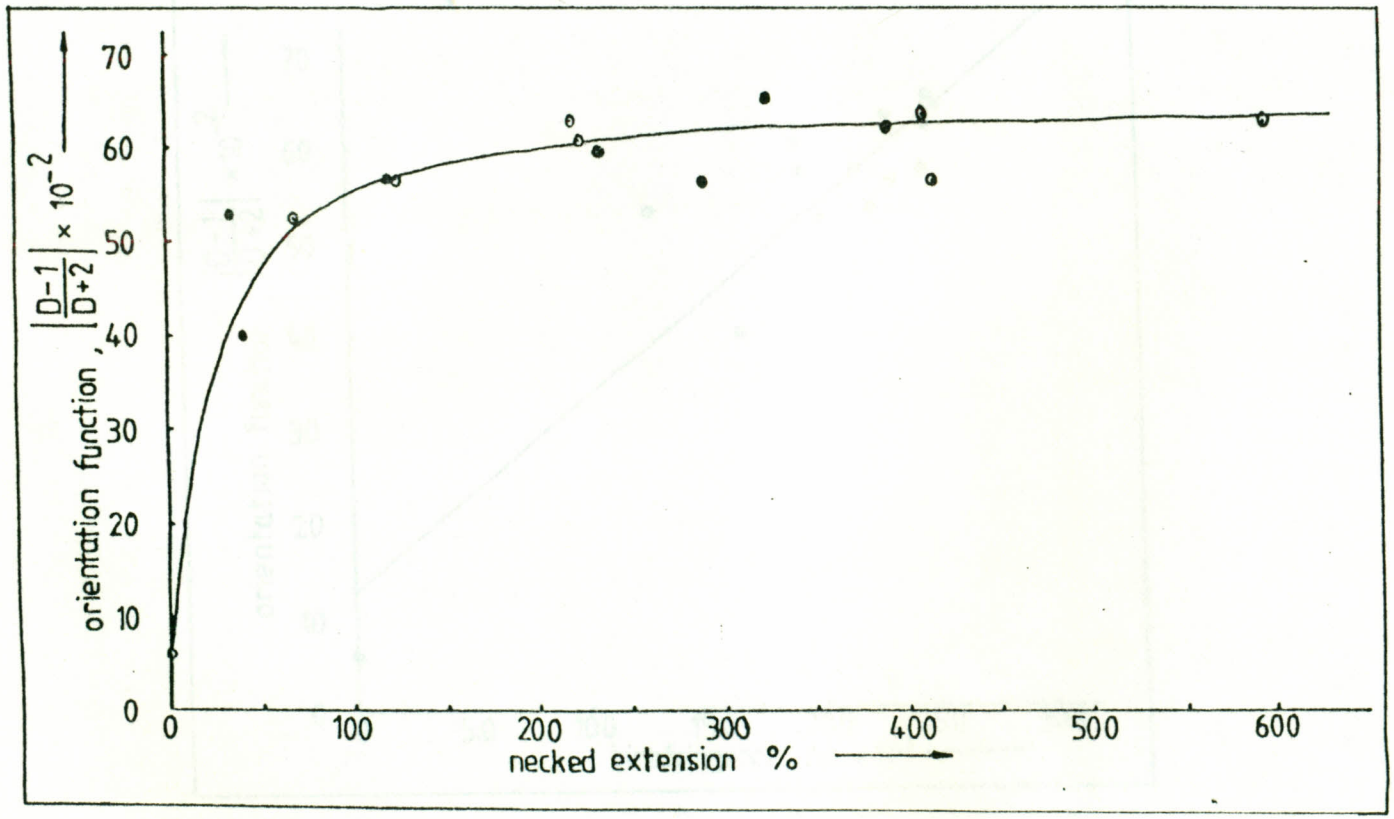

Fig. 33. The dependence of "orientation function" on extension.

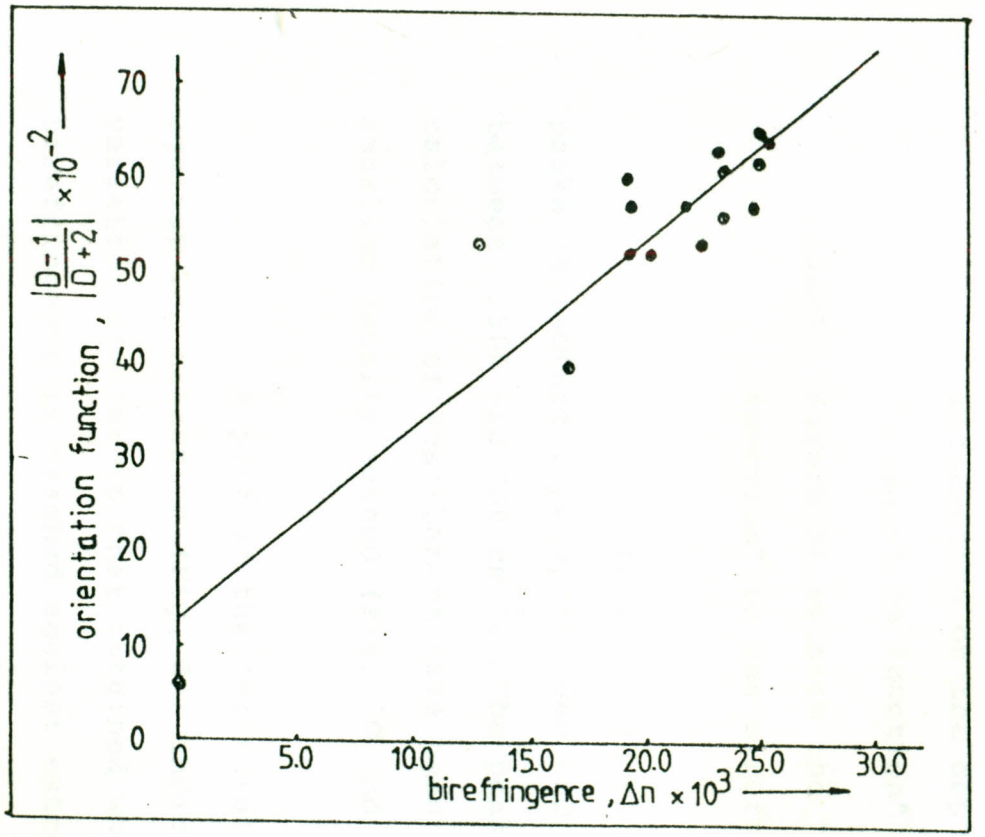

Fig. 34. The variation of "orientation function" with birefringence.

(ii) Figures 30 and 31 show the resolution of the infrared scan of a specimen for horizontal and vertical absorptions of the polarised beam, at the wavenumber 1365 cm^{-1}.

(iii) Table 18 and figure 33 provide information on the dependence of "Orientation function" on extension %.

(iv) Figure 34 relates the "Orientation function" to the birefringence.

The figure 29 gives the characteristic peaks of isotactic polypropylene and they lie between 1500 and 700 cm^{-1}. The peaks for the calculation of absorbances have been resolved by the baseline density method (fig. 30 and 31).

A plot of the "orientation function" against the extension (Fig. 33) indicates a trend of variation similar to that obtained when birefringence is graphed against extension (Fig 32). "Orientation function" was also plotted against birefringence (Fig. 34). By means of linear regression analysis, a straight line was drawn through the points, with a correlation coefficient of +0.92.

CHAPTER 5

DISCUSSION AND CONCLUSIONS

5.0 DISCUSSION

5.0.1 BIREFRINGENCE

The observations made in figs. 12 and 13 indicate that birefringence changes are more sensitive to extension than to the thickness variation. The thickness range considered did not affect the general trend of the birefringence - extension relation significantly. This should be as a result of the polymer molecules and crystallites aligning in the direction of stretch. Since the polymer molecules are long, their anisotropy lengthwise far outweighs that in the lateral direction. This explains why birefringence as a function of extension dominates over its variation with thickness.

While a stretched polymer is held at constant extension for a period of time and at a given annealing temperature (fig. 14 and 15) the processes of orientation and crystallization are expected to take place. Orientation processes would proceed if they had not reached completion during the hot-stretching, whereas crystallization would proceed until thermodynamic equilibrium is attained. During the annealing, at constant tension, of specimens whose data is given in figs. 14 and 15, the orientation and crystallization processes were expected to proceed, and this is evidently shown by the slight rise in birefringence.

It has been observed by Keller[57] that under orientation forces, crystallization occurs, and a number of molecules would crystallize into closely packed chainfolds. These structures would manifest in the form of increased birefringence with annealing.

The specimens that had been pre-stretch annealed for various periods (fig. 16-22) had birefringence and extension results that could be explained by examining the internal structure of polypropylene. Polypropylene is a semi-crystalline polymer and hence is expected to crystallize from the melt into crystalline and amorphous phases. Before stretching, the specimens were heated to soften at 115°C, a temperature close to the crystal mobility temperature of isotactic polypropylene. Takayanagi et al.[58] have reported the crystal mobility temperature of polypropylene as 100°C.

The deformation caused by uniaxial draw leads to orientation of the film substructure. The crystalline phase deforms through the folded chain lamellae. Crystallites, in the form of folded chain lamellae constitute the radial fibrils that radiate from the nucleus, from which the spherulite grew. The lamellae may deform by intralamellar or interlamellar slips. The chainfolds in the lamellae may pull out in a chain straightening process, and these deformations would be observed in the change

in shape of the spherulites.

A spherulite under stress may become ellipsoidal in shape, in the case of an affine deformation; otherwise it may stress at the apex, or even contract at the "waist", yielding along the radii perpendicular to the direction of stretch, both being non-affine types of deformation. The position of the crystallites within the deformed spherulite would depend on the initial positions of the lamellae or radial fibrils along which they are located.

The crystalline phase is embedded in the amorphous phase and the various spherulites are connected through tie molecules. During the deformation process, the coiled and entangled polymeric molecules may uncoil and come out of entanglement. The deformation may proceed by cooperative action between the crystalline and amorphous components through tie molecules. As extension of the polymer film proceeds further, the deformation may take a path from the spherulitic and lamellar into microfibrillar structures.

The initial steep rise in the value of birefringence with extension (fig. 23-24) may be viewed as the result of a combination of the

orientation of the crystalline and amorphous phases emanating from deformations, of which the amorphous phase contributes a greater part. The crystalline component does not orient as easily and quickly as the amorphous phase, given its complex path of deformation. However, as the extension rises higher, the rate of increase of birefringence lowers as the limiting birefringence is approached (fig. 23 and 24). At the regions of high extensions, for example, beyond 300% (draw ratio 4) most of the structure of the oriented specimen becomes fibrillar.

At extensions between 0 and 200% the magnitudes of birefringence tended to decrease with increased annealing time, but having an upturn after 22 hours, by very slightly rising with extension (figs. 23 and 24). The graphs in figure 25, showing the changes in birefringence with pre-stretch annealing time for both low (0-200°) and high extensions (beyond 200%) suggest an approach of the internal structure to a common substructure.

The initial steep rise in birefringence as a function of pre-stretch annealing time may also be attributed to the crystal to amorphous ratio which was high before stretch (table 15). The ratio decreases

tremendously as the extension is made higher, because the spherulitic structure transforms into the microfibrillar structure. Thus, although we would expect stress-induced crystallinity under such circumstances, the net effect may not completely offset the crystallinity lost due to transformation of the spherulitic structure into the microfibrillar type.

The behaviour of pre-stretch annealed specimens at low extension may be explained by invoking Samuels'[54,59] findings, that the intrinsic birefringence of the amorphous region is several times larger than that of the crystalline region. This observation means that for fairly equal phases and equal orientation, a higher birefringence value for the amorphous phase after stretch may be observed. By considering that the crystalline content ranges from half to two thirds for the specimens considered, we may assume that the amorphous birefringence would dominate at the initial drawing stages. This would be more so, in view of the fact that the amorphous phase orients more easily than the crystalline phase. This inference supports the observations that were made especially for the specimens annealed for $1^{1}/4$, $2^{1}/4$, 3, 6 and 22 hours (Fig. 23). It should be noted however that in the real polymer the amorphous phase is never perfectly aligned, nor is the crystallite ever perfect, as it is implied

in the intrinsic birefringence values.

At high extensions, it is expected that random chain portions stretch out, and chainfolds become aligned and pulled out to varying extents. The lamellae may break up into small chainfolded blocks and remain strung together to form beaded structures. The whole assembly would thus become an assembly of microfribrils[60]. Since chainfolds may still be found in the microfibrils, full extension of the chains is not yet achieved.

The tendency of the birefringence-extension curves of the pre-stretch annealed specimens to lump together may be attributed to the narrow range of the original crystallinity as indicated initially (table 15 and fig. 26). The crystallinity of the pre-stretch annealed specimens was observed to rise fairly rapidly in the first 6 hours and then the changes became less significant with longer times. The variation may be described as inverse tangential. It may be said that the initial state of crystallinity of the oriented specimens seems only to matter in the earlier low extensions upto about 300% (figs. 23, 24, and 25) but has insignificant effect on later orientations, during which close packing of chains and microfribrils seem to have set in.

5.0.2 WIDE-ANGLE X-RAY DIFFRACTION

The degree of crystallinity was observed to increase with pre-stretch annealing time, but the 2θ values tended to fluctuate slightly (table 16), suggesting little or no change in Bragg spacing. The observed change in crystallinity was however consistent with Migwi's[61] findings. Since a shift in 2θ values would have been expected due to crystal thickening[62], the change in crystallite size was relatively small.

By comparing the arcs (figs. 28a, b, c, d) with those obtained by Samuels and other authors the planes (110), (040) and (130) were identified as c-axis oriented.[54, 55, 56] c-axis orientation is important in the sense that the polymer molecules constituting the lamellae orient in the fibre axis, i.e the direction of uniaxial orientation.

The change observed in Braggs spacing as a function of extention (fig. 27) is infinitesimal, compared to the change of birefringence with extension (figs. 16-22 and 32). However, while the spacing tends to decrease with extension, the birefringence increases with the same.

5.0.3 INFRARED DICHROISM

The infrared dichroism measurements show

that the variation of the "Orientation function" with extension is similar to the variation of birefringence with extension (fig. 32 and 33). The correlation between birefringence and "orientation function" was found to be strong (fig. 34). The "Orientation function" plotted against extension suggests that the deformation in the specimens involves rapid transformation from the crystalline to fibrillar structure within the low extensions, i.e. about 200% and below (fig. 32). From the above observation, the behaviour of the "orientation function" indirectly tells us how the orientation parameter, $\langle \cos^2\theta \rangle$ is affected. This means that birefringence and orientation parameter are influenced in a similar manner by the stretching process, hence molecular orientation.

A graphical comparison of the trends of "orientation function" - extension curve (fig. 33) and Wilchinsky's model curve of orientation parameter $\langle \cos^2\theta \rangle$ versus extension (fig. 35) shows that the experimental curve is initially steeper, but becomes less steep and levels off much earlier. The difference between the curves may be attributed to (i) the ideal assumptions of Wilchinsky's model (ii) the non-affine nature of the deformation of the films used in this study. The close trends however affirm the basic assumption of an initially semi-crystalline structure of the films, which later breaks down towards a fibrillar structure.

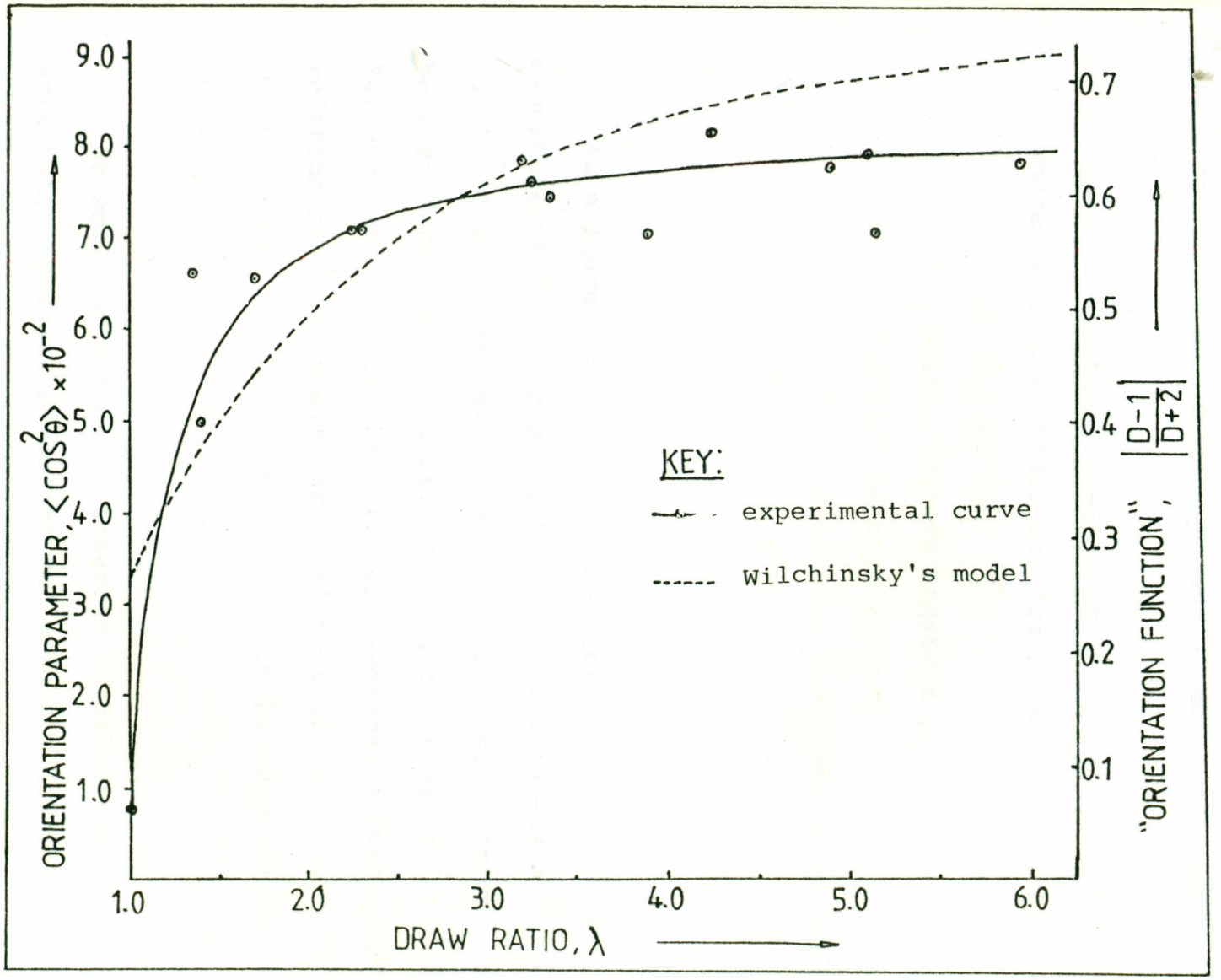

Fig. 35. Comparison of experimental curve with Wilchinsky's Model.

It should be noted that vertical scales for the two functions are proportional to each other (ref. eq.6 pg. 18 and eq. 12 pg.22). The "orientation function" curve seems to fit on an inverse tangential curve of form

$$f(\lambda) = K \tan^{-1}(\lambda^n - 1)^{\frac{1}{2}} + M$$

where λ is the extension (draw) ratio

n an integer

k a multiplicative constant or function of crystallinty

M an additive constant, dependent on initial orientation of film

$f(\lambda)$ is $\frac{D-1}{D+2}$ ("orientation function")

As n increases from 1, both initial steepness and magnitude of $f(\lambda)$ increase, but the curve levels off quickly towards an asymptote. The observed relation between "orientation function" and birefringence (fig. 34) suggests that the birefringence-extension functional relation may have a similar model to that above (figs. 23 and 35). Such an indication is given by the overlapped curves in fig. 23.

It would have been of interest to calculate the orientation parameter $\langle \cos^2\theta \rangle$ and even the transition moment, but the information available was insufficient to calculate D_o, the dichroic ratio of an ideally

oriented specimen.

5.1 CONCLUSIONS

(a) There is a steep rise in both the birefringence and "orientation function" at low extensions of 0 - 200% (draw ratios of 0 -3), which is a sign of rapid deformation or change in the structure of the films and is associated mainly with the amorphous phase chain orientation of the sample.

(b) The birefringence and "orientation function" both approach common values at high extensions irrespective of the initial crystalline states of the specimens. This suggests that at high extensions these properties of the specimens may be determined uniquely.

(c) The variation of crystallinity as a function of annealing time and the variations of birefringence and "orinentation function" as functions of extension exhibit an inverse tangential relationship. The inverse tangential function suggests the tendency of crystallinity, birefringence and "Orientation function" towards equilibrium values at high extensions and high annealing times respectively.

(d) The observation that the birefringence of pre-stretch annealed specimens tends to decrease with longer

annealing times, especially in the shorter periods of annealing, at low extensions indicates that a higher crystalline content leads to a correspondingly lower birefringence. The difference in crystalline content has a bearing on how the initial deformation occurs. At higher extensions most or all of the initial crystalline structure will have broken down and instead a more fibrillar structure will have formed. This perhaps may be the reason why high extension birefringence does not seem to depend on initial crystallinity.

(e) The uniaxial drawing of specimens has been found to change Bragg Spacings by very slightly decreasing them. This may be explained by assuming crystallization under stress, coupled with close packing and chain straightening of the polymer molecules.

LIMITATIONS AND RECOMMENDATIONS

(a) In this study the cooling of the mold was performed by using natural air-cooling. It would be interesting to have a much wider range of initial crystalline levels, hence physical states, by using different cooling rates, possibly by means of a temperature controlled hot-press.

(b) Another way by which crystallinity would have been varied in this work is by varying the annealing temperature, but due to non-availability of time this was not done.

(c) The orientation parameter $\langle \cos^2\theta \rangle$ mentioned in the discussion section above, may be found if D_o can be found. One method to find D_o would be to obtain the crystalline orientation functions f_c for specimens of various draw ratios according to the method adopted by Wilchinsky[63] using wide-angle X-ray diffraction. An X-ray apparatus with pole diagram facilities would, however, be necessary. The dichroic ratio, D, for the same specimens would be found and a plot of f_c against $\frac{D-1}{D+2}$ made. The slope would then provide D_o.

REFERENCES

1. E.Meinecke ., "Optical Properties", in Encyclopedia of Polymer Science and Technology, (eds.) N.M. Bikales, J. Conrad, A. Ruks, and J. Perlman, Interscience Publishers, New York, 1972, Vol.9, p. 64.

2. F.W. Billmeyer Jr.,A Textbook of Polymer Science, John Wiley and Sons, Inc., New York, 1984, p. 368.

3. E.A. Collins, J. Bare's, and F.W. Billmeyer Jr., Experiments in Polymer Science, John Wiley and Sons, Inc., New York, 1973, p. 222.

4. H.D. Keith, F.J. Padden, N.M. Walter Jr., and H.W. Wychoff, I. Appl. Phys. 30, 1485 (1959).

5. P.H. Geil, Polmer Single Crystals, Interscience Publishers, New York, 1963.

6. D.R. Morrow and B.A. Newman, J. Appl. Phys. 39 4944 (1968).

7. H. Kolsky and A.C. Shearman, Proc. Phys. Soc. London 55, 383 (1943).

8. W. Heller and Oppenheimer, J. Colloid Sci. 3, 33 (1948).

9. R.D. Andrews and J.F. Rudd, J. Appl. Phys. 28 1091 (1957).

10. E.N. Lawrence and R. Buchdahl, J. Appl. Phys. 21 488 (1950)

11. R.S. Moore and G. Gieniewski, J. Appl. Phys. 41 4367 (1970).

12. R.J. Samuels, Structured Polymer Properties, A Wiley Interscience Publication, New York, 1974.

13. R.S. Stein, J. Polymer Science. 31, 327 (1958).

14. J. Petermann and J.M. Schultz, J. Mater Sci. 13 2188 (1978).

15. A. Keller and O' Connor, , Nature 180, 1289 (1957).

16. W.O. Statton, J. Polymer Sci. 41, 143 (1959).

17. A.Peterlin, J. Polymer Sci. C9, 61 (1965).

18. J. Petermann and H. Gleiter, Phil. Mag. 31 929 (1975).

19. A. Keller and M.J. Machin, J. Makromol. Sci. Phys. 1, 41 (1967).

20. D. Krueger and G.S.Y Yeh, J. MaCromol. Sci. Phys. 6, 431 (1972).

21. K. Hess and H. Kiessig, Z. Phys. Chem. A193 196 (1944).

22. E.W. Fischer and H. Göddar, J. Polymer Sci. C16, 4405 (1969).

23. R.A. Horsely and H.A. Nancarrow, Brit. J. Appl. Phys. 2, 345 (1951).

24. S. Bahadur, J. Mater. Sci. 10, 1425 (1975).

25. A. Peterlin and F.J. Balta'-calleja, J. Appl. Phys. 40, 4238 (1969).

26. A. Peterlin, J. Appl. Phys. 48, 4099 (1977).

27. M.A McRae, W.F. Maddams and J.E. Preedy, J. Mater. Sci. 11 , 2036 (1976)

28. A. Brown, J. Appl. Phy. 20, 552 (1949).

29. R.S. Stein and F.H. Norris, J. Polymer Sci. 21, 381 (1956).

30. S.L. Aggarwal, G.P. Tilley and D.J. Sweeting, J. Polymer Sci. 51, 551 (1961).

31. D. Shinozaki and G.W. Grooves, J. Mater Sci. Letters 11, 2356 (1976).

32. D. Pope and A. Keller,
J. Polymer Sci. 13, 533 (1975).

33. R.J. Young, P.B. Bowden, J.M. Ritchie, and
J.G. Rider, J. Mater Sci.8, 23 (1973).

34. D. Shinozaki and G.W. Grooves,
J. Mater Sci. 8, 1012 (1973).

35. M.D. Rhodes and R.S. Stein, J. Appl. Phys.
32, 2344 (1961).

36. K. Sasaguri, S. Hoshino and R.S. Stein, J. Appl.
Phys. 35, 47 (1964).

37. R.G. Crystal and D.Hansen, J. Appl. Phys. 38
3103 (1967).

38. M.R. Miller, The Structure of Polymers,
Reinhold Publishing Corporation, New York,
1966, p. 573.

39. R.D.B. Fraser, J. Chem. Phys. 21, 1511 (1953).

40. J.J. Hermans, P.H. Hermans, D. Vermass, and
A. Weidinger, Rec. Trav. Chim. 65, 427 (1946).

41. R.S. Stein, J. Appl. Phys. 32, 1280 (1961).

42. E.F. Gurnee, J. Appl. Phys. 25, 1232 (1954).

43. W.R.R. Park and J. Conrad,
"Biaxial Orientation", in Encylopedia of
Polymer Science and Technology, Eds. JO Conrad)
J. Perlman, F.L. Dankberg, J.J. Kerstein,
L.L. Strauss, Interscience Publishers,
New York, Vol. 2, p. 339.

44. Z.W. Wilchinsky, Polymer 5, 271 (1964).

45. J.P. Colson and R.K. Eby,
J. Appl. Phys. 44, 4332 (1973).

46. P.I. Vincent, "Fracture", in Encylopedia of
Polymer Science and Technology, (eds.)
J. Conrad, C. Comiskey, and A. Ruks.
Interscience Publishers, New York, 1967.
vol. 7, p. 293.

47. Table of function for the Rotatory Compensator
by Ehringhaus with Quartz combination
plates, Carl Zeiss Company, West Germany.

48. R.L. Miller, "Crystallinity", in Encylopedia of
Polymer Science and technology, (eds).
J. Conrad, J. Perlman, J.J. Kerstein and
A. Ruks, Interscience Publishers, New York,
1966, Vol. 4, p. 481.

49. G. Natta and G. Corradini, Rend. Accad.
Naz. Luccei 8, 11 (1957).

50. P.H. Hermans and A. Weidinger,
Makromol. Chem. 50, 98 (1961).

51. G. Farrow, Polymer 1, 518 (1960).

52. H.P. Klug and L.E. Alexander, X-ray diffraction Procedures for Polycrystalline and Amorphous Materials, A Wiley-Interscience Publication, New York, 1974.

53. V.J.I. Zicky, "Quantitative Analysis of Polymeric Materials", in Laboratory Methods in Infrared spectroscopy, (eds.) R.G.J. Miller and B.C. Stace, Heyden and son Ltd., London, 1972, p.51.

54. R.J. Samuels, J. Polymer Sci. A3, 1741 (1965).

55. E.J. Addink and J. Buntema, J. Polymer 2, 185 (1961).

56. H.D. Keith, F.J. Padden, N.M. Walter Fr., and H.W. Wyckoff, J. Appl. Phys. 30, 1485 (1959).

57. A. Keller, "Polymer Crystallisation: A Survey and Current Salient Issues", in Recent Advances in the Field of Crystallization and Fusion of Polymers, (eds.) J.P. Mercies and R. Legras, an Interscience Publication, New York, 1977, p.1.

58. M. Takayanagi, S. Minami, and H. Nagatoshi, Asahi Garasii Kogyo Gijutsu Shoreikai, 7, 127 (1961).

59. R.J. Samuels, J. Polymer Sci., A-2, 6, 1101 (1968)

60. A. Peterlin, J. Mater. Sci. 6, 480 (1971)

61. M. Migwi, "Correlation of the Experimental Crystallinity with Mechanical Properties of Isotactic Polypropylene", M.Sc. Thesis, Kenyatta University, 1987.

62. I.C. Sanchez, "Problems and Theories of Polymer Crystallization", in Advances in the field of Crystallization and Fusion of Polymers, (eds.) J.P. Mercier and R. Legras, an Interscience publication, New York, 1977, p. 109.

63. Z.W. Wilchinsky, J. Appl. Phys. 31, 1969 (1960).

APPENDIX I

1. The correlation coefficient in figure [34] was obtained by using the Peason's correlation coefficient formula:

$$r = \frac{\Sigma xy - (\Sigma x)(\Sigma y)/n}{\left\{\left[\Sigma x^2 - (\Sigma x)^2/n\right]\left[\Sigma y^2 - (\Sigma y)^2/n\right]\right\}^{\frac{1}{2}}}$$

where

r is the correlation coefficient

x, y are the quantities to be correlated

n is the number of points of each of the quantities to be correlated.

2. To fit the straight line, the slope of the line was obtained from:

$$b = \frac{\Sigma xy - (\Sigma x)(\Sigma y)/n}{\Sigma x^2 - (\Sigma x)^2/n}$$

APPENDIX II

X- RAY DIFFRACTOGRAMS

FIGURES 36-42.

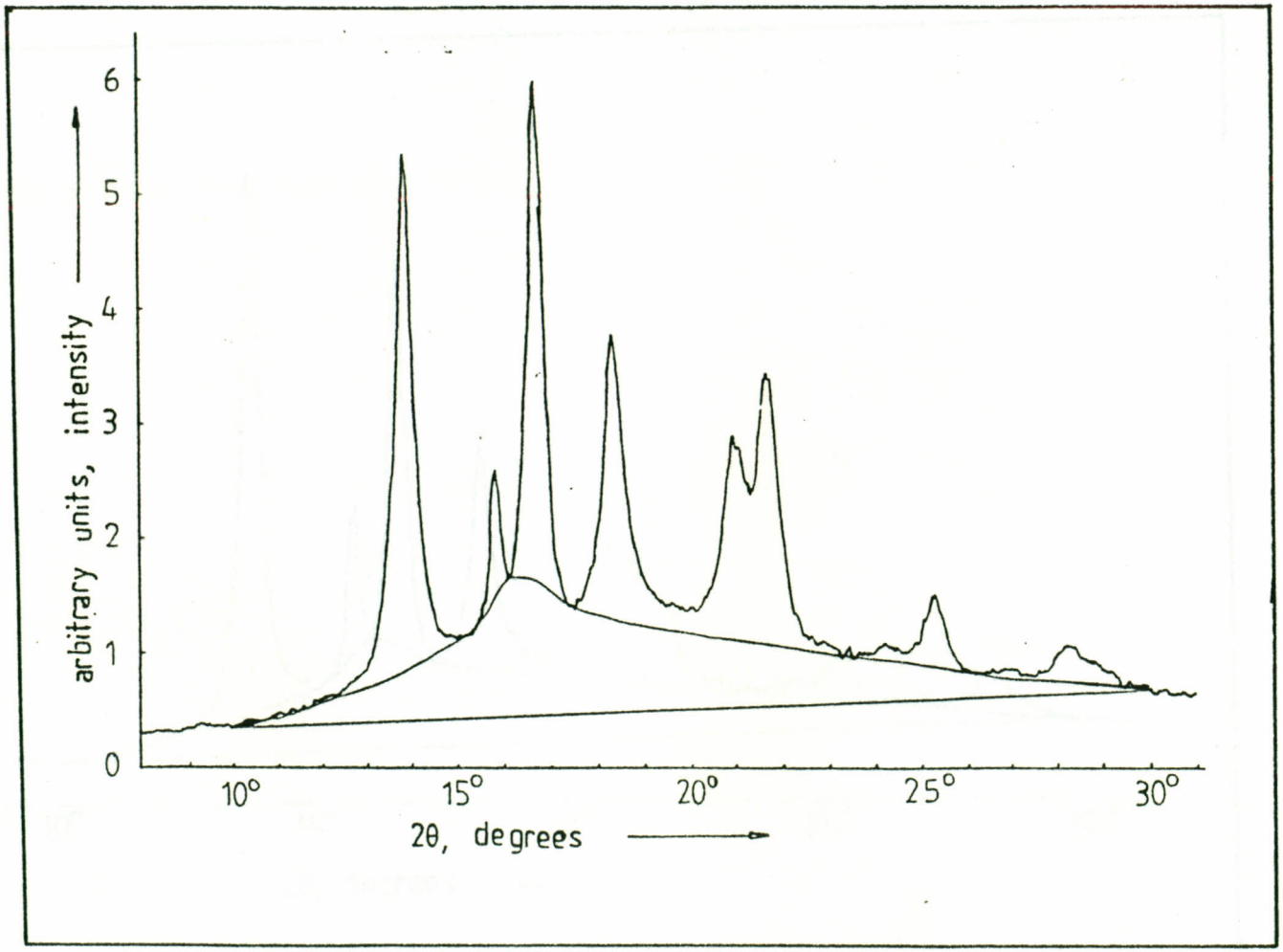

Fig. 36. Specimen unannealed; annealing time = 0 hours.

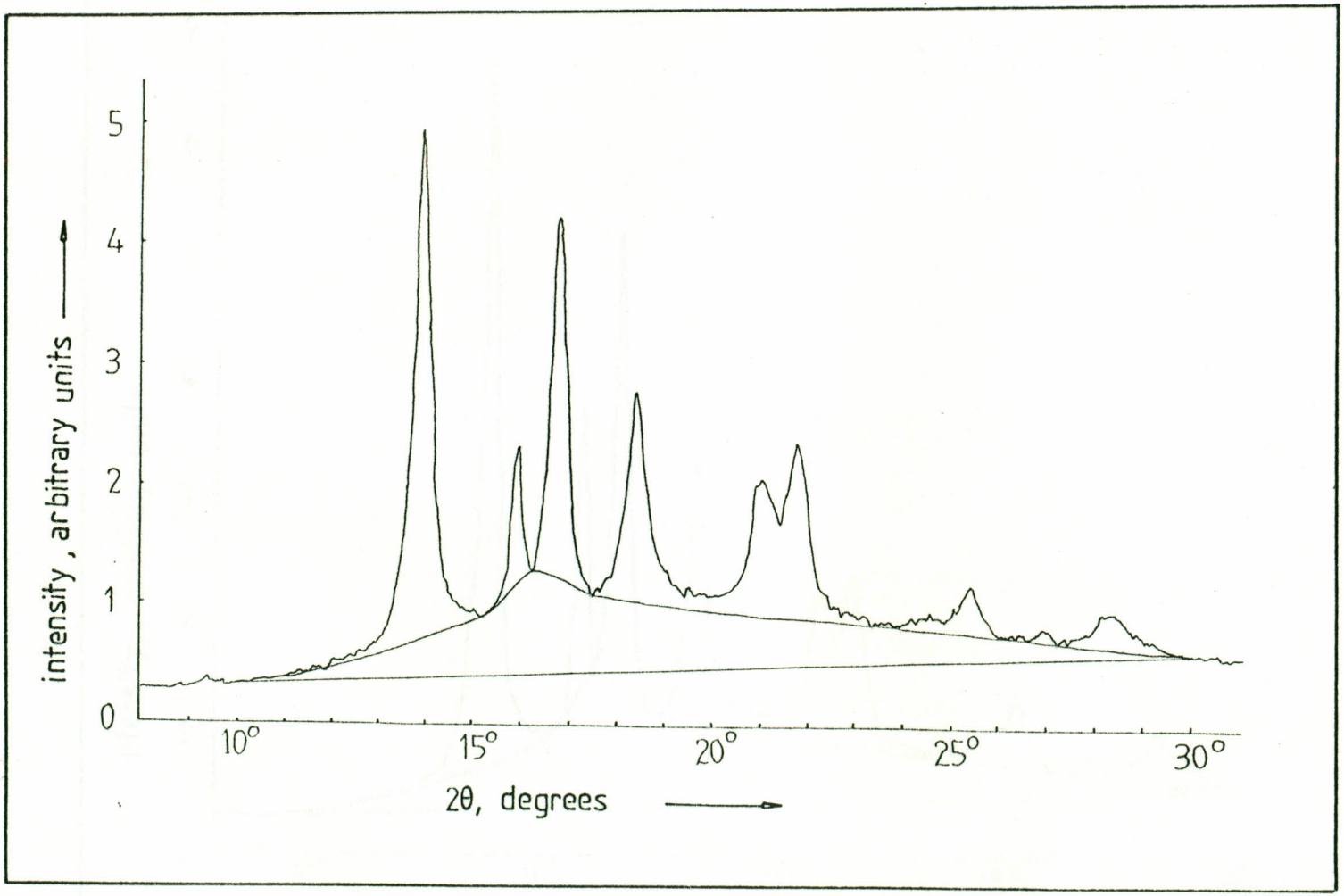

Fig. 37. Specimen annealed for 1¼ hours.

Fig. 38. Specimen annealed for 3 hours.

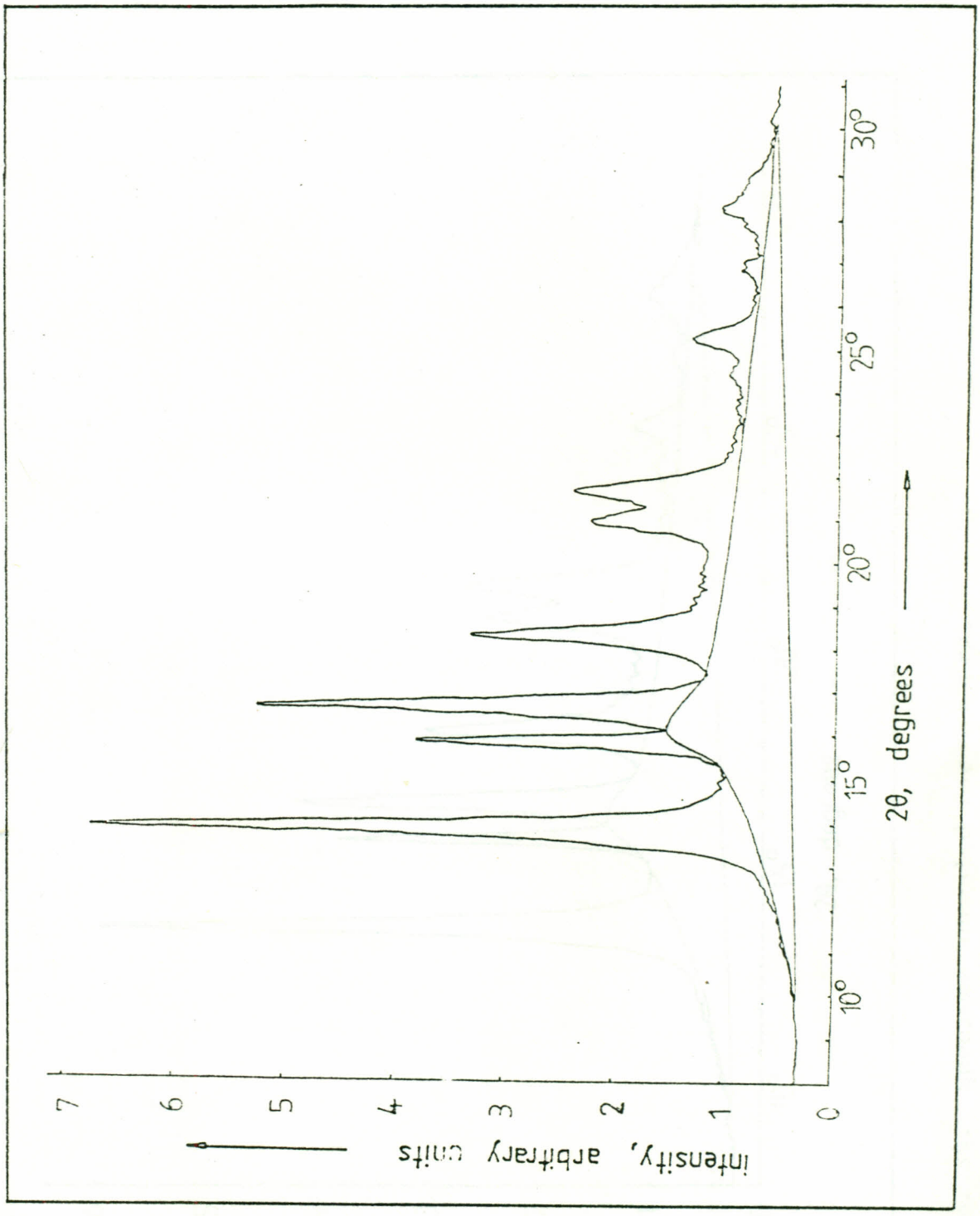

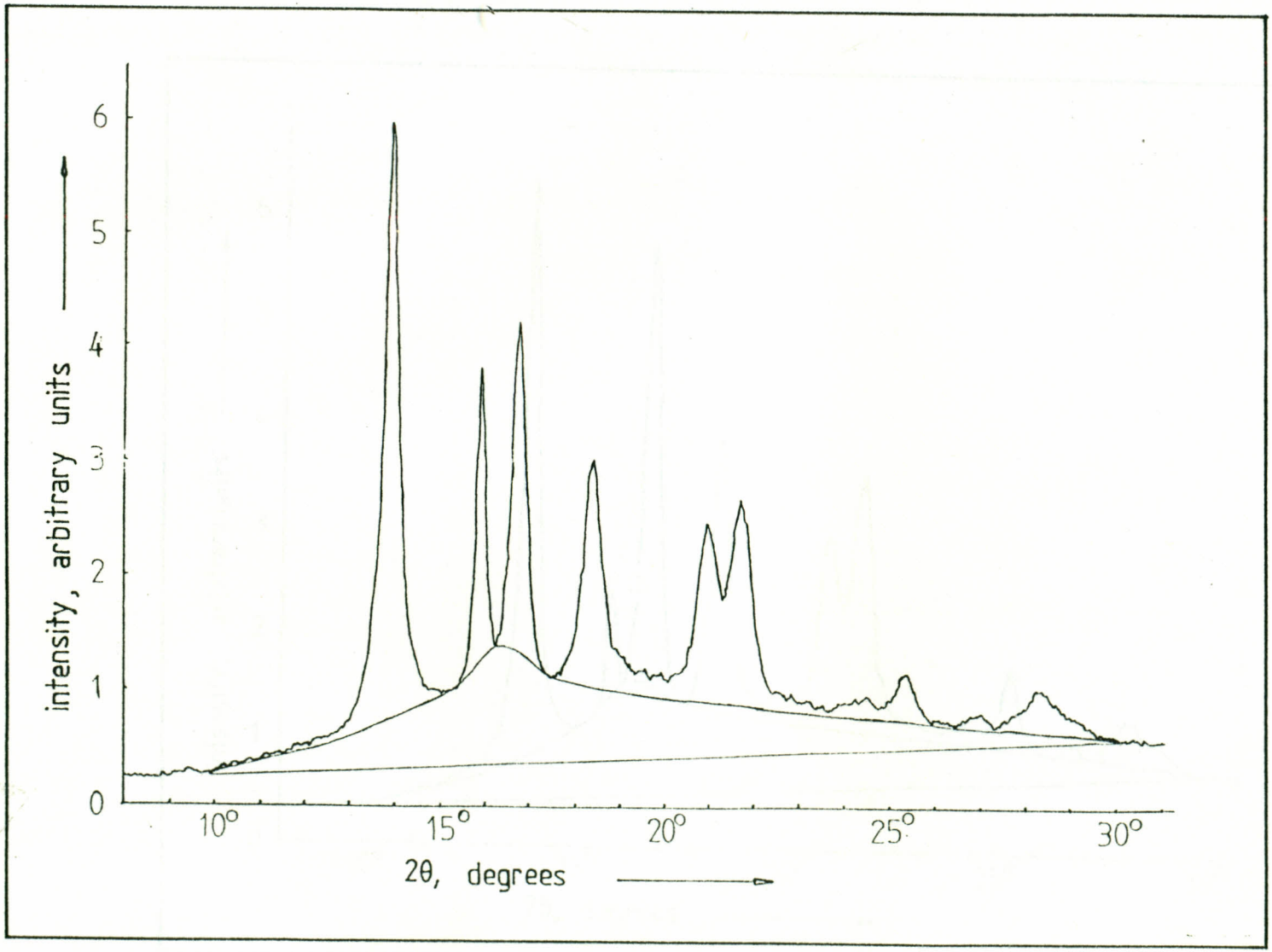

Fig. 39. Specimen annealed for 6 hours.

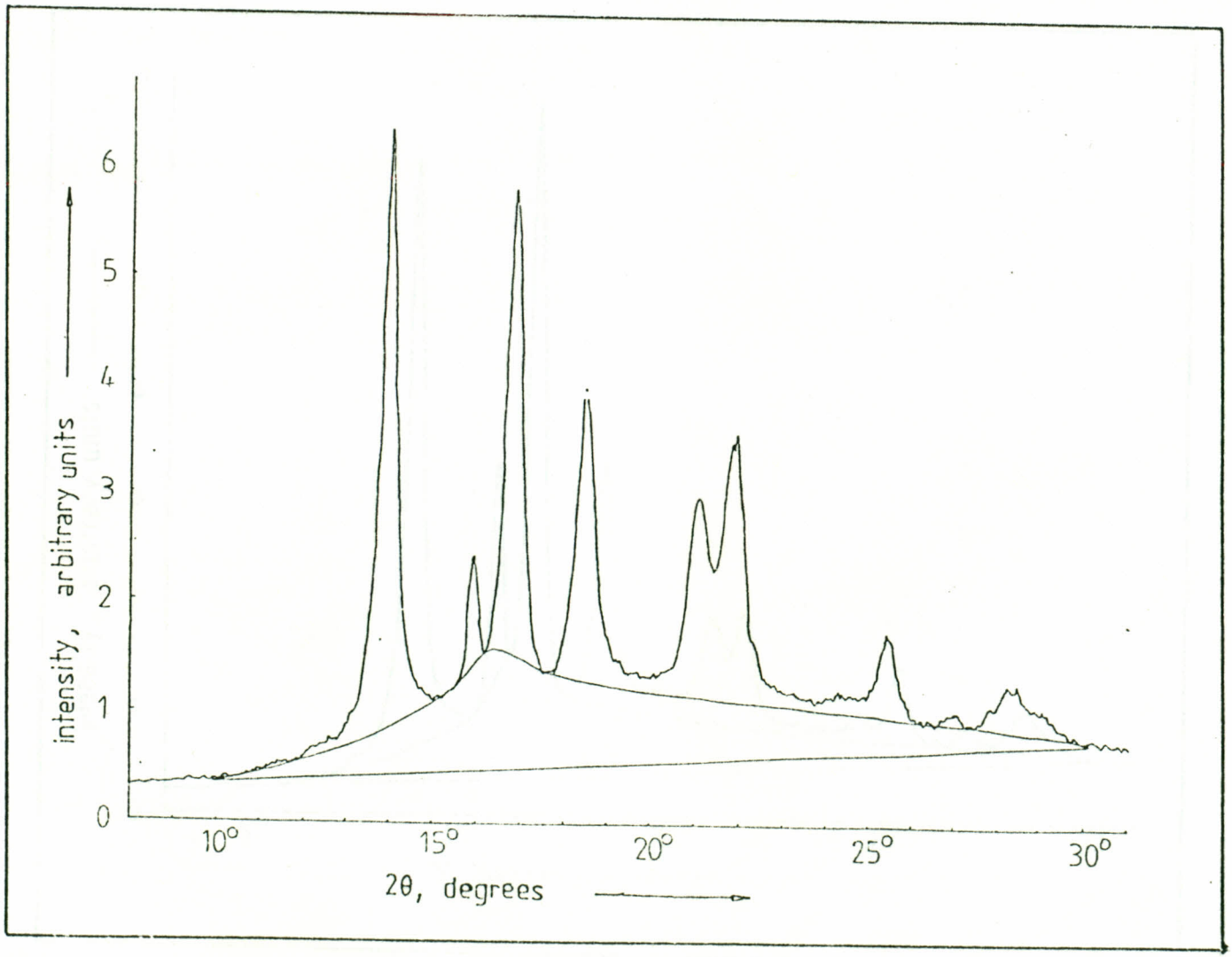

Fig. 40. Specimen annealed for 22 hours.

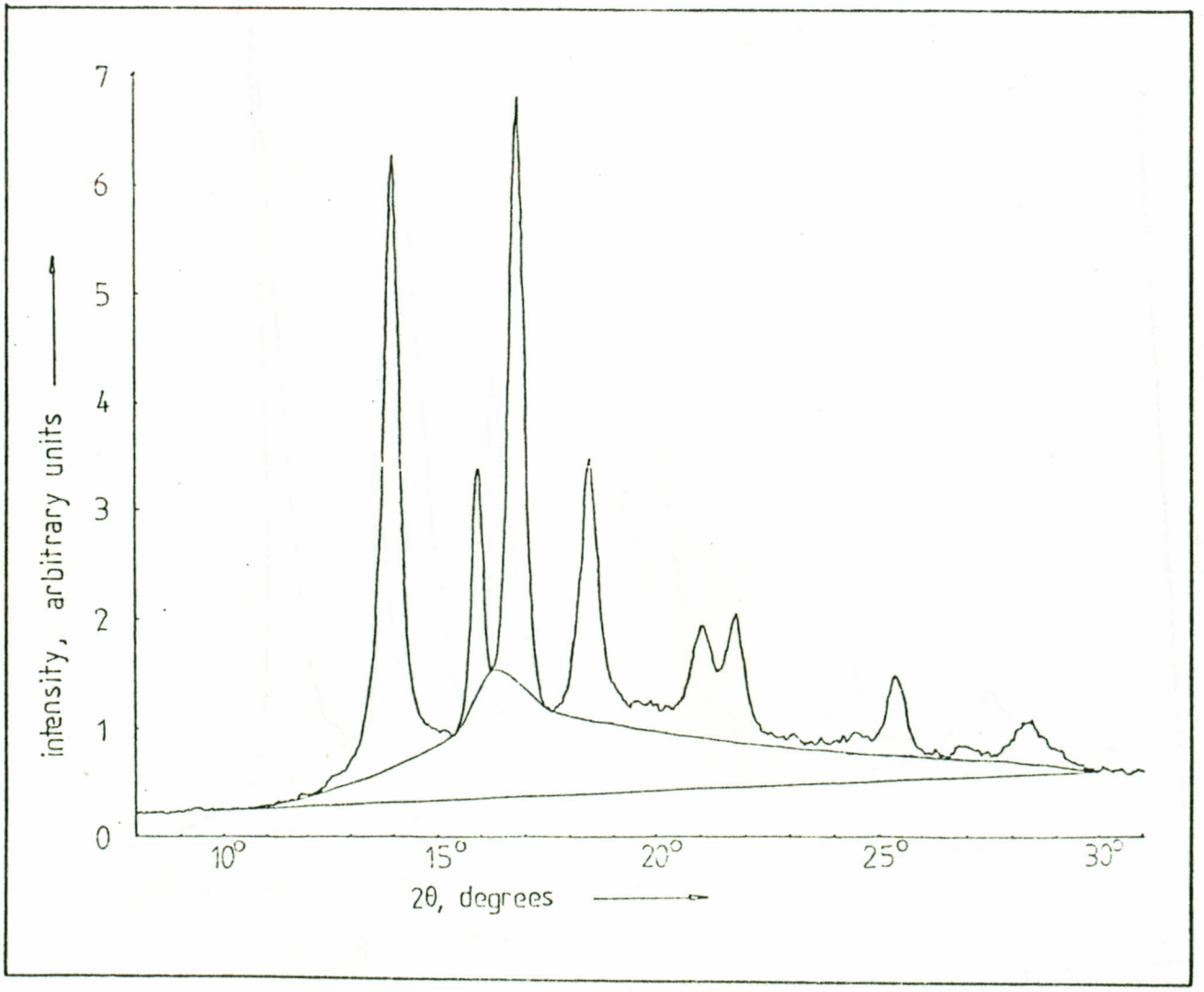

Fig. 41. Specimen annealed for $47^{2}/3$ hours.

Fig. 42. Specimen annealed for 72 hours.

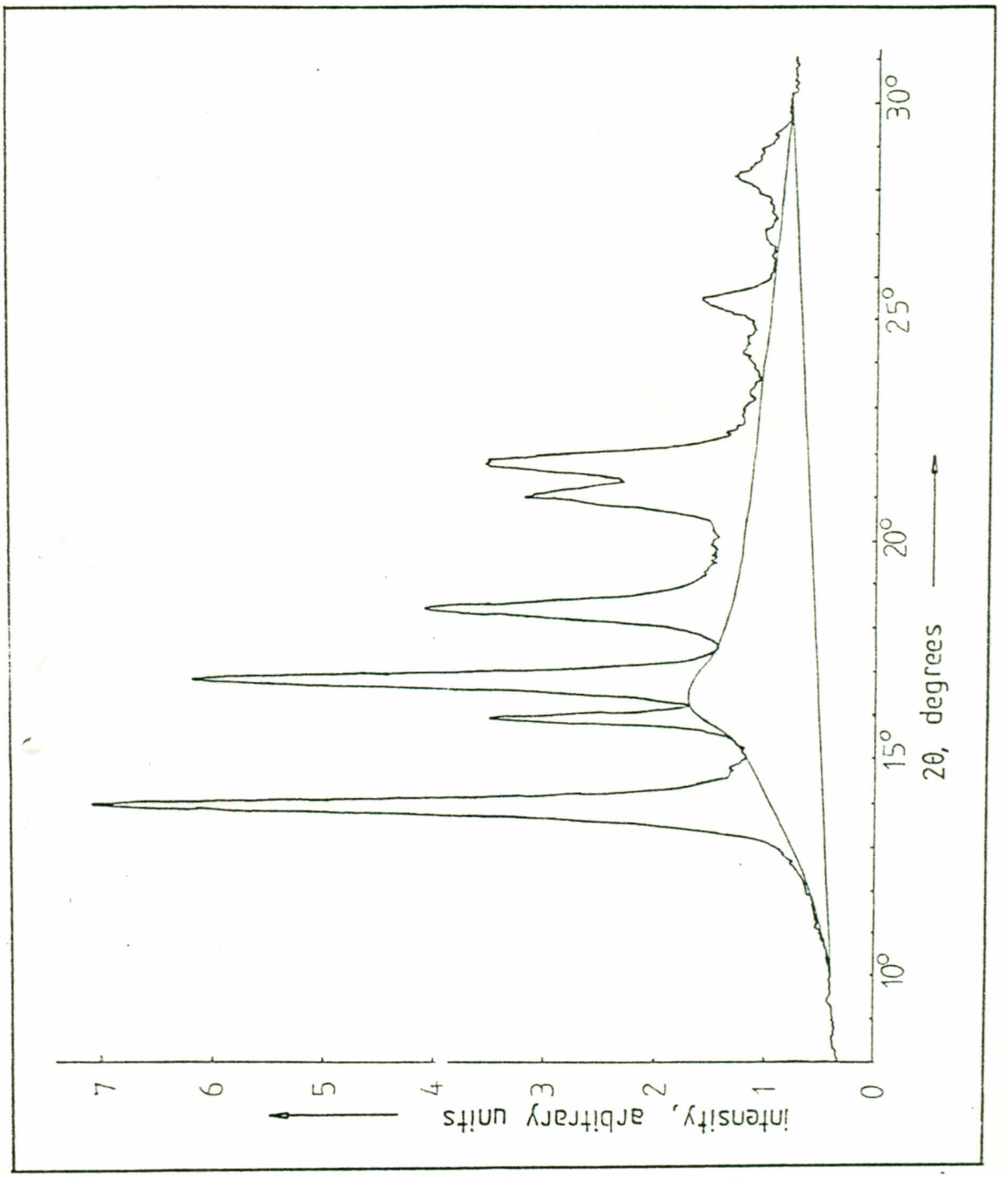

APPENDIX III

TABLES 1-20

TABLE 1. EFFECT OF RE-STRETCH ON BIREFRINGENCE

SPECIMEN NO.	INITIAL		FINAL	
	EXTENSION %	BF, $\Delta n \times 10^3$	EXTENSION %	BF, $\Delta n \times 10^3$
SR-1	43	18.55	68	22.54
SR-2	63	24.83	130	25.15
SR-3	80	19.70	150	25.37
SR-4	213	22.19	273	25.05
SR-5	278	18.40	323	19.28

TABLE 2. VARIATION OF BIREFRINGENCE WITH THICKNESS AT CONSTANT EXTENSION = 25%

SPECIMEN NO.	THICKNESS (mm)	BF, $\Delta n \times 10^3$
ST-1	0.085	17.97
ST-2	0.098	17.95
ST-3	0.110	17.55
ST-4	0.118	18.73
ST-5	0.139	18.42
ST-6	0.170	21.06

TABLE 3. VARIATION OF BIREFRINGENCE WITH EXTENSION FOR CONTROLLED THICKNESS RANGE (0.085 - 0.095 mm)

SPECIMEN NO.	NECKED EXTENSION %	THICKNESS (mm)	STRETCH RATE mm/min	BF, $\Delta n \times 10^3$
SE-1	22.5	0.095	10.8	19.15
SE-2	25.0	0.085	13.3	17.97
SE-3	27.5	0.085	16.5	19.17
SE-4	87.5	0.089	18.3	22.25
SE-5	95.0	0.085	18.9	20.62
SE-6	120	0.90	21.5	24.63
SE-7	140	0.095	32.7	23.93
SE-8	200	0.095	31.4	25.56
SE-9	315	0.093	21.6	27.06

Mean thickness ≈ 0.090 ± 0.005 mm

TABLE 4. SPECIMENS ANNEALED FOR 10 MINUTES AFTER STRETCH, AND THEN 30 MINUTES AFTER STRETCH. ANNEALING TEMPERATURE = 115°C

SPECIMEN NO.	NECKED EXTENSION %	INITIAL BF, $\Delta n \times 10^3$	FINAL BF, $\Delta n \times 10^3$
SA-A1	40	17.10	18.15
SA-A2	63	24.84	25.66
SA-A3	138	26.34	26.06
SA-A4	210	25.59	26.98
SA-A5	270	23.68	28.44

TABLE 5. SPECIMENS ANNEALED FOR 10 MINUTES AFTER STRETCH, AND THEN 60 MINUTES AFTER STRETCH. ANNEALING TEMPERATURE = 115°C

SPECIMEN NO.	NECKED EXTENSION %	INITIAL BF, $\Delta n \times 10^3$	FINAL BF, $\Delta n \times 10^3$
SA-B1	25	15.77	15.91
SA-B2	43	15.85	19.26
SA-B3	63	22.65	23.26
SA-B4	125	24.90	24.94
SA-B5	143	22.66	25.81
SA-B6	205	24.32	25.48
SA-B7	250	25.20	27.00

TABLE 6. SPECIMENS ANNEALED FOR 1½ HOURS BEFORE STRETCH, AT 115°C

SPECIMEN NO.	NECKED EXTENSION %	THICKNESS (mm)	STRETCH RATE mm/min	BF, $\Delta n \times 10^3$
SB-A1	40	0.075	30.0	20.79
SB-A2	60	0.070	30.0	24.48
SB-A3	90	0.078	28.2	27.73
SB-A4	110	0.112	25.3	24.64
SB-A5	125	0.088	29.3	28.20
SB-A6	270	0.077	21.9	30.38
SB-A7	290	0.080	27.8	30.54
SB-A8	435	0.073	30.2	30.56

Note: After stretch, the specimens were annealed for 10 minutes at constant tension, at 115°C.

TABLE 7. SPECIMENS ANNEALED FOR 2¼ HOURS BEFORE STRETCH, AT 115°C

SPECIMEN	NECKED EXTENSION %	THICKNESS (mm)	STRETCH RATE mm/min	BF, $\Delta n \times 10^3$
SB-B1	50	0.063	28.5	21.69
SB-B2	110	0.075	30.3	25.20
SB-B3	195	0.068	29.1	27.94
SB-B4	215	0.089	27.8	27.33
SB-B5	260	0.072	26.7	29.16
SB-B6	285	0.081	32.7	28.06
SB-B7	430	0.090	37.5	29.96
SB-B8	440	0.103	30.4	30.50
SB-B9	445	0.103	27.4	30.66
SB-B10	475	0.141	27.3	28.25

Note: After stretch the specimens were annealed for 10 minutes at constant tension, at 115°C.

TABLE 8. SPECIMENS ANNEALED FOR 3 HOURS BEFORE STRETCH, AT 115°C

SPECIMEN NO.	NECKED EXTENSION %	THICKNESS (mm)	STRETCH RATE mm/min	BF, $\Delta n \times 10^3$
SB-C1	30	0.069	33.0	20.13
SB-C2	100	0.069	26.3	26.81
SB-C3	105	0.060	27.8	24.83
SB-C4	170	0.075	29.0	28.96
SB-C5	180	0.067	30.5	25.74
SB-C6	280	0.068	32.0	29.00
SB-C7	360	0.075	31.5	30.51
SB-C8	450	0.089	27.9	31.07
SB-C9	460	0.115	29.8	29.55
SB-C10	555	0.133	31.8	29.45

Note: After stretch, the specimens were annealed for 10 minutes at contant tension, at 115°C.

TABLE 9. SPECIMENS ANNEALED FOR 6 HOURS BEFORE STRETCH, AT 115°C

SPECIMEN NO.	NECKED EXTENSION %	THICKNESS (mm)	STRETCH RATE mm/min	BF, $\ln \times 10^3$
SB-D1	30	0.052	36.0	18.59
SB-D2	45	0.087	36.0	19.35
SB-D3	50	0.102	31.5	18.92
SB-D4	65	0.093	30.0	23.57
SB-D5	75	0.115	38.6	23.61
SB-D6	80	0.107	36.0	25.26
SB-D7	95	0.078	24.8	23.52
SB-D8	150	0.107	26.0	24.36
SB-D9	215	0.092	28.1	28.41
SB-D10	260	0.077	27.4	29.25
SB-D11	300	0.100	26.3	29.94
SB-D12	550	0.119	30.4	28.64

Note: Specimens were annealed for 10 minutes after stretch at constant tension, at 115°C.

TABLE 10. SPECIMENS ANNEALED FOR 22 HOURS BEFORE STRETCH, AT 115°C

SPECIMEN NO.	NECKED EXTENSION %	THICKNESS (mm)	STRETCH RATE mm/min	BF, $\Delta n \times 10^3$
SB-E1	20	0.70	24.0	16.50
SB-E2	30	0.084	36.0	10.46
SB-E3	35	0.211	36.0	14.18
SB-E4	40	0.075	32.0	18.74
SB-E5	55	0.087	33.0	20.88
SB-e6	90	0.090	28.0	23.23
SB-E7	145	0.106	30.6	25.02
SB-E8	165	0.103	29.0	25.80
SB-E9	195	0.105	29.1	26.25
SB-E10	270	0.105	31.3	27.65
SB-E11	355	0.105	30.8	29.19
SB-E12	405	0.100	34.8	28.91
SB-E13	490	0.100	34.6	31.66
SB-E14	520	0.101	32.4	39.56

Note: Specimens were annealed for 10 minutes after stretch at constant tension, at 115°C.

TABLE 11. SPECIMENS ANNEALED FOR $47\frac{2}{3}$ HOURS BEFORE STRETCH, AT 115°C

SPECIMEN NO.	NECKED EXT. %	THICKNESS (mm)	STRETCH RATE mm/min	BF, $\Delta n \times 10^3$
SB-F1	20	0.096	33.0	9.90
SB-F2	40	0.092	34.0	15.42
SB-F3	50	0.068	31.5	19.16
SB-F4	55	0.086	31.5	20.63
SB-F5	95	0.093	32.0	23.03
SB-F6	100	0.101	31.5	22.93
SB-F7	145	0.077	30.6	26.30
SB-F8	150	0.095	30.6	24.52
SB-F9	185	0.083	31.0	27.17
SB-F10	245	0.083	28.7	27.06
SB-F11	275	0.085	32.0	28.53
SB-F12	285	0.085	29.1	28.87
SB-F13	340	0.115	30.0	28.19
SB-F14	355	0.088	30.5	29.90
SB-F15	400	0.089	27.8	28.29
SB-F16	470	0.107	0.107	28.43
SB-F17	495	0.070	28.8	30.50
SB-F18	535	0.151	30.7	28.77
SB-F19	540	0.082	31.2	31.50
SB-F20	565	0.115	31.1	29.10
SB-F21	635	0.105	33.2	31.31

TABLE 12. SPECIMENS ANNEALED FOR 72 HOURS BEFORE STRETCH, AT 115°C

SPECIMEN NO.	NECKED EXT. %	THICKNESS (mm)	STRETCH RATE mm/min	BF, $\Delta n \times 10^3$
SB-G1	35	0.072	28.0	17.56
SB-G2	50	0.085	30.0	20.37
SB-G3	55	0.097	30.0	18.87
SB-G4	85	0.085	30.0	23.61
SB-G5	125	0.092	32.3	25.39
SB-G6	155	0.084	32.4	25.86
SB-G7	165	0.098	28.5	26.07
SB-G8	225	0.098	28.5	25.84
SB-G9	235	0.110	24.0	28.02
SB-G10	280	0.083	31.3	28.22
SB-G11	310	0.099	33.0	28.08
SB-G12	375	0.098	32.5	27.46
SB-G13	425	0.079	33.7	29.03
SB-G14	495	0.120	34.4	29.84
SB-G15	520	0.094	30.3	31.42
SB-G16	595	0.111	34.8	31.23

TABLE 13 BIREFRINGENCE ~ ANNEALING TIME VARIATION AT GIVEN EXTENSIONS

PRE- STRETCH ANNEALING TIME	BF, $\Delta n \times 10^3$, AT GIVEN NECKED EXTENSIONS %							
(hours)	50	100	150	200	250	300	350	400
$1\frac{1}{4}$	23.1	26.9	28.7	29.7	30.3	30.6	30.8	31.1
$2\frac{1}{4}$	20.8	24.5	26.6	27.9	29.0	29.5	29.2	30.2
3	21.3	25.1	27.0	28.1	29.0	29.6	30.2	30.6
6	20.2	24.1	26.4	28.0	29.1	29.9	30.5	30.8
22	19.8	23.5	25.4	26.4	27.2	27.9	28.6	29.2
$47\frac{2}{3}$	18.3	23.2	25.6	26.9	27.9	28.5	29.1	29.5
72	20.0	24.4	26.2	27.2	28.1	28.6	29.0	29.5

TABLE 14. BIREFRINGENCE MEASUREMENTS FOR IR-SCAN SPECIMENS, UNANNEALED BEFORE STRETCH, BUT ANNEALED FOR 15 MINUTES AFTER STRETCH, AT 115°C.

SPECIMEN NO.	NECKED EXT. %	THICKNESS (mm)	STRETCH RATE mm/min	BF, $\Delta n \times 10^3$
IR-1	35	0.110	27.0	12.75
IR-2	40	0.091	25.2	16.60
IR-3	70	0.068	32.0	19.25
IR-4	125	0.091	28.2	19.79
IR-5	130	0.097	25.2	21.65
IR-6	160	0.083	29.5	20.66
IR-7	165	0.105	30.5	20.29
IR-8	220	0.085	25.7	23.14
IR-9	225	0.098	29.6	23.38
IR-10	235	0.117	27.3	19.25
IR-11	285	0.095	29.4	25.52
IR-12	290	0.083	30.3	25.32
IR-13	325	0.090	28.5	24.99
IR-14	390	0.101	27.2	24.94
IR-15	405	0.115	27.4	22.36
IR-16	410	0.087	30.6	25.39
IR-17	415	0.117	32.5	24.66
IR-18	510	0.120	30.5	26.43
IR-19	595	0.099	34.0	23.21

TABLE 15 DEGREE OF CRYSTALLINITY AS A FUNCTION OF ANNEALING TIME

SPECIMEN NO.	ANNEALING PERIOD BEFORE STRETCH	DEGREE OF CRYSTALLINITY
DC-1	Unannealed	52.3±2.2
DC-2	1½ hour	53.7±3.3
DC-3	3 hour	55.3±1.4
DC-4	6 "	54.5±2.4
DC-5	22 "	55.8±2.3
DC-6	$47\frac{2}{3}$ "	58.4±1.3
DC-7	72 "	57.5±2.7

TABLE 16 BRAGG SPACING, d_{hkl} - FROM DIFFRACTOGRAMS AS A FUNCTION OF ANNEALING TIME

ANNEALING TIME (hours)	BRAGG SPACING, d_{hkl}			
	(110)	(040)	(130)	(131) (041)
0	6.37	5.29	4.84	4.10
1½	6.35	5.26	4.81	4.08
3	6.37	5.31	4.84	4.10
6	6.35	5.29	4.82	4.10
22	6.33	5.28	4.81	4.07
$47\frac{2}{3}$	6.33	5.26	4.80	4.08
72	6.33	5.28	4.81	4.08

TABLE . 17. BRAGG SPACINGS (AVERAGE) AS A FUNCTION OF EXTENSION %.

SPECIMEN NO.	NECKED EXT. %	BRAGG SPACING, d_{hkl} (Å)			
		1 (110)	2 (040)	3 (130)	4 $\overline{(131)}$, (041)
DS-1	0	6.30	5.35	4.79	4.12
DS-2	25	6.52	5.39	4.82	4.20
DS-3	30	6.28	5.29	4.69	4.09
DS-4	90	6.30	5.30	4.77	4.14
DS-5	125	6.30	5.33	4.78	4.20
DS-6	140	6.22	5.21	4.67	4.03
DS-7	165	6.54	5.34	4.85	4.24
DS-8	230	6.35	5.26	4.74	4.11
DS-9	240	6.30	5.29	4.76	4.20
DS-10	265	6.16	5.20	4.65	4.05
DS-11	325	6.34	5.31	4.76	4.16
DS-12	365	6.29	5.32	4.74	4.09
DS-13	405	6.38	5.30	4.76	4.13
DS-14	435	6.28	5.28	4.73	4.07
DS-15	460	6.30	5.28	4.74	4.11
DS-16	505	6.29	5.21	4.68	3.95
DS-17	550	6.31	5.31	4.75	4.12

TABLE 18 BIREFRINGENCE, DICHROIC RATIO AS FUNCTIONS OF EXTENSION

SPECIMEN NO.	WAVELENGTH≈1365 cm^{-1}		NECKED EXT. %	D	$\left\|\frac{D-1}{D+2}\right\|$	BF, $\Delta n \times 10^3$
	VERTICAL ABSORB. $\log \frac{FG}{GH}$	HORIZ. ABSORB. $\log \frac{FG}{GH}$				
Unoriented	1.000	1.2041	0	0.83	0.06	0
IR-1	1.2253	0.2804	35	4.37	0.529	12.75
IR-2	1.0640	0.3554	40	2.99	0.399	16.60
IR-3	0.8939	0.2078	70	4.30	0.524	19.25
IR-4	0.9138	0.1865	125	4.90	0.565	19.79
IR-5	0.8800	0.1793	130	4.91	0.566	21.65
IR-8	0.8246	0.1369	220	6.02	0.626	23.14
IR-9	0.8876	0.1568	225	5.66	0.608	23.38
IR-10	1.0280	0.1895	235	5.42	0.596	19.23
IR-12	0.8598	0.1774	290	4.85	0.562	23.32
IR-13	0.7270	0.1093	325	6.65	0.653	24.99
IR-14	0.9777	0.1645	390	5.94	0.622	24.94
IR-16	0.9247	0.1480	410	6.25	0.636	25.39
IR-17	0.8451	0.1728	415	4.89	0.565	24.66
IR-19	0.9011	0.1486	595	6.06	0.628	23.21

TABLE 19 MEASURED ARCLENGTH (PHOTOGRAPHIC FILMS)

Unit of distance: mm

SPECIMEN NO.	DIST. BET. COLL. & EXIT HOLES	RING/ ARC NO.	X_1	X_2	X_1+X_2	X_2-X_1
DS-1	90.25	1(a)	78.1	92.2	170.3	14.1
		(b)	78.1	92.2	170.3	14.1
		(c)	78.1	92.2	170.3	14.1
		2(a)	76.8	93.5	170.3	16.7
		(b)	76.9	93.5	170.4	16.6
		(c)	76.9	93.5	170.4	16.6
		3(a)	75.9	94.4	170.3	18.5
		(b)	75.9	94.5	170.4	18.6
		(c)	75.9	94.5	170.4	18.6
		4(a)	74.3	96.0	170.3	21.7
		(b)	74.4	95.9	170.3	21.5
		(c)	74.3	96.0	170.3	21.7
DS-2	90.35	1(a)	84.5	98.1	182.6	13.6
		(b)	84.5	98.2	182.7	13.7
		(c)	84.5	98.1	182.6	13.6
		2(a)	83.1	99.6	182.7	16.5
		(b)	83.1	99.6	182.7	16.5
		(c)	83.1	99.6	182.7	16.5
		3(a)	82.1	100.5	182.6	18.4
		(b)	82.1	100.6	182.7	18.5
		(c)	82.1	100.6	182.7	18.5

(Cont.)

SPECIMEN NO.	DIST. BET. COLL. & EXIT HOLES	RING/ ARC NO.	X_1	X_2	X_1+X_2	X_2-X_1
		4(a)	80.7	102.0	182.7	21.3
		(b)	80.8	102.0	182.8	21.2
		(c)	80.8	102.0	182.8	21.2
DS-3	89.70	1(a)	100.4	114.4	214.8	14.0
		(b)	100.4	114.5	214.9	14.1
		(c)	100.5	114.5	215.0	14.0
		2(a)	99.1	115.8	214.9	16.7
		(b)	99.1	115.8	214.9	16.7
		(c)	99.1	115.8	214.9	16.7
		3(a)	98.0	116.9	214.9	18.9
		(b)	98.1	116.9	215.0	18.8
		(c)	98.0	116.9	214.9	18.9
		4(a)	96.7	118.3	215.0	21.6
		(b)	96.6	118.3	214.9	21.7
		(c)	96.6	118.2	214.8	21.7
DS-4	90.25	1(a)	53.6	67.7	121.3	14.1
		(b)	53.6	67.7	121.3	14.1
		(c)	53.6	67.7	121.3	14.1
		2(a)	52.3	69.1	121.4	16.8
		(b)	52.3	69.0	121.3	16.7
		(c)	52.3	69.1	121.4	16.8
		3(a)	51.3	70.0	121.3	18.7
		(b)	51.4	70.0	121.4	18.6

(Cont.)

SPECIMEN NO.	DIST. BET. COLL & EXIT HOLES	RING/ ARC NO.	X_1	X_2	X_1+X_2	X_2-X_1
		(c)	51.4	70.0	121.4	18.6
		4(a)	49.9	71.4	121.3	21.5
		(b)	49.8	71.4	121.2	21.6
		(c)	49.9	71.3	121.2	21.4
DS-5	90.35	1(a)	45.6	59.8	105.4	14.2
		(b)	45.7	59.8	105.5	14.1
		(c)	45.7	59.7	105.4	14.0
		2(a)	44.3	61.1	105.4	16.8
		(b)	44.3	61.0	105.3	16.7
		(c)	44.4	61.0	105.4	16.6
		3(a)	43.4	62.1	105.5	18.7
		(b)	43.4	62.0	105.4	18.6
		(c)	43.4	62.0	105.4	18.6
		4(a)	42.0	63.5	105.5	21.5
		(b)	42.2	63.3	105.5	21.1
		(c)	42.2	63.3	105.5	21.1
DS-6	87.85	1(a)	72.2	86.2	158.4	14.0
		(b)	72.3	86.2	158.5	13.9
		(c)	72.3	86.1	158.4	13.8
		2(a)	70.8	87.5	158.3	16.7
		(b)	70.9	87.6	158.5	16.7
		(c)	70.9	87.4	158.3	16.5
		3(a)	69.9	88.5	158.4	18.6

(Cont.)

SPECIMEN NO.	DIST. BET. COLL. & EXIT HOLES	RING/ ARC NO.	X_1	X_2	X_1+X_2	X_2-X_1
		(b)	70.0	88.5	158.5	18.5
		(c)	69.9	88.5	158.5	18.6
		4(a)	68.4	90.0	158.4	21.6
		(b)	68.5	90.0	158.5	21.5
		(c)	68.4	89.9	158.3	21.5
DS-7	91.05	1(a)	92.5	106.2	198.7	13.7
		(b)	92.5	106.2	198.7	13.7
		(c)	92.5	106.2	198.7	13.7
		2(a)	90.9	107.7	198.6	16.8
		(b)	90.9	107.7	198.6	16.8
		(c)	91.0	107.8	198.8	16.8
		3(a)	90.2	108.7	198.9	18.5
		(b)	90.2	108.7	198.9	18.5
		(c)	90.1	108.6	198.7	18.5
		4(a)	88.8	110.0	198.8	21.2
		(b)	88.8	110.0	198.8	21.2
		(c)	88.8	110.0	198.8	21.2
DS-8	90-10	1(a)	65.5	79.5	145.0	14.0
		(b)	65.5	79.5	145.0	14.0
		(c)	65.5	79.5	145.0	13.9
		2(a)	64.0	80.9	144.9	16.9
		(b)	64.1	80.9	145.0	16.8
		(c)	64.1	80.9	144.9	16.9

(Cont.)

SPECIMEN NO.	DIST. BET. COLL. & EXIT HOLES	RING/ ARC NO.	X_1	X_2	X_1+X_2	X_2-X_1
		3(a)	63.1	81.8	144.9	18.7
		(b)	63.1	81.8	144.9	18.7
		(c)	63.0	81.8	144.8	18.8
		4(a)	61.7	83.3	145.0	21.6
		(b)	61.7	83.4	145.1	21.7
		(c)	61.7	83.4	145.1	21.7
DS-9	90.35	1(a)	54.4	68.5	122.9	14.1
		(b)	54.4	68.5	122.9	14.1
		(c)	54.4	68.5	122.9	14.1
		2(a)	53.1	69.9	123.0	16.8
		(b)	53.1	70.0	123.1	16.9
		(c)	53.1	69.9	123.0	16.8
		3(a)	52.2	70.9	123.1	18.7
		(b)	52.2	70.9	123.1	18.7
		(c)	52.2	70.9	123.1	18.7
		4(a)	50.8	72.1	122.9	21.3
		(b)	50.9	72.1	123.0	21.2
		(c)	50.9	72.1	123.0	21.2
DS-10	88.45	1(a)	73.2	87.4	160.6	14.2
		(b)	73.2	87.3	160.5	14.1
		(c)	73.3	87.3	160.6	14.1
		2(a)	71.9	88.7	160.6	16.8
		(b)	71.9	88.7	160.6	16.8

Cont.

SPECIMEN NO.	DIST. BET. COLL. & EXIT HOLES	RING/ ARC NO.	X_1	X_2	X_1+X_2	X_1-X_1
		(c)	71.9	88.6	160.5	16.7
		3(a)	70.9	89.6	160.5	18.7
		(b)	70.9	89.7	160.6	18.8
		(c)	70.9	89.7	160.6	18.8
		4(a)	69.5	91.1	160.6	21.6
		(b)	69.6	91.1	160.7	21.5
		(c)	69.5	91.0	160.5	21.5
DS-11	90.35	1(a)	61.9	75.9	137.8	14.0
		(b)	61.9	75.9	137.8	14.0
		(c)	61.9	75.9	137.8	14.0
		2(a)	60.5	77.3	137.8	16.8
		(b)	60.6	77.3	137.9	16.7
		(c)	60.5	77.3	137.8	16.3
		3(a)	59.6	78.3	137.9	18.7
		(b)	59.6	78.3	137.9	18.7
		(c)	59.6	78.3	137.9	18.7
		4(a)	58.2	79.7	137.9	21.5
		(b)	58.2	79.6	137.3	21.4
		(c)	58.2	79.6	137.8	21.4
DS-12	89.85	1(a)	98.7	112.7	211.4	14.0
		(b)	98.7	112.8	211.5	14.1
		(c)	98.7	112.8	211.5	14.1
		2(a)	97.4	114.1	211.5	16.7

(Cont.)

SPECIMEN N NO.	DIST. BET. COLL. & EXIT HOLES	RING/ ARC NO.	X_1	X_2	X_1+X_2	X_2-X_1
		(b)	97.4	114.1	211.5	16.7
		(c)	97.4	114.0	211.4	16.6
		3(a)	96.3	115.1	211.4	18.8
		(b)	96.4	115.1	211.5	18.7
		(c)	96.4	115.0	211.4	18.6
		4(a)	94.9	116.6	211.5	21.7
		(b)	95.0	116.6	211.6	21.6
		(c)	94.9	116.7	211.6	21.8
DS-13	88.80	1(a)	61.3	75.0	136.3	13.7
		(b)	61.3	75.0	136.3	13.7
		(c)	61.3	75.0	136.3	13.7
		2(a)	59.9	76.4	136.3	16.5
		(b)	59.9	76.4	136.3	16.5
		(c)	59.8	76.3	136.1	16.5
		3(a)	59.0	77.3	136.3	18.3
		(b)	58.9	77.4	136.3	18.5
		(c)	58.9	77.3	136.2	18.4
		4(a)	57.5	78.7	136.2	21.2
		(b)	57.6	78.8	136.4	21.2
		(c)	57.5	78.8	136.3	21.3
DS-14	89.75	1(a)	66.3	80.3	146.6	14.0
		(b)	66.3	80.4	146.7	14.1
		(c)	66.2	80.3	146.5	14.1

(Cont.)

SPECIMEN NO.	DIST. BET. COLL. & EXIT HOLES	RING/ ARC NO.	X_1	X_2	X_1+X_2	X_2-X_1
		2(a)	65.0	81.7	146.7	16.7
		(b)	64.9	81.7	146.6	16.8
		(c)	64.9	81.6	146.5	16.7
		3(a)	63.9	82.6	146.5	18.7
		(b)	64.0	82.7	146.7	18.7
		(c)	63.9	82.6	146.5	18.7
		4(a)	62.4	84.2	146.6	21.8
		(b)	62.5	84.2	146.7	21.7
		(c)	62.4	84.2	146.6	21.8
DS-15	90.0	1(a)	67.2	81.3	148.5	14.1
		(b)	67.2	81.3	148.5	14.1
		(c)	67.2	18.2	148.4	14.0
		2(a)	65.9	82.7	148.6	16.8
		(b)	65.9	82.7	148.6	16.8
		(c)	65.9	82.7	148.6	16.8
		3(a)	64.9	83.7	148.6	18.8
		(b)	65.0	83.7	148.7	18.7
		(c)	64.9	83.6	148.5	18.7
		4(a)	63.5	85.1	148.6	21.6
		(b)	63.6	85.1	148.6	21.6
		(c)	63.5	85.1	148.6	21.6
DS-16	84.95	1(a)	64.7	78.0	142.7	13.3
		(b)	64.7	78.1	142.8	13.4

(Cont.)

SPECIMEN NO.	DIST. BET. COLL. & EXIT HOLES	RING/ ARC NO.	X_1	X_2	X_1+X_2	X_2-X_1
		(c)	64.8	78.0	142.8	13.2
		2(a)	63.3	79.4	142.7	16.1
		(b)	63.4	79.4	142.8	16.0
		(c)	63.3	79.4	142.7	16.1
		3(a)	62.5	80.4	142.9	17.9
		(b)	62.6	80.4	143.0	17.8
		(c)	62.4	80.4	142.8	18.0
		4(a)	60.7	82.1	142.8	21.4
		(b)	60.7	82.2	142.9	21.5
		(c)	61.0	81.9	142.9	20.9
DS-17	90.10	1(a)	70.7	84.8	155.5	14.1
		(b)	70.8	84.8	155.4	14.0
		(c)	70.8	84.9	155.7	14.1
		2(a)	69.4	86.1	155.5	16.7
		(b)	69.4	86.2	155.6	16.8
		(c)	69.4	86.1	155.5	16.7
		3(a)	68.5	87.2	155.7	18.7
		(b)	68.4	87.2	155.6	18.8
		(c)	68.5	87.1	155.6	18.6
		4(a)	67.0	88.6	155.6	21.6
		(b)	67.0	88.6	155.6	21.6
		(c)	67.0	88.6	155.6	21.6

TABLE 20 BRAGG SPACINGS ; DATA FROM TABLE 19.

SPECIMEN NO.	NECKED EXT. %	RING/ ARC NO.	OBS. RED. X_2-X_1 =S=2θ	CORR. FACTOR	CORR. READING S'	d-SPACING
DS-1	0	1(a)	14.1	$\frac{90}{90.25}$	14.06	6.30
		(b)	14.1		14.06	6.30
		(c)	14.1		14.06	6.30
		2(a)	16.7		16.65	5.33
		(b)	16.6		16.55	5.36
		(c)	16.6		16.55	5.36
		3(a)	18.5		18.45	4.81
		(b)	18.6		18.55	4.78
		(c)	18.6		18.55	4.78
		4(a)	21.7		21.64	4.11
		(b)	21.5		21.44	4.14
		(c)	21.7		21.64	4.11
DS-2	25	1(a)	13.6	$\frac{90}{90.35}$	13.55	6.54
		(b)	13.7		13.65	6.49
		(c)	13.6		13.55	6.54
		2(a)	16.5		16.44	5.39
		(b)	16.5		16.44	5.39
		(c)	16.5		16.44	5.39
		3(a)	18.4		18.32	4.84
		(b)	18.5		18.43	4.81
		(c)	18.5		18.43	4.81
		4(a)	21.3		21.22	4.19

(Cont.)

SPECIMEN NO.	NECKED EXT. %	RING/ ARC NO.	OBS. RED. X_2-X_1 $=S=2\theta$	CORR. FACTOR	CORR. READING S'	d-SPACING
		(b)	21.2		21.12	4.21
		(c)	21.2		21.12	4.21
DS-3	30	1(a)	14.0	$\frac{90}{89.7}$	14.05	6.30
		(b)	14.1		14.15	6.26
		(c)	14.0		14.05	6.30
		2(a)	16.7		16.76	5.29
		(b)	16.7		16.76	5.29
		(c)	16.7		16.76	5.29
		3(a)	18.9		18.96	4.68
		(b)	18.8		18.86	4.71
		(c)	18.9		18.96	4.68
		4(a)	21.6		21.67	4.10
		(b)	21.7		21.77	4.08
		(c)	21.7		21.77	4.08
DS-4	90	1(a)	14.1	$\frac{90}{90.25}$	14.06	6.30
		(b)	14.1		14.06	6.30
		(c)	14.1		14.06	6.30
		2(a)	16.8		16.75	5.29
		(b)	16.7		16.65	5.33
		(c)	16.8		16.75	5.29
		3(a)	18.7		18.65	4.76
		(b)	18.6		18.55	4.78
		(c)	18.6		18.55	4.78

(Cont.)

SPECIMEN NO.	NECKED EXT. %	RING/ ARC NO.	OBS. RED. X_2-X_1 =S=2θ	CORR. FACTOR	CORR. READING S'	d-SPACING
		4(a)	21.5		21.44	4.14
		(b)	21.6		21.54	4.13
		(c)	21.4		21.34	4.16
DS-5	125	1(a)	14.2	$\frac{90}{90.35}$	14.14	6.26
		(b)	14.1		14.05	6.30
		(c)	14.0		13.95	6.35
		2(a)	16.8		16.73	5.30
		(b)	16.7		16.64	5.33
		(c)	16.6		16.54	5.36
		3(a)	18.7		18.63	4.76
		(b)	18.6		18.53	4.79
		(c)	18.6		18.53	4.79
		4(a)	21.5		21.42	4.15
		(b)	21.1		21.02	4.23
		(c)	21.1		21.02	4.23
DS-6	140	1(a)	14.0	$\frac{90}{87.85}$	14.34	6.18
		(b)	13.9		14.24	6.22
		(c)	13.8		14.14	6.26
		2(a)	16.7		17.10	5.19
		(b)	16.7		17.10	5.19
		(c)	16.5		16.90	5.25
		3(a)	18.6		19.06	4.66
		(b)	18.5		18.95	4.68

(Cont.)

SPECIMEN NO.	NECKED EXT. %	RING/ ARC NO.	OBS. RED. X_2-X_1 =S=2θ	CORR. FACTOR	CORR. READING S'	d-SPACING
		(c)	18.6		19.06	4.66
		4(a)	21.6		22.13	4.02
		(b)	21.5		22.03	4.04
		(c)	21.5		22.03	4.04
DS-7	165	1(a)	13.7	$\frac{90}{91.05}$	13.54	6.54
		(b)	13.7		13.54	6.54
		(c)	13.7		13.54	6.54
		2(a)	16.8		16.61	5.34
		(b)	16.8		16.61	5.34
		(c)	16.8		16.61	5.34
		3(a)	18.5		18.29	4.85
		(b)	18.5		18.29	4.85
		(c)	18.5		18.29	4.85
		4(a)	21.2		20.96	4.24
		(b)	21.2		20.96	4.24
		(c)	21.2		20.96	4.24
DS-8	230	1(a)	14.0	$\frac{90}{90.1}$	13.98	6.34
		(b)	14.0		13.98	6.34
		(c)	13.9		13.88	6.38
		2(a)	16.9		16.88	5.25
		(b)	16.8		16.78	5.28
		(c)	16.9		16.88	5.25

(Cont.)

SPECIMEN NO.	NECKED EXT. %	RING/ ARC NO.	OBS. RED. X_2-X_1 =S=2θ	CORR. FACTOR	CORR. READING S'	d-SPACING
		3(a)	18.7		18.68	4.75
		(b)	18.7		18.68	4.75
		(c)	18.8		18.78	4.73
		4(a)	21.6		21.58	4.12
		(b)	21.7		21.68	4.10
		(c)	21.7		21.68	4.10
DS-9	240	1(a)	14.1	$\frac{90}{90.35}$	14.05	6.30
		(b)	14.1		14.05	6.30
		(c)	14.1		14.05	66.30
		2(a)	16.8		16.73	5.30
		(b)	16.9		16.84	5.27
		(c)	16.8		16.73	5.30
		3(a)	18.7		18.63	4.76
		(b)	18.7		18.63	4.76
		(c)	18.7		18.63	4.76
		4(a)	21.3		21.22	4.19
		(b)	21.2		21.12	4.12
		(c)	21.2		21.12	4.12
DS-10	265	1(a)	14.2	$\frac{90}{88.45}$	14.45	6.13
		(b)	14.1		14.35	6.17
		(c)	14.1		14.35	6.17
		2(a)	16.8		17.09	5.19
		(b)	16.8		17.09	5.19

(Cont.)

SPECIMEN NO.	NECKED EXT. %	RING/ ARC NO.	OBS. RED. X_2-X_1 $=S=2\theta$	CORR. FACTOR	CORR. READING S'	d-SPACING
		(c)	16.7		16.99	5.22
		3(a)	18.7		19.03	4.66
		(b)	18.8		19.13	4.64
		(c)	18.8		19.13	4.64
		4(a)	21.6		21.98	4.04
		(b)	21.5		21.88	4.06
		(c)	21.5		21.88	4.06
DS-11	325	1(a)	14.0	$\frac{90}{90.35}$	13.95	6.34
		(b)	14.0		13.95	6.34
		(c)	14.0		13.95	6.34
		2(a)	16.8		16.73	5.30
		(b)	16.7		16.64	5.33
		(c)	16.8		16.73	5.30
		3(a)	18.7		18.63	4.76
		(b)	18.7		18.63	4.76
		(c)	18.7		18.63	4.76
		4(a)	21.5		21.42	4.15
		(b)	21.4		21.32	4.17
		(c)	21.4		21.32	4.17
DS-12	365	1(a)	14.0	$\frac{90}{89.85}$	14.02	6.32
		(b)	14.1		14.12	6.27
		(c)	14.1		14.12	6.27
		2(a)	16.7		16.73	5.30

(Cont.)

SPECIMEN NO.	NECKED EXT. %	RING/ ARC NO.	OBS. RED. X_2-X_1 =S=2θ	CORR. FACTOR	CORR. READING S'	d-SPACING
		(b)	16.7		16.73	5.30
		(c)	16.6		16.63	5.33
		3(a)	18.8		18.83	4.71
		(b)	18.7		18.73	4.74
		(c)	18.6		18.63	4.76
		4(a)	21.7		21.74	4.09
		(b)	21.6		21.64	4.11
		(c)	21.8		21.84	4.07
DS-13	405	1(a)	13.7	$\frac{90}{88.8}$	13.89	6.38
		(b)	13.7		13.89	6.38
		(c)	13.7		13.89	6.38
		2(a)	16.5		16.72	5.30
		(b)	16.5		16.72	5.30
		(c)	16.5		16.72	5.30
		3(a)	18.3		18.55	4.78
		(b)	18.5		18.75	4.73
		(c)	18.4		18.65	4.76
		4(a)	21.2		21.49	4.14
		(b)	21.2		21.49	4.14
		(c)	21.3		21.59	4.12
DS-14	435	1(a)	14.0	$\frac{90}{89.75}$	14.04	6.31
		(b)	14.1		14.14	6.26
		(c)	14.1		14.14	6.26

(Cont.)

SPECIMEN NO.	NECKED EXT. %	RING/ ARC NO.	OBS. RED. X_2-X_1 =S=2θ	CORR. FACTOR	CORR. READING S'	d-SPACING
		2(a)	16.7		16.75	5.29
		(b)	16.8		16.85	5.26
		(c)	16.8		16.85	5.26
		3(a)	18.7		18.75	4.73
		(b)	18.7		18.75	4.73
		(c)	18.7		18.75	4.73
		4(a)	21.8		21.86	4.07
		(b)	21.7		21.76	4.08
		(c)	21.8		21.86	4.07
DS-15	460	1(a)	14.1	$\frac{90}{90}$	14.1	6.28
		(b)	14.1		14.1	6.28
		(c)	14.0		14.0	6.33
		2(a)	16.8		16.8	5.28
		(b)	16.8		16.8	5.28
		(c)	16.8		16.8	5.28
		3(a)	18.8		18.8	4.72
		(b)	18.7		18.7	4.75
		(c)	18.7		18.7	4.75
		4(a)	21.6		21.6	4.11
		(b)	21.6		21.6	4.11
		(c)	21.6		21.6	4.11
DS-16	505	1(a)	13.3	$\frac{90}{84.95}$	14.09	6.28
		(b)	13.4		14.20	6.24

(Cont.)

SPECIMEN NO.	NECKED EXT. %	RING/ ARC NO.	OBS. RED. X_2-X_1 $=S=2\theta$	CORR. FACTOR	CORR. READING S'	d-SPACING
		(c)	13.2		13.98	6.34
		2(a)	16.1		17.06	5.20
		(b)	16.0		16.95	5.23
		(c)	16.1		17.06	5.20
		3(a)	17.9		18.96	4.68
		(b)	17.8		18.86	4.71
		(c)	18.0		19.07	4.65
		4(a)	21.4		22.67	3.92
		(b)	21.5		22.78	3.90
		(c)	20.9		22.14	4.02
DS-17	550	1(a)	14.1	$\frac{90}{90.1}$	14.08	6.29
		(b)	14.0		13.98	6.34
		(c)	14.1		14.08	6.29
		2(a)	16.7		16.68	5.32
		(b)	16.8		16.78	5.28
		(c)	16.7		16.68	5.32
		3(a)	18.7		18.68	4.75
		(b)	18.8		18.78	4.73
		(c)	18.6		18.58	4.78
		4(a)	21.6		21.58	4.12
		(b)	21.6		21.58	4.12
		(c)	21.6		21.58	4.12